

This is a postprint version of the following published document:

Serrano, O., Zaera, R., Fernández-Sáez, J. (2018) Band structure analysis of a thin plate with periodic arrangements of slender beams, *Journal of Sound and Vibration*, v. 420, pp.: 330-345.

DOI: <https://doi.org/10.1016/j.jsv.2017.11.016>

© 2017 Elsevier Ltd. All rights reserved.



This work is licensed under a [Creative Commons AttributionNonCommercialNoDerivatives 4.0 International License](https://creativecommons.org/licenses/by-nc-nd/4.0/)

1  
2  
3  
4  
5  
6  
7  
8  
9  
10  
11  
12  
13  
14  
15  
16  
17  
18  
19  
20  
21

# Band structure analysis of a thin plate with periodic arrangements of slender beams

12  
13  
14  
15  
16  
17  
18  
19  
20  
21

Ó. Serrano<sup>a,\*</sup>, R. Zaera<sup>a</sup>, and J. Fernández-Sáez<sup>a</sup>

16  
17  
18  
19  
20  
21

*<sup>a</sup>Department of Continuum Mechanics and Structural Analysis, University Carlos III of Madrid, Av. de la Universidad 30, 28911 Leganés, Madrid, Spain.*

---

22  
23  
24  
25  
26  
27  
28  
29  
30  
31  
32  
33  
34  
35  
36  
37  
38  
39  
40  
41  
42

## Abstract

24  
25  
26  
27  
28  
29  
30  
31  
32  
33  
34  
35  
36  
37

This work analyzes the wave propagation in structures composed of a periodic arrangement of vertical beams rigidly joined to a plate substrate. Three different configurations for the distribution of the beams have been analyzed: square, triangular, and hexagonal. A dimensional analysis of the problem indicates the presence of three dimensionless groups of parameters controlling the response of the system. The main features of the wave propagation have been found using numerical procedures based on the Finite Element Method, through the application of the Bloch's theorem for the corresponding primitive unit cells. Illustrative examples of the effect of the different dimensionless parameters on the dynamic behavior of the system are presented, providing information relevant for design.

38  
39  
40  
41  
42

*Keywords:* Lattice structure, beam arrays, Bloch's theorem, band gap, dimensional analysis.

---

43  
44  
45  
46  
47  
48  
49  
50  
51  
52  
53  
54  
55

## 1. Introduction

45  
46  
47  
48  
49  
50  
51

The design and use of structures able to promote directivity in wave propagation, or even to cancel it at certain frequencies ranges (band gaps) have attracted a great interest in several scientific and technological fields. It is well known that periodic solids, which can be treated as lattice structures, provide the above characteristics.

52  
53  
54  
55

Among the great variety of periodic solids, structures composed by an array of parallel nanobeams located normal to a nanoplate (substrate) have

---

56  
57  
58  
59  
60  
61  
62  
63  
64  
65

\*Corresponding author. E-mail address: oscar.serrano@uc3m.es.

1  
2  
3  
4  
5  
6  
7  
8  
9  
10  
11  
12  
13  
14  
15  
16  
17  
18  
19  
20  
21  
22  
23  
24  
25  
26  
27  
28  
29  
30  
31  
32  
33  
34  
35  
36  
37  
38  
39  
40  
41  
42  
43  
44  
45  
46  
47  
48  
49  
50  
51  
52  
53  
54  
55  
56  
57  
58  
59  
60  
61  
62  
63  
64  
65

been used in several applications related to nanosensors, water photoelectrolysis, hydrogen storage devices and gas sensing [1, 2].

The dynamic behavior of this kind of system has been analyzed by several authors (Collet *et al.* [3], Tsung-Tsong *et al.* [4], Tzung-Chen *et al.* [5] and Zi-Gui *et al.* [6]). The above works focus on periodic stubbed surfaces where short beams with circular [3, 4, 5] or square-cross sections [6] are distributed in a square arrangement over the surface. The predicted band structures have been verified with experimental results [4, 5]. Tsung-Tsong *et al.* [4] and Tzung-Chen *et al.* [5] showed the corresponding band structures for different ratios of beam length to plate thickness, while Zi-Gui *et al.* [6] studied the influence on the first band gaps of the rotated angle of the square cross-section of the stubs around its longitudinal axis. These analyses are rather specific because only one configuration (square arrangements of the stubs) and the variation of only one parameter is considered.

Other authors focus on a kind of structure with a higher beam-length to plate-thickness ratio. Tanaka *et al.* [7] showed some characteristics of these kinds of structures, in which a polymer surrounds the arrangement of beams. Eremeyev *et al.* [8, 9] conducted an analytical study of the dynamic behavior of a system composed by ZnO nanocrystals (slender nanobeams) clamped to a sapphire substrate (nanoplate). It was found that the eigenfrequencies of the system can be determined as a combination of the eigenfrequencies of a single nanocrystal and those of the substrate [8]. Elsewhere [9] a dense continuous distribution of beams over the substrate is presented.

The control of location and width of the band gaps is a key design issue of this type of structure in order to achieve the desired performance related to a specific application. Sugino *et al.* [10] studied the case of a plate with a square arrangement of resonators (masses and springs vibrating perpendicularly to the plate). These authors finished with the evidence of a band gap located at the resonant frequency of the spring-mass resonator and the width depending on the ratio of resonator mass to plate mass. This technological interest stimulates the proposal of methodologies for *optimal* design, aiming at selecting the parameters of the system that can position the band gap within a certain range. Some authors explored the use of topology optimization as a systematic way to design phononic band-gap materials [11, 12]. In topology optimization, a given design layout is discretized by a large number of elements, commonly coinciding with the FE mesh, allowing the material type or density in each element to be treated as a design variable. By defining objective functions, the above-cited authors determine the characteristics of

1  
2  
3  
4  
5  
6  
7  
8  
9 the solid for the maximization of the band gaps. Despite the interest of this  
10 methodology to define entirely new topologies tailored for specific loads and  
11 boundary conditions, the overall picture of the physical behavior of the solid  
12 frequently remains hidden. Moreover, the presence of multiple optima, i.e.  
13 non-unique solutions, introduces uncertainties in the design process. Here we  
14 follow an alternative pathway, grounded in the knowledge of the dimension-  
15 less groups governing the solution to the problem. This enables us to specify  
16 which parameters are relevant (and which are not), how they influence the  
17 band structure, and where the global extrema are located.

18  
19 In this work, we analyze the dynamic behavior of a periodic array of slender  
20 beams normal to a thin substrate, considering it as a lattice structure.  
21 This periodicity permits the use of Bloch's methodology. On the basis of the  
22 formulation by Eremeyev *et al.* [9], we develop a dimensional analysis which  
23 reveals three dimensionless groups of variables governing the dynamic be-  
24 havior of the lattice. Three different geometrical distributions for the crystal  
25 are considered (square, triangular, and hexagonal). For each configuration  
26 an analysis of band structures and directivity of wave propagation is shown.  
27 Also, illustrative results on the influence of the different dimensionless groups  
28 of variables on the location and width of the band gaps are presented.

29  
30 The paper is organized as follows. Section 1 provides a brief introduc-  
31 tion and Section 2 describes the problem and the geometries involved in the  
32 study. Section 3 offers the dimensional analysis of the problem while Section  
33 4 describes the methodology used to apply Bloch's theorem together with  
34 the Finite Element Method on the different primitive unit cells. Section 5  
35 presents some illustrative examples on the wave-propagation characteristics  
36 of the three studied lattice structures. Section 6 illustrates the influence of  
37 the different dimensionless parameters in the behavior of the system. Finally  
38 Section 7 summarizes the main results of the work.

## 39 40 41 42 43 44 45 46 **2. Problem formulation**

47  
48 Let us consider a system consisting of an infinite plate parallel to the plane  
49  $\{x, y\}$ , and an infinite array of beams perpendicular to the plate and with  
50 their lower ends joined to it. The assumed constraint condition at the beam-  
51 plate interface is that of equal rotations and out-of-plane displacement. The  
52 plate has surface density  $\rho$  and bending stiffness  $D$ . The beams have length  
53  $l$ , linear density  $\rho_*$  and the same bending stiffness  $C$  in both directions. Let  
54  $(U, V, W)$  be displacements and  $(\theta_x, \theta_y, \theta_z)$  rotations, the degrees of freedom  
55  
56  
57  
58

1  
2  
3  
4  
5  
6  
7  
8  
9  
10  
11  
12  
13  
14  
15  
16  
17  
18  
19  
20  
21  
22  
23  
24  
25  
26  
27  
28  
29  
30  
31  
32  
33  
34  
35  
36  
37  
38  
39  
40  
41  
42  
43  
44  
45  
46  
47  
48  
49  
50  
51  
52  
53  
54  
55  
56  
57  
58  
59  
60  
61  
62  
63  
64  
65

of the system are  $W, \theta_x, \theta_y$  for the plate, and  $U, V, W, \theta_x, \theta_y$  for the beams. Fig. 1 illustrates the degrees of freedom considered. Moreover, the beams are considered inextensible. As stated above, thin plate and slender beams are considered, thus permitting the use of the Kirchhoff and Euler-Bernoulli models respectively, neglecting the effect of shear strains.

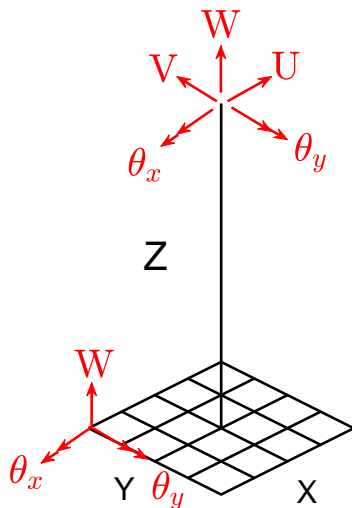


Figure 1: Scheme of a lattice structure with the degrees of freedom considered.

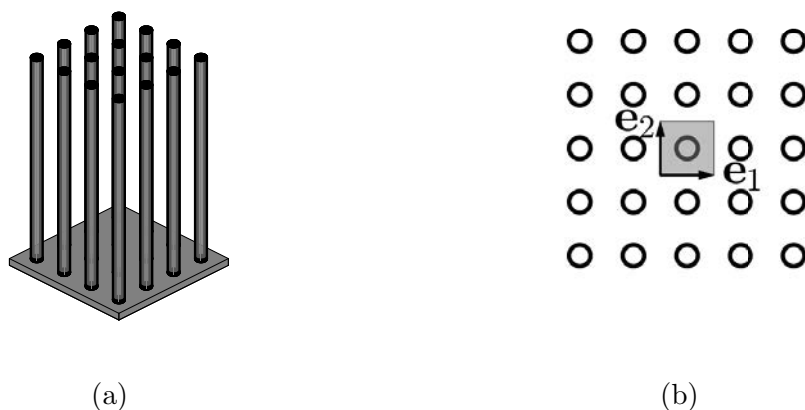


Figure 2: Lattice structure with square configuration: (a) Isometric view, (b) Top view with primitive unit cell.

1  
2  
3  
4  
5  
6  
7  
8  
9  
10  
11  
12  
13  
14  
15  
16  
17  
18  
19  
20  
21  
22  
23  
24  
25  
26  
27  
28  
29  
30  
31  
32  
33  
34  
35  
36  
37  
38  
39  
40  
41  
42  
43  
44  
45  
46  
47  
48  
49  
50  
51  
52  
53  
54  
55  
56  
57  
58  
59  
60  
61  
62  
63  
64  
65

The position of the beams is assumed to follow a periodic arrangement in the  $\{x, y\}$  plane, thus constituting a lattice structure. Three different arrangements are studied: square, triangular, and hexagonal, with connection points located at the vertices of the corresponding regular polygons. The primitive unit cells  $\Omega_c$  consist of one beam in the center of a square substrate for the square lattice, one beam in the center of a rhombic substrate for the triangular lattice, and two beams in the center of the two contiguous equilateral triangles for the hexagonal lattice. The corresponding primitive unit cells are presented in Figs. 2b to 4b as shaded quadrilaterals, and Table 1 shows their lattice vectors  $\mathbf{e}_1$  and  $\mathbf{e}_2$  and reciprocal lattice vectors  $\mathbf{b}_1$  and  $\mathbf{b}_2$  ( $\mathbf{e}_i \cdot \mathbf{b}_j = \delta_{ij}$ , being  $\delta_{ij}$  the Kronecker delta) in terms of a characteristic dimension  $a$ .

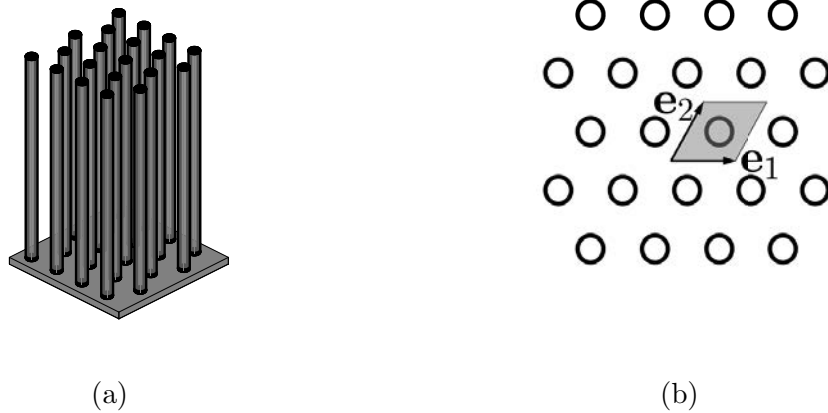


Figure 3: Lattice structure with triangular configuration: (a) Isometric view, (b) Top view with primitive unit cell.

lattice	$\mathbf{e}_1$	$\mathbf{e}_2$	$\mathbf{b}_1$	$\mathbf{b}_2$
square	$a\mathbf{i}$	$a\mathbf{j}$	$\frac{1}{a}\mathbf{i}$	$\frac{1}{a}\mathbf{j}$
triangular and hexagonal	$a\mathbf{i}$	$a\left(\frac{1}{2}\mathbf{i} + \frac{\sqrt{3}}{2}\mathbf{j}\right)$	$\frac{1}{a}\left(\mathbf{i} - \frac{1}{\sqrt{3}}\mathbf{j}\right)$	$\frac{1}{a}\left(\frac{2}{\sqrt{3}}\mathbf{j}\right)$

Table 1: Vectors of lattices ( $\mathbf{e}_1$  and  $\mathbf{e}_2$ ) and reciprocal lattices ( $\mathbf{b}_1$  and  $\mathbf{b}_2$ ) in terms of the characteristic dimension  $a$  for the configurations studied.

1  
2  
3  
4  
5  
6  
7  
8  
9  
10  
11  
12  
13  
14  
15  
16  
17  
18  
19  
20  
21  
22  
23  
24  
25  
26  
27  
28  
29  
30  
31  
32  
33  
34  
35  
36  
37  
38  
39  
40  
41  
42  
43  
44  
45  
46  
47  
48  
49  
50  
51  
52  
53  
54  
55  
56  
57  
58  
59  
60  
61  
62  
63  
64  
65

Eremeyev *et al.* [9] formulated the governing equation of the vibrations of the above system leading to the following eigenvalue problem

$$D\Delta\Delta W - \rho\omega^2 W = \sum_i \left( \rho_* l \omega^2 W \delta(x - x_i) \delta(y - y_i) - \frac{C\kappa}{g(\kappa l)} \nabla \cdot [(\nabla W) \Big|_{x=x_i, y=y_i} \delta(x - x_i) \delta(y - y_i)] \right), \quad (1)$$

where  $\omega$  is the eigenfrequency,  $(x_i, y_i)$  are the coordinates of junctions between plate and beam of unit cell  $i$ ,  $\kappa = \sqrt[4]{\rho_*/C} \sqrt{\omega}$ ,  $\nabla$  the 2D gradient operator,  $\Delta$  the 2D Laplacian operator and  $g(\kappa l)$  the dimensionless function

$$g(\kappa l) = \frac{1 + \cos(\kappa l) \cosh(\kappa l)}{\sin(\kappa l) \cosh(\kappa l) - \cos(\kappa l) \sinh(\kappa l)}. \quad (2)$$

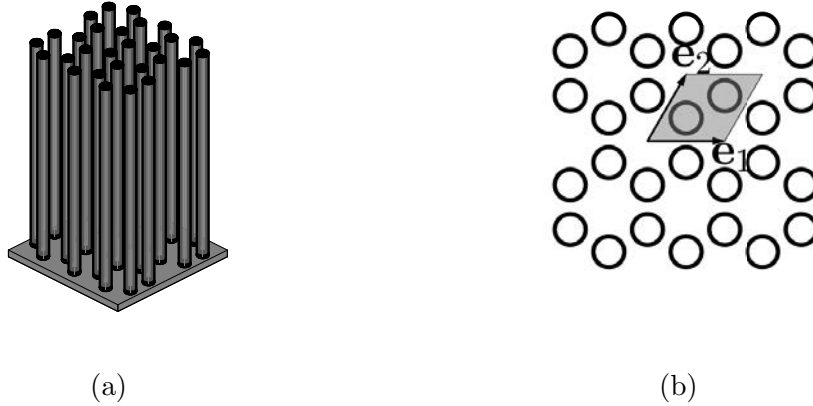


Figure 4: Lattice structure with hexagonal configuration: (a) Isometric view, (b) Top view with primitive unit cell.

Eq. (1) provides valuable information to identify the group of parameters that govern the solution of the problem, as it will be shown next.

### 3. Nondimensional form of the governing equation: dimensionless groups

Using the following dimensionless spatial variables  $\bar{W} = W/a$ ,  $\bar{x} = x/a$  and  $\bar{y} = y/a$ , Eq. (1) may be written in nondimensional form, leading to the

following expression

$$\begin{aligned} \Delta\Delta\bar{W} - A_1A_2^4A_3^2\bar{\lambda}^4\bar{W} = \sum_i \left( A_2^2A_3\bar{\lambda}^4\bar{W}\delta(\bar{x} - \bar{x}_i)\delta(\bar{y} - \bar{y}_i) - \right. \\ \left. - \frac{A_3\bar{\lambda}}{g(\bar{\lambda})}\nabla \cdot [(\nabla\bar{W})\Big|_i\delta(\bar{x} - \bar{x}_i)\delta(\bar{y} - \bar{y}_i)] \right), \end{aligned} \quad (3)$$

where  $A_1$ ,  $A_2$ , and  $A_3$  are the dimensionless groups relating the plate to beam density, the cell dimension to beam length, and the beam to plate stiffness, respectively

$$A_1 = \frac{\rho}{\rho_*/l}, \quad A_2 = \frac{a}{l}, \quad A_3 = \frac{C/l}{D} \quad (4)$$

and  $\bar{\lambda}$  is the dimensionless eigenvalue

$$\bar{\lambda} = \sqrt[4]{\frac{\rho_*l^4}{C}}\sqrt{\omega}. \quad (5)$$

The dimensionless groups related to a physical phenomenon give intrinsic information about the problem. While the same value is maintained for all the dimensionless groups ( $A_1$ ,  $A_2$ ,  $A_3$ ), the physical parameters (beam length, plate thickness, etc.) involved in the problem can be modified without changing the response of the physical system. In other words, if two different lattices ( $l1$ ), defined by  $(\rho, \rho_*, l, a, C, D)^{l1}$ , and ( $l2$ ), defined by  $(\rho, \rho_*, l, a, C, D)^{l2}$ , lead to the same values of  $A_1$ ,  $A_2$ ,  $A_3$  ( $A_1^{l1} = A_1^{l2}$ ,  $A_2^{l1} = A_2^{l2}$ ,  $A_3^{l1} = A_3^{l2}$ ), then  $\bar{\lambda}^{l1} = \bar{\lambda}^{l2}$ .

Therefore, given a certain periodic distribution of beams,  $\bar{\lambda}$  is a function of  $A_1$ ,  $A_2$ ,  $A_3$ . The groups  $A_1$ ,  $A_2$  and  $A_3$  provide valuable information for the analysis of the dispersion properties and band gaps of this type of lattice structures, and for tailoring their dynamic behavior. In the following sections, this study will be performed using the Bloch's theorem combined with the Finite Element Method.

#### 4. Numerical Analysis

Now, we develop the application of Bloch's theorem to the beam-plate lattice, which enables us to analyze the dispersive properties in the primitive



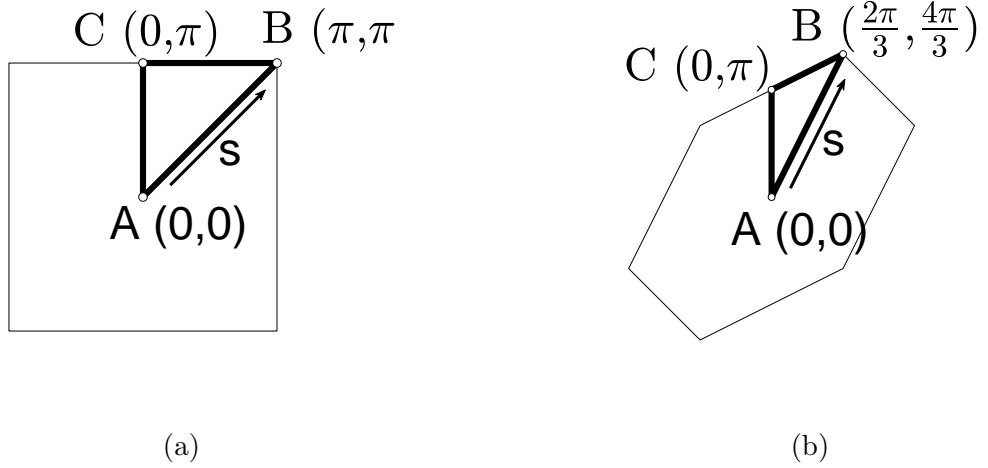


Figure 5: Reciprocal lattice in  $k_1$ - $k_2$  space: (a) Square configuration, (b) Triangular and hexagonal configurations.

unit cell (Figs. 2b to 4b) instead of investigating them in the entire domain, thus saving huge computation time. For that aim a self-made Finite Element code has been developed.

#### 4.1. Application of the Bloch's theorem

Bloch's theorem is commonly applied in photonics and quantum mechanics [13], and has been progressively employed in the mechanics of periodic solids as well. It can be understood as a multidimensional version of Floquet's theorem [14]. A brief explanation of Bloch's theorem is presented below. For a more detailed description, see for instance the works of Collet *et al.* [3], Gonella *et al.* [15], Phani *et al.* [16], and Tie *et al.* [17].

Due to the periodicity of the lattice, any point  $\mathbf{x}$  of the plate can be parametrized with respect to a point  $\mathbf{p}$  of the reference primitive unit cell  $\Omega_c$  as

$$\mathbf{x} = \mathbf{p} + n_j \mathbf{e}_j, \quad j = 1, 2, \quad (6)$$

with  $n_j \in \mathbb{Z}$  being the indexes identifying the cell. According to the Bloch's theorem, the vector of dofs  $\mathbf{u}$  at points  $\mathbf{x}$  and  $\mathbf{p}$  for a plane wave (harmonic motion) are related as

$$\mathbf{u}(\mathbf{x}) = \mathbf{u}(\mathbf{p}) e^{i\mathbf{k} \cdot (n_j \mathbf{e}_j)}, \quad (7)$$

with  $\mathbf{k}$  being the wavevector in the Cartesian coordinate system. Then, the motion in the periodic domain can be expressed in terms of the response of a reference cell and an exponential term defining the phase changes as the wave propagates through the lattice. Consequently, the dispersive characteristics of the lattice structure can be determined from the analysis of the primitive unit cell.

To explore directivity and band gaps in wave propagation, we can represent the wavevectors in the reciprocal lattice with primitive unit cell  $\Omega_r$  [18], whose reciprocal lattice basis  $\mathbf{b}_1$  and  $\mathbf{b}_2$  are defined in Table 1. Due to the periodicity of the reciprocal lattice, the dispersive characteristics can be explored just in the first Brillouin zone, which coincides with  $\Omega_r$ . Fig. 5 shows the first Brillouin zone for the three lattices in the lattice basis. Commonly the wavevector is expressed on the basis of the vectors of the lattices:  $k_i = \mathbf{k} \cdot \mathbf{e}_i, i = 1, 2$ . If the band gap structure is to be determined, only the wavevectors pointing to the edges of a given subdomain of  $\Omega_r$  (irreducible zone) are studied, since the band extrema almost always occur along the boundaries of this region [19]. The irreducible zone is represented by the shaded triangle  $ABC$  in Fig. 5 for each of the three configurations.

#### 4.2. FEM Model

The harmonic motion of the reference primitive unit cell is numerically studied by the application of the Finite Element Method. As stated above, the vertical rods were modeled as Euler-Bernoulli beams and the substrate as a Kirchhoff plate. Two-node linear elements (10 dofs) were used for the beam. The square cell of the square lattice was modeled with the four-node MZC (Melosh, Zienkiewicz and Cheung) elements (12 dofs). The rhombic cell of the triangular and hexagonal lattices was modeled with the three-node CKZ (Cheung, King and Zienkiewicz) elements (9 dofs). The shape functions for these elements can be found in a previous work [20]. The models correspond to the primitive unit cell shown in Figs. 2b to 4b. According to the hypotheses of the problem, the beams are assumed to be inextensible and rotation around its axis is not permitted. Also, the in-plane displacements of the plate and the rotation around the normal axis are disabled.

Finally, the discretized equation of motion reads

$$[\mathbf{K} - \omega^2 \mathbf{M}] \hat{\mathbf{U}} = \mathbf{F}, \quad (8)$$

where  $\mathbf{K}$  and  $\mathbf{M}$  are the stiffness and mass matrices, and  $\hat{\mathbf{U}}$  and  $\mathbf{F}$  are the nodal dofs and load vectors of the discretized cell.

According to Bloch's theorem, a relation in nodal displacements and in nodal loads exist between the dofs located at the edges of the primitive unit cell. This enables us to establish the following relations

$$\hat{\mathbf{U}} = \mathbf{W}_a \hat{\mathbf{U}}_r, \quad \mathbf{F} = \mathbf{W}_b \mathbf{F}_r, \quad (9)$$

$\hat{\mathbf{U}}_r$  and  $\mathbf{F}_r$  being the vectors containing the displacement and load of the independent dofs of the nodes, respectively.  $\mathbf{W}_a = \mathbf{W}_a(k_1, k_2)$ ,  $\mathbf{W}_b = \mathbf{W}_b(k_1, k_2)$  are the matrices resulting from the application of Eq. (7) to displacements and forces, respectively. Finally, introducing Eq. (9) into Eq. (8), pre-multiplying by  $\mathbf{W}_a^H$  (Hermitian transpose of  $\mathbf{W}_a$ ), and taking into account  $\mathbf{W}_a^H \mathbf{F} = \mathbf{0}$  [21], we get the eigenvalue problem

$$[\mathbf{K}_r(k_1, k_2) - \omega^2 \mathbf{M}_r(k_1, k_2)] \hat{\mathbf{U}}_r = \mathbf{0}, \quad (10)$$

where  $\mathbf{K}_r = \mathbf{W}_a^H \mathbf{K} \mathbf{W}_a$  and  $\mathbf{M}_r = \mathbf{W}_a^H \mathbf{M} \mathbf{W}_a$  are the respective reduced stiffness and mass matrices.

## 5. Analysis of results

The band structure and the phase and group velocities are the main features characterizing wave propagation in lattice structures. Both can be derived from the solution of the eigenvalue problem given by Eq. (10), leading to the dispersion surfaces

$$\omega = \omega(k_1, k_2). \quad (11)$$

The phase and group velocities expressed in the  $\{x, y\}$  space ( $\mathbf{i}_1, \mathbf{i}_2$  on the basis of the Cartesian coordinate system) are defined by

$$\mathbf{v}_{\text{phase}} = \frac{\omega}{|\mathbf{k}|^2} \mathbf{k}, \quad \mathbf{v}_{\text{group}} = \mathbf{R} \cdot \left( \frac{d\omega}{dk_1}, \frac{d\omega}{dk_2} \right)^T, \quad (12)$$

with  $\mathbf{k} = k_1 \mathbf{b}_1 + k_2 \mathbf{b}_2$  and,  $\mathbf{R}$  given by

$$\mathbf{R} = \begin{pmatrix} \mathbf{e}_1 \cdot \mathbf{i}_1 & \mathbf{e}_2 \cdot \mathbf{i}_1 \\ \mathbf{e}_1 \cdot \mathbf{i}_2 & \mathbf{e}_2 \cdot \mathbf{i}_2 \end{pmatrix}.$$

Band structure and velocities will be presented for a reference set of values of the nondimensional groups  $A_1^* = 0.65$ ,  $A_2^* = 0.5$ , and  $A_3^* = 823.69$ . These

1  
2  
3  
4  
5  
6  
7  
8  
9 values correspond to the mechanical properties of steel (Young Modulus,  
10  $E = 2.1 \cdot 10^{11}$  N/m<sup>2</sup>; Poisson's ratio,  $\nu = 0.3$ ; and volumetric mass density,  
11  $\rho_{\text{vol}} = 7800$  kg/m<sup>3</sup>) for beam and plate, and the following dimensions: plate  
12 thickness  $t = 0.005$  m, primitive unit cell parameter  $a = 1.0$  m, beam length  
13  $l = 2.0$  m, and beam diameter (considering circular cross section)  $d = 0.14$  m.  
14 Note that the same reference values of the parameters will be used for the  
15 three lattices. A mesh convergence analysis was performed in order to define  
16 a suitable number of elements for both plate and beams.  
17  
18  
19

### 20 *5.1. Band structures and dispersion surfaces*

21  
22 The band structures and dispersion surface related to the three configura-  
23 tions are presented below.  
24

#### 25 *5.1.1. Square configuration*

26  
27 The band structure is presented in Fig. 6a along the edges of the irre-  
28 ducible zone, which can be identified by the triangle  $ABC$  depicted in Fig.  
29 5a. A detail of the first modes is presented in Fig. 6b. The vertical axis in  
30 the Figure 6a represents the square of the dimensionless eigenfrequency  $\bar{\lambda}$   
31 Eq. (5). The horizontal axis represents the wavenumber through the path  
32 defined by the edges of the irreducible zone.  
33

34  
35 The dispersion curve corresponding to the first mode starts from  $\bar{\lambda}^2 = 0$ ,  
36 representing a translational displacement in  $z$  direction. The appearance  
37 of wide complete band gaps (light gray) and partial band gaps (dark gray)  
38 in the lattices allows us to envisage the square configuration as an efficient  
39 vibration filter. Fig. 6a presents two complete band gaps (3rd-4th and 4th-  
40 5th modes) and several partial band gaps through the different edges of the  
41 irreducible zone.  
42  
43  
44  
45  
46  
47  
48  
49  
50  
51  
52  
53  
54  
55  
56  
57  
58

1  
2  
3  
4  
5  
6  
7  
8  
9  
10  
11  
12  
13  
14  
15  
16  
17  
18  
19  
20  
21  
22  
23  
24  
25  
26  
27  
28  
29  
30  
31  
32  
33  
34  
35  
36  
37  
38  
39  
40  
41  
42  
43  
44  
45  
46  
47  
48  
49  
50  
51  
52  
53  
54  
55  
56  
57  
58  
59  
60  
61  
62  
63  
64  
65

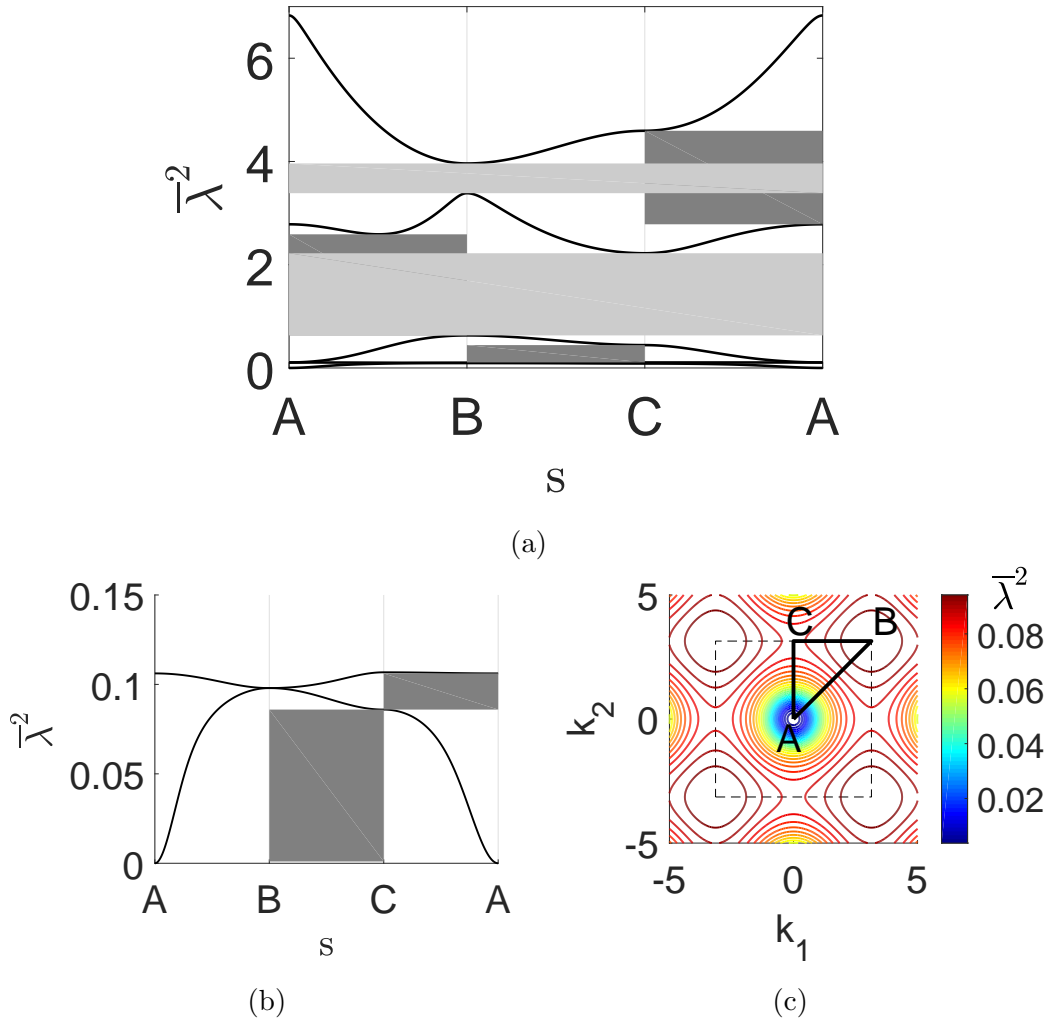


Figure 6: Square configuration: (a) Band structure: 1st to 5th modes, (b) Detail of band structure: 1st and 2nd modes, (c) 1st mode dispersion surface presented in the contour plot.

The square configuration has been commonly used for the case of stubbed surfaces. One of these was presented by Tsung-Tsong et al. [4], who showed a complete band gap from 114 kHz to 146 kHz for this kind of structure. An analysis of an equivalent square lattice with slender beams has been performed, using the same material and the same geometry for the plate and a slender ratio for the geometry of the beam of  $d=0.07L$ . The results show

1  
2  
3  
4  
5  
6  
7  
8  
9  
10  
11  
12  
13  
14  
15  
16  
17  
18  
19  
20  
21  
22  
23  
24  
25  
26  
27  
28  
29  
30  
31  
32  
33  
34  
35  
36  
37  
38  
39  
40  
41  
42  
43  
44  
45  
46  
47  
48  
49  
50  
51  
52  
53  
54  
55  
56  
57  
58  
59  
60  
61  
62  
63  
64  
65

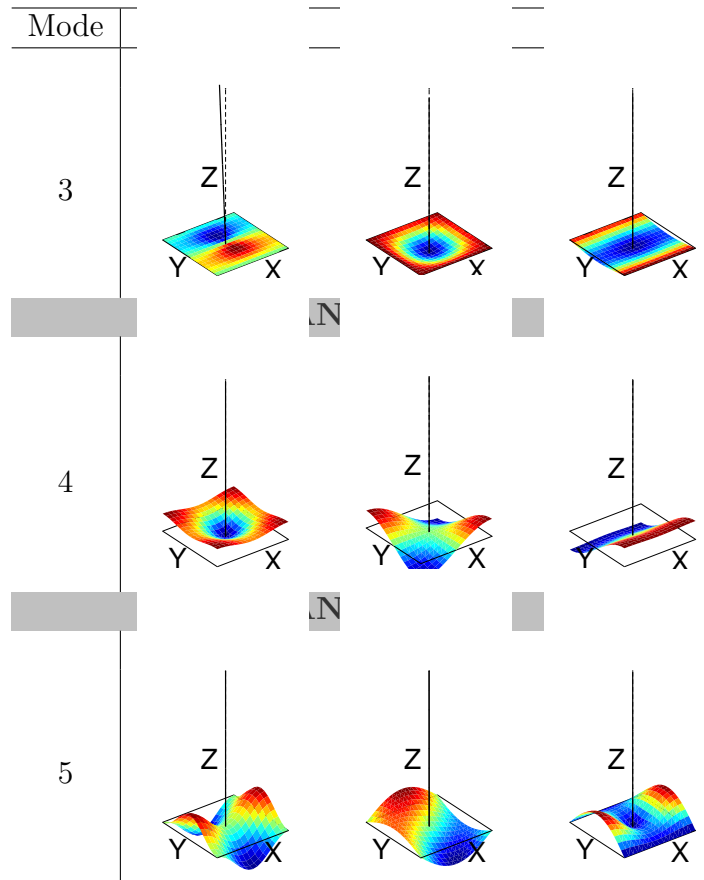


Table 2: Square configuration: Shapes of modes surrounding the band gaps.

that a plate with slender beams creates wide band gaps at lower frequencies than a plate with stubs: from 11.3 kHz to 15.6 kHz, 15.8 kHz to 29 kHz, and 32.5 kHz to 34.4 kHz. This is consistent with the fact that slender beams have lower resonant frequencies than do stubs of the same total mass.

The shapes of the modes surrounding the band gaps at points A, B, and C of the Brillouin zone are presented in Table 2. To ascertain which mechanism is present at each point, we have decoupled the problem as follows: 1) the first is represented by a unit cell composed of a plate with a point mass equal to that of the beam and located at the joint. This model captures the effect of the inertia of the beam in the out-of-plane direction, as a result of its inextensibility. Numerically, this condition is fulfilled by transferring the total mass of the beam to the junction node; 2) the second is represented

Mode	A	B	C
1	Common	Type 2	Type 2
2	Type 2	Type 2	Type 2
3	Type 2	Type 1	Type 1
<b>BAND GAP</b>			
4	Type 1	Common	Type 2
<b>BAND GAP</b>			
5	Common	Type 2	Type 1

Table 3: Square configuration: Summary of the predominant problem types.

by a unit cell composed of a plate with a beam that lacks mass in the  $z$  direction. This model captures the effect of transverse vibration of the beam in directions  $x$  and  $y$ . This uncoupling makes it possible to match, at specific points of the dispersion diagram, the eigenvalues (as well as eigenfunctions) of the complete system with those of the two uncoupled systems, enabling us to distinguish whether the vibration of the system is driven by the inertia of the beam in the out-of-plane direction or by the transverse vibration of the beam. Additionally, at specific wavenumbers and for specific modes, the dynamics of the complete system is common to both problem types. It was proved that these eigenvalues (and eigenfunctions) correspond also to the case of a plate in the absence of beams.

Thus, for each mode and for each vertex of the irreducible zone of the complete system, the vibration corresponds to one or both of the following problems:

- Type 1: plate with point-mass.
- Type 2: plate with beam lacking mass in the  $z$  direction.

Table 3 summarizes the predominant problem type for each mode, where equivalent modes can be identified in the different problem types. It can be seen that the first modes are related to Type 2, Fig. 9a.

The dispersion surface of the first mode is presented in Fig. 6c in the form of iso-frequency contours over the  $k_1 - k_2$  space. The boundaries of the first Brillouin zone and of the irreducible zone are also presented in this Figure. The four-fold rotational symmetry of the lattice with square configuration becomes evident in Fig. 6c. It should be noted that circular iso-frequency curves associated with a low wavenumber (vicinity of point A in Fig. 6c)

1  
2  
3  
4  
5  
6  
7  
8  
9  
10  
11  
12  
13  
14  
15  
16  
17  
18  
19  
20  
21  
22  
23  
24  
25  
26  
27  
28  
29  
30  
31  
32  
33  
34  
35  
36  
37  
38  
39  
40  
41  
42  
43  
44  
45  
46  
47  
48  
49  
50  
51  
52  
53  
54  
55  
56  
57  
58  
59  
60  
61  
62  
63  
64  
65

suggest isotropic wave propagation. As the wave number approaches the boundaries of the Brillouin zone, the iso-frequency curves deform and the angular-dependent dispersion relation reveals the underlying symmetry of the lattice. There exists a frequency range where the iso-frequency curves change from convex to concave. At the limit between concavity and convexity, curves take the form close to a square and the energy flux collimates in two perpendicular directions according to the preferential orientations of the group velocity vector, which is normal to the iso-frequency contours.

### 5.1.2. *Triangular configuration*

The band structure is presented in Fig. 7a along the edges of the irreducible zone, which can be identified by the triangle  $ABC$  depicted in Fig. 5b. A detail of the first modes is presented in Fig. 7b.



1  
2  
3  
4  
5  
6  
7  
8  
9  
10  
11  
12  
13  
14  
15  
16  
17  
18  
19  
20  
21  
22  
23  
24  
25  
26  
27  
28  
29  
30  
31  
32  
33  
34  
35  
36  
37  
38  
39  
40  
41  
42  
43  
44  
45  
46  
47  
48  
49  
50  
51  
52  
53  
54  
55  
56  
57  
58  
59  
60  
61  
62  
63  
64  
65

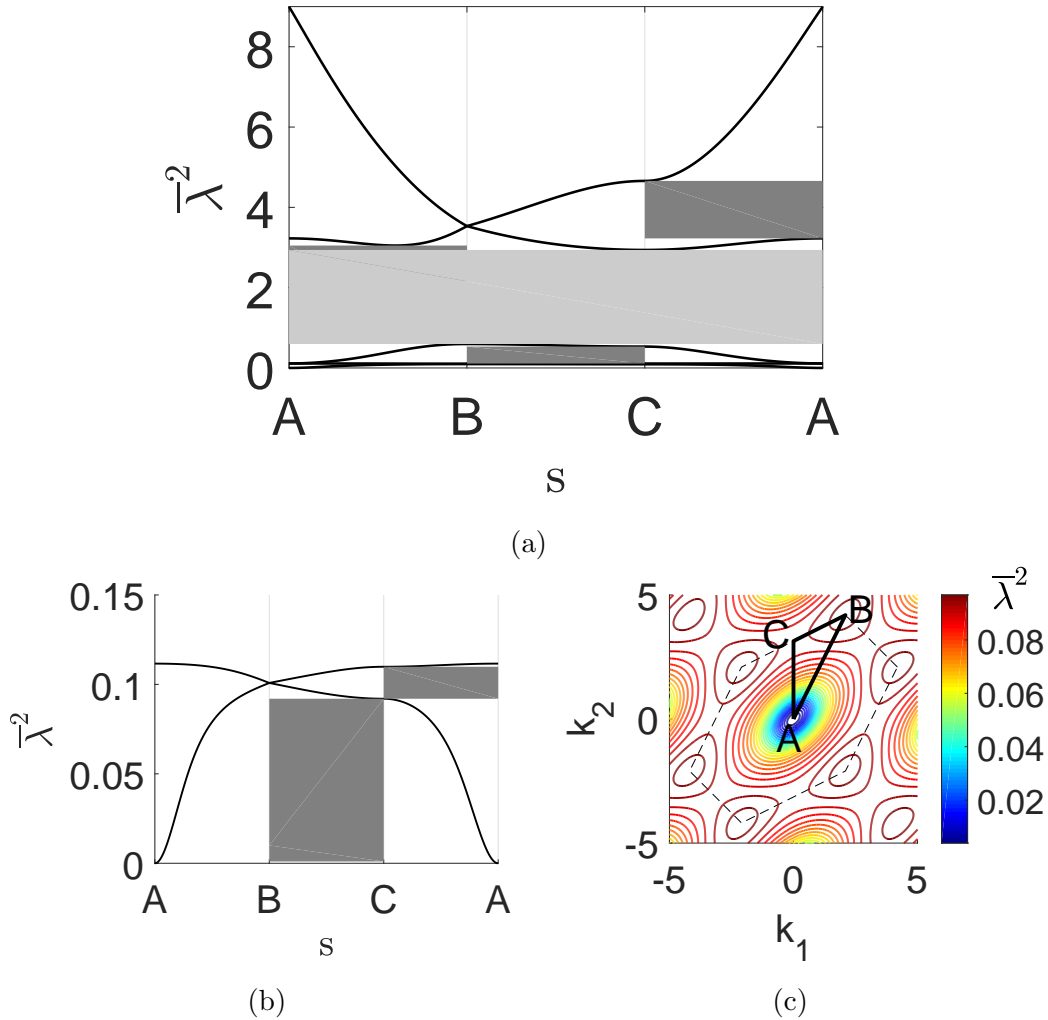


Figure 7: Triangular configuration: (a) Band structure: 1st to 5th modes, (b) Detail of band structure: 1st and 2nd modes, (c) 1st mode dispersion surface presented in the contour plot.

Changing the arrangement of beams from square to triangular configuration results in a single complete band gap (3rd-4th modes) (see Fig. 7a), but with a larger width. Several partial band gaps appear through the different edges of the irreducible zone. Moreover, this configuration features veering of the 1st and 2nd modes (Fig. 7b) and 4th and 5th modes (Fig. 7a), whose dispersion surfaces approach each other and then suddenly diverge. There-

1  
2  
3  
4  
5  
6  
7  
8  
9  
10  
11  
12  
13  
14  
15  
16  
17  
18  
19  
20  
21  
22  
23  
24  
25  
26  
27  
28  
29  
30  
31  
32  
33  
34  
35  
36  
37  
38  
39  
40  
41  
42  
43  
44  
45  
46  
47  
48  
49  
50  
51  
52  
53  
54  
55  
56  
57  
58  
59  
60  
61  
62  
63  
64  
65

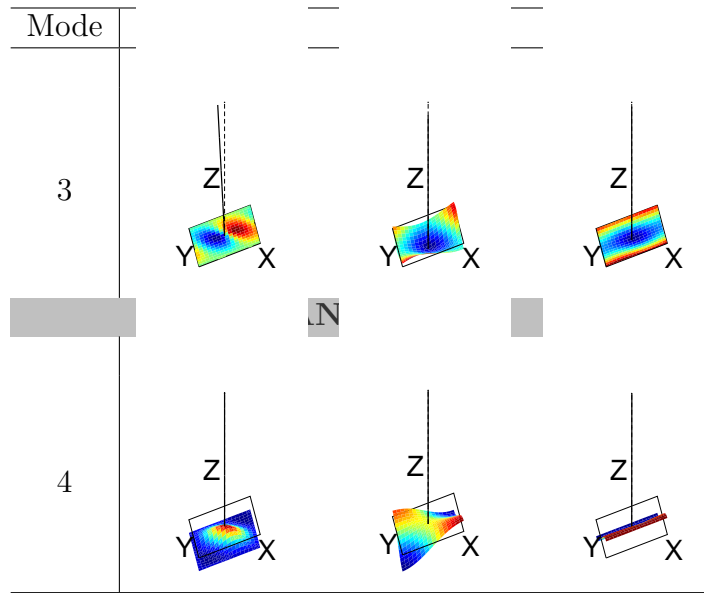


Table 4: Triangular configuration: Shapes of modes surrounding the band gap.

fore, a slight change in the excitation frequency of the lattice in the transition zone leads to a sudden change in the wave-propagation mode.

The shapes of the modes surrounding the band gap at points A, B, and C of the Brillouin zone are presented in Table 4. Table 5 summarizes the predominant problem type for each mode, where equivalent modes can be identified in the different problem types. As in the square configuration, it can be observed that the first modes are related to problem Type 2 (Fig. 9b).

The dispersion surface of the first mode (Fig. 7c) shows elliptical iso-

Mode	A	B	C
1	Common	Type 2	Type 2
2	Type 2	Type 2	Type 2
3	Type 2	Type 1	Type 1
<b>BAND GAP</b>			
4	Type 1	Type 2	Type 2
5	Common	Type 2	Type 1

Table 5: Triangular configuration: Summary of the predominant problem types.

1  
2  
3  
4  
5  
6  
7  
8  
9  
10  
11  
12  
13  
14  
15  
16  
17  
18  
19  
20  
21  
22  
23  
24  
25  
26  
27  
28  
29  
30  
31  
32  
33  
34  
35  
36  
37  
38  
39  
40  
41  
42  
43  
44  
45  
46  
47  
48  
49  
50  
51  
52  
53  
54  
55  
56  
57  
58  
59  
60  
61  
62  
63  
64  
65

frequency curves in the  $k_1 - k_2$  space (circular in the  $k_x - k_y$  space) in the low wave number regime, denoting isotropic wave propagation. Unlike the square configuration, iso-frequency curves bend into an hexagonal shape as the wave number increases, while the dispersion surface becomes virtually flat as indicated by the lower density of curves towards the edges of the Brillouin zone. In this region, straight sections of iso-frequency curves entail a strong directionality of the energy flux along the six main directions of the lattices. Likewise, the six-fold symmetry of the lattice with triangular configuration is apparent in Fig. 7c.

### 5.1.3. Hexagonal configuration

The band structure is presented in Fig. 8a along the edges of the irreducible zone Fig. 5b. A detail of the first modes is presented in Fig. 8b.

1  
2  
3  
4  
5  
6  
7  
8  
9  
10  
11  
12  
13  
14  
15  
16  
17  
18  
19  
20  
21  
22  
23  
24  
25  
26  
27  
28  
29  
30  
31  
32  
33  
34  
35  
36  
37  
38  
39  
40  
41  
42  
43  
44  
45  
46  
47  
48  
49  
50  
51  
52  
53  
54  
55  
56  
57  
58  
59  
60  
61  
62  
63  
64  
65

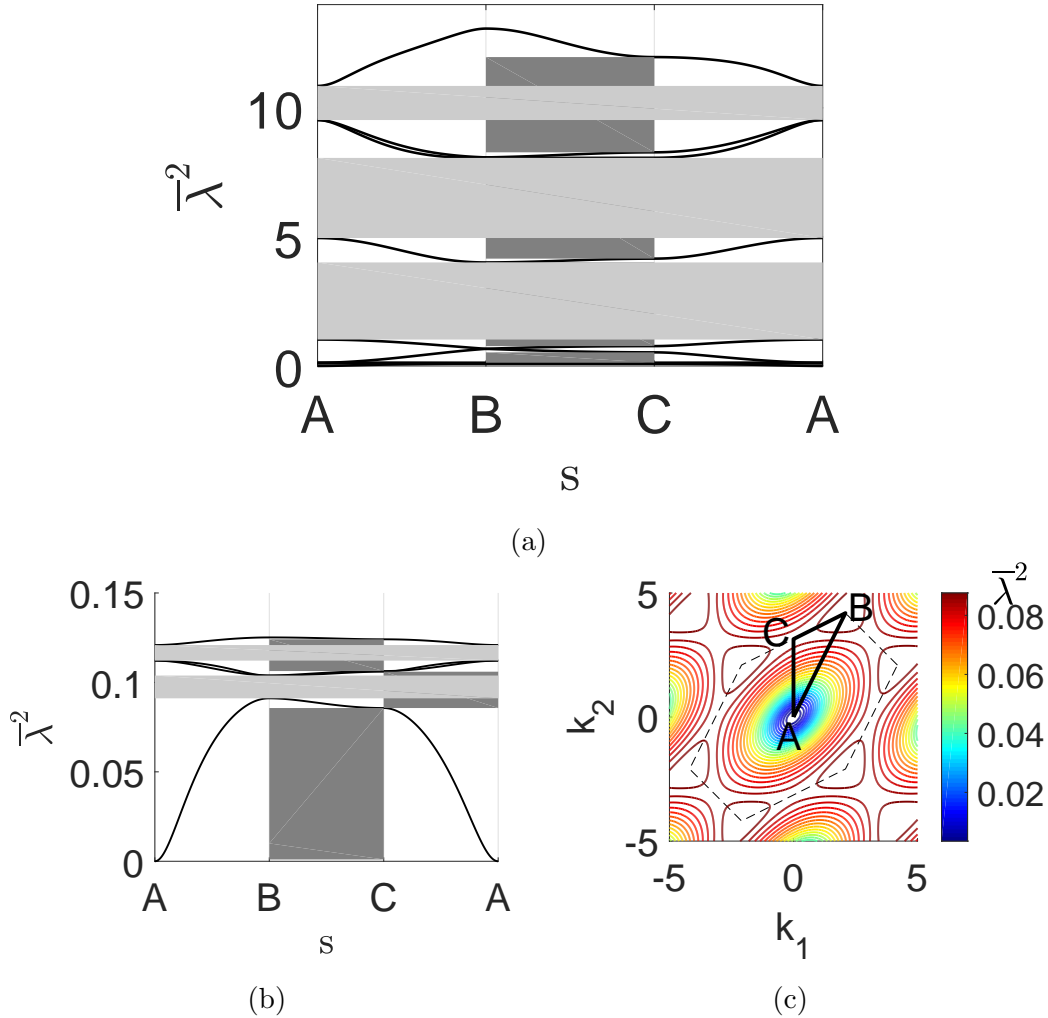


Figure 8: Hexagonal configuration: (a) Band structure: 1st to 10th modes, (b) Detail of band structure: 1st and 4th modes, (c) 1st mode dispersion surface presented in the contour plot.

The change in the dispersion structure is also evident when moving to the hexagonal configuration, which presents two narrow complete stop bands in the lower-frequency regime (1st-2nd and 3rd-4th modes) and three wide complete stop bands in the higher-frequency regime (6th-7th, 7th-8th, and 9th-10th modes). Several partial band gaps appear mainly through the edge  $BC$  of the irreducible zone. The hexagonal configuration likewise shows

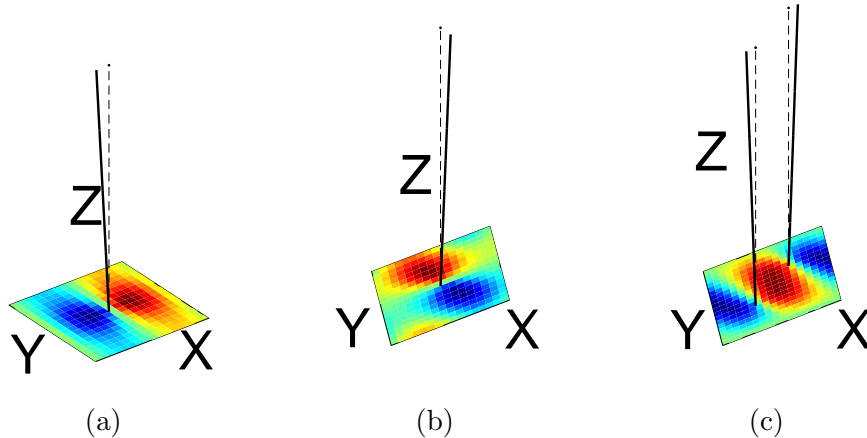


Figure 9: Example of mode shape in problem Type 2 (Mode 2, Point A): (a) Square configuration, (b) Triangular configuration, (c) Hexagonal configuration.

veering of the 5th and 6th modes (Fig. 8a).

The shapes of the modes surrounding the band gaps at points A, B, and C of the Brillouin zone are presented in Table 6, while Table 7 summarizes the predominant problem type for each mode. Equivalent modes to those of the different problem types have also been identified (Fig. 9c). However, in contrast to the previous cases, this equivalence has not been completely accomplished for the higher modes. The existence of two beams in the cell increases the coupling between the two problem types.

The dispersion surface of the first mode is presented in Fig. 8c. As in the triangular configuration, the hexagonal one presents isotropic wave propagation in the low wavenumber regime. Towards the edges of the Brillouin zone, straight sections of iso-frequency curves entail a strong directionality of the energy flux along the six principal directions of the lattices. The six-fold symmetry of the lattice is apparent in Fig. 8c.

#### 5.1.4. Remarks

An important difference in the behavior of a plate with resonators (mass-spring system) becomes evident from the results presented in Figs. 6a to 8a. As Sugino et al. [10] pointed out, a plate with an arrangement of resonators (masses and springs vibrating perpendicularly to the plate) generates a band gap at the resonant frequency of the resonator. For the case of a plate with an arrangement of beams, this rule cannot be generalized. As reflected in the above-mentioned figures, for the mechanical properties selected in the anal-

1  
2  
3  
4  
5  
6  
7  
8  
9  
10  
11  
12  
13  
14  
15  
16  
17  
18  
19  
20  
21  
22  
23  
24  
25  
26  
27  
28  
29  
30  
31  
32  
33  
34  
35  
36  
37  
38  
39  
40  
41  
42  
43  
44  
45  
46  
47  
48  
49  
50  
51  
52  
53  
54  
55  
56  
57  
58  
59  
60  
61  
62  
63  
64  
65

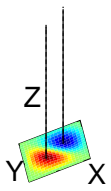
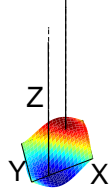
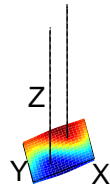
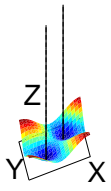
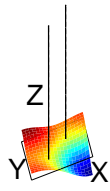
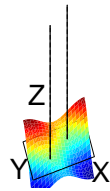
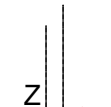
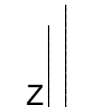
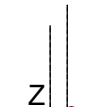
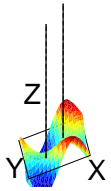
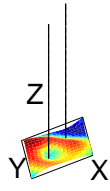
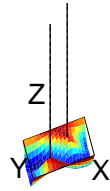
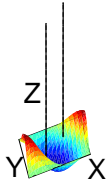
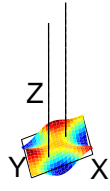
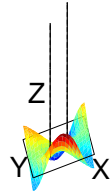
Mode	—	—	
6			
	LN		
7			
	LN		
8			
	LN		
9			
	LN		
10			

Table 6: Hexagonal configuration: Shapes of modes surrounding the band gaps.

1  
2  
3  
4  
5  
6  
7  
8  
9  
10  
11  
12  
13  
14  
15  
16  
17  
18  
19  
20  
21  
22  
23  
24  
25  
26  
27  
28  
29  
30  
31  
32  
33  
34  
35  
36  
37  
38  
39  
40  
41  
42  
43  
44  
45  
46  
47  
48  
49  
50  
51  
52  
53  
54  
55  
56  
57  
58  
59  
60  
61  
62  
63  
64  
65

Mode	A	B	C
1	Common	Type 2	Type 2
<b>BAND GAP</b>			
2	Type 2	Type 2	Type 2
3	Type 2	Type 2	Type 2
<b>BAND GAP</b>			
4	Type 2	Type 2	Type 2
5	Type 2	Type 2	Type 2
6	Type 1	Not present	Not present
<b>BAND GAP</b>			
7	Type 1	Type 2	Not present
<b>BAND GAP</b>			
8	Type 2	Not present	Type 2
9	Type 2	Not present	Not present
<b>BAND GAP</b>			
10	Type 2	Type 2	Not present

Table 7: Hexagonal configuration: Summary of the predominant problem types.

ysis, a band gap including the first resonant frequency of a clamped beam ( $\bar{\lambda}^2=3.51$ ) is found only for the square and hexagonal configurations but not for the triangular one. Moreover, for other sets of mechanical properties, the resonant frequency of the clamped beam is no longer included in the band gap, even for square and hexagonal configurations. The dynamic response of this system is more complex than that of the system studied in [10], since the former is influenced by the inertia of the beam in the out-of-plane direction and by the transverse vibration of the beam. This interaction can be detected in the vibration modes.

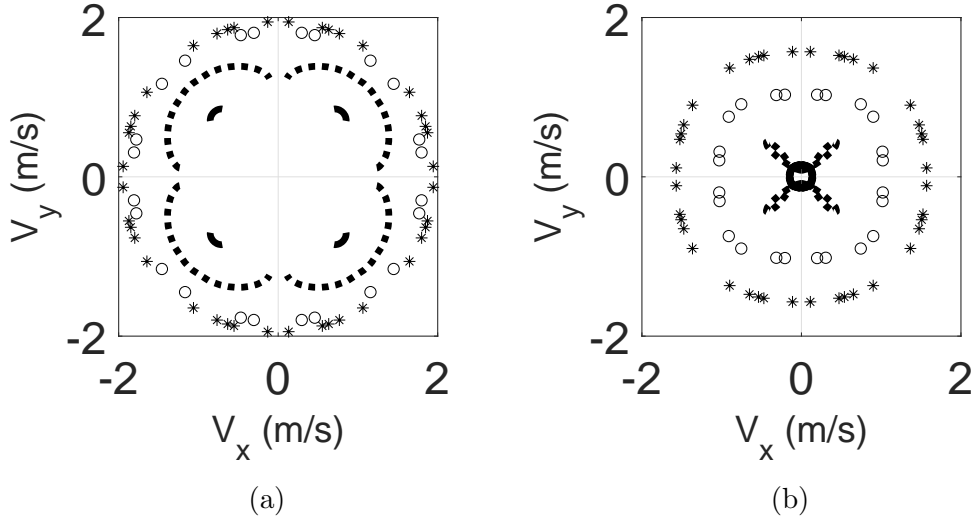
### 5.2. Phase and group velocities

The band structure provides a tidy representation of the dispersive features and forbidden frequencies of the lattice. In a complementary way, the analysis of phase and group velocities helps identify anisotropic behavior and preferred directions of energy flow. Both diagrams provide insight for effective insulation or focusing of the mechanical energy [22].

The phase and group velocities are shown in Figs. 10 to 12 for the three configurations. The results correspond to the first vibration mode of each

1  
2  
3  
4  
5  
6  
7  
8  
9 configuration. Both phase and group velocities are presented in coordinates  
10  $\{x, y\}$ , for different frequency values.

11  
12 The three lattices behave as isotropic solids at low frequencies, as antici-  
13 pated from the circular shape of iso-frequency curves for low wave numbers.  
14 As the frequency increases, the anisotropy becomes manifest by the angu-  
15 lar variation of both phase and group velocity moduli. The curves present  
16 four folds –for square configuration, Fig. 10– or six folds –for triangular and  
17 hexagonal configurations, Figs. 11 and 12–, in accordance with the sym-  
18 metries in the arrangements of the beams. As observed in Figs. 10b and  
19 12b the three configurations can create caustics (loops in the group velocity  
20 plot), which are related to powerful energy focusing for propagating wave  
21 trains [22]. This feature most commonly appears in anisotropic media.  
22  
23  
24  
25



44 Figure 10: Square configuration: (a) Phase velocity, (b) Group velocity. 1st mode at  
45 various frequencies: ‘\*’  $\omega = 0.65 \cdot \omega_{max}$ , ‘o’  $\omega = 0.75 \cdot \omega_{max}$ , ‘dashed line’  $\omega = 0.88 \cdot \omega_{max}$ ,  
46 ‘solid line’  $\omega = 0.99 \cdot \omega_{max}$ .  $\omega_{max}$  = maximum value of  $\omega$  for the 1st mode.  
47  
48  
49  
50  
51  
52  
53  
54  
55  
56  
57  
58  
59  
60  
61  
62  
63  
64  
65



1  
2  
3  
4  
5  
6  
7  
8  
9  
10  
11  
12  
13  
14  
15  
16  
17  
18  
19  
20  
21  
22  
23  
24  
25  
26  
27  
28  
29  
30  
31  
32  
33  
34  
35  
36  
37  
38  
39  
40  
41  
42  
43  
44  
45  
46  
47  
48  
49  
50  
51  
52  
53  
54  
55  
56  
57  
58  
59  
60  
61  
62  
63  
64  
65

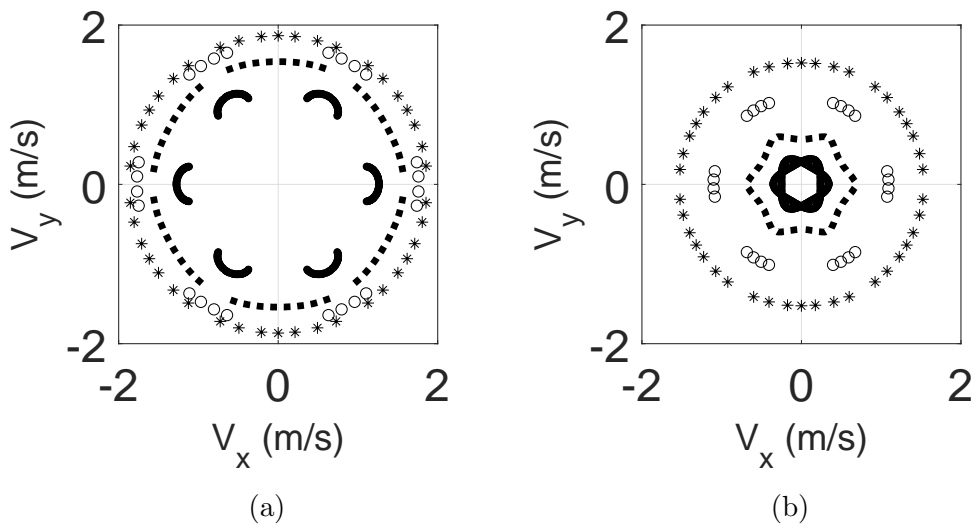


Figure 11: Triangular configuration: (a) Phase velocity, (b) Group velocity. 1st mode at various frequencies: ‘\*’  $\omega = 0.65 \cdot \omega_{max}$ , ‘o’  $\omega = 0.75 \cdot \omega_{max}$ , ‘dashed line’  $\omega = 0.85 \cdot \omega_{max}$ , ‘solid line’  $\omega = 0.95 \cdot \omega_{max}$ .  $\omega_{max}$  = maximum value of  $\omega$  for the 1st mode.

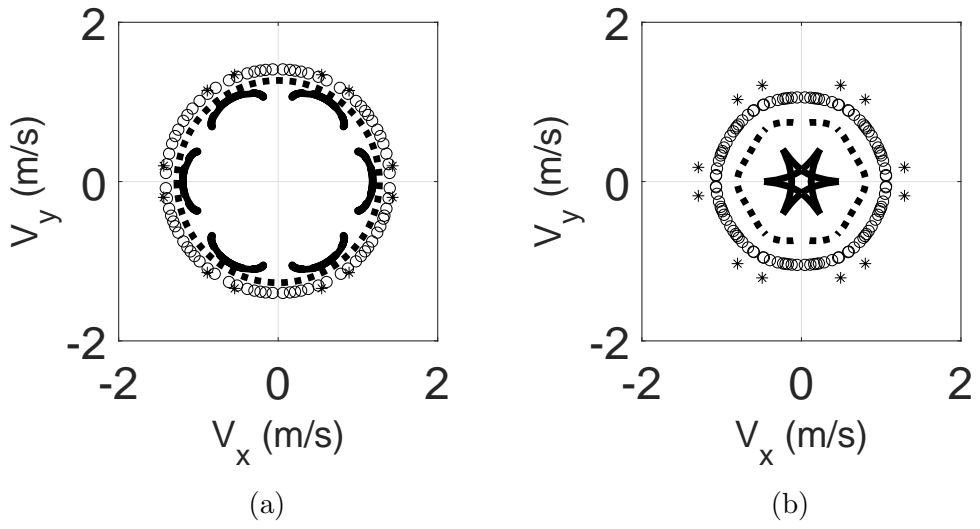


Figure 12: Hexagonal configuration: (a) Phase velocity, (b) Group velocity. 1st mode at various frequencies: ‘\*’  $\omega = 0.65 \cdot \omega_{max}$ , ‘o’  $\omega = 0.75 \cdot \omega_{max}$ , ‘dashed line’  $\omega = 0.85 \cdot \omega_{max}$ , ‘solid line’  $\omega = 0.95 \cdot \omega_{max}$ .  $\omega_{max}$  = maximum value of  $\omega$  for the 1st mode.

## 6. Effect of dimensionless parameters in the band structure

For the three configurations, the change in the mean value and width of the first band gap from Figs. 6a to 8a was analyzed for different values of the dimensionless groups. Assuming that this band gap is located between modes  $i$  and  $i + 1$ , we calculate its dimensionless mean value and width as

$$\bar{\lambda}_{\text{mean}}^{-2} = \frac{\omega_{i+1}^{\min} + \omega_i^{\max}}{2\omega_0}, \quad \bar{\lambda}_{\text{width}}^{-2} = \frac{\omega_{i+1}^{\min} - \omega_i^{\max}}{\omega_0}, \quad (13)$$

where  $\omega_{i+1}^{\min}$  and  $\omega_i^{\max}$  are the minimum and maximum frequencies corresponding to modes  $i + 1$  and  $i$ , respectively, and  $\omega_0 = \sqrt{\frac{C}{\rho_* l^4}}$ .

The evolution of the band gaps for values of the dimensionless parameters within the intervals  $A_1 \in [0.45, 0.85]$ ,  $A_2 \in (0, 3]$ , and  $A_3 \in [673, 973]$ , which include the reference values  $A_1^*$ ,  $A_2^*$ ,  $A_3^*$  quoted in previous sections, is presented in Figs. 13 to 15. Thus, the whole set of geometrical and mechanical characteristics is involved in the analysis. Notice that the results presented and the following analyses are limited to the intervals considered and to the first band gap.

As can be seen in Figs. 13 to 15, the influence of the dimensionless parameters is similar in the three configurations, with  $A_2$  emerging as the most influencing dimensionless group in terms of both location and width of the band gap. The location of the band gap monotonically increases as  $A_2$  decreases. Although  $A_2$  enables us to easily adjust the band gap at the required frequency, as it tends to zero,  $A_3$  becomes relevant on the width value (see Fig. 13b). It can be also seen that the width approaches to zero as  $A_2 \rightarrow 0$  or as  $1/A_2 \rightarrow 0$ . Within these two limits, the band-gap width reaches a maximum that can be exploited for design purposes.

These results lead to the idea that for  $a \ll l$  ( $A_2 \rightarrow 0$ ) and  $a \gg l$  ( $1/A_2 \rightarrow 0$ ) the lattice structures lack the ability to stop wave propagation. In the first case, the beams can be assumed to be continuously distributed over the plate area, thus becoming a dense lattice. It bears remarking that within the continuum limit  $A_2 \rightarrow 0$ , Eq. (3) leads to a dispersion relation without band gaps, as stated by Eremeyev *et al.* [9]. In the second case, the beams can be assumed to be sufficiently disperse that the effect of the beams become negligible in the wave propagation behavior of the lattice, thus resembling a continuous plate, which lacks of band gaps. This can be clearly shown by comparing the dispersion relation of the Kirchoff plate

1  
2  
3  
4  
5  
6  
7  
8  
9  
10  
11  
12  
13  
14  
15  
16  
17  
18  
19  
20  
21  
22  
23  
24  
25  
26  
27  
28  
29  
30  
31  
32  
33  
34  
35  
36  
37  
38  
39  
40  
41  
42  
43  
44  
45  
46  
47  
48  
49  
50  
51  
52  
53  
54  
55  
56  
57  
58  
59  
60  
61  
62  
63  
64  
65

$$\omega(k_x, k_y) = \sqrt{\frac{D}{\rho} (k_x^4 + 2k_x^2 k_y^2 + k_y^4)} \quad (14)$$

derived by imposing a plane-wave solution  $W(x, y, t) = A_0 e^{i(k_x x + k_y y - \omega t)}$  to the governing equation  $D\Delta\Delta W + \rho\partial^2 W/\partial t^2 = 0$ , with the dispersion relation corresponding to the first mode of a primitive unit cell with constant size  $a$  and decreasing values of the beam length  $l$ . Fig. 16 shows this comparison for the lattice with the square configuration along the edges of the triangle defined in Fig. 5a (a similar trend can be found for any of the configurations). As expected, the dispersion relation of the lattice converges with that of the continuum Kirchoff plate as  $l$  decreases ( $A_2$  increases).

Unlike other works, where the evolution of the band gap is analyzed for a single physical parameter, an alternative and more complete analysis of the parameters is developed here. In this section the mean value and width of the first band gap is presented for different values of the dimensionless groups ( $A_1, A_2, A_3$ ). Figs. 13 to 15 show the change in the characteristics of the band gaps when a nondimensional parameter is modified while keeping the other two constant, no matter which physical parameters are modified. In particular, given a requirement of a band gap at a certain frequency with a specific width, the figure gives the corresponding value of  $A_1, A_2$ , and  $A_3$ . Then, this set of values can be determined by an infinite combination of the physical parameters.

1  
2  
3  
4  
5  
6  
7  
8  
9  
10  
11  
12  
13  
14  
15  
16  
17  
18  
19  
20  
21  
22  
23  
24  
25  
26  
27  
28  
29  
30  
31  
32  
33  
34  
35  
36  
37  
38  
39  
40  
41  
42  
43  
44  
45  
46  
47  
48  
49  
50  
51  
52  
53  
54  
55  
56  
57  
58  
59  
60  
61  
62  
63  
64  
65

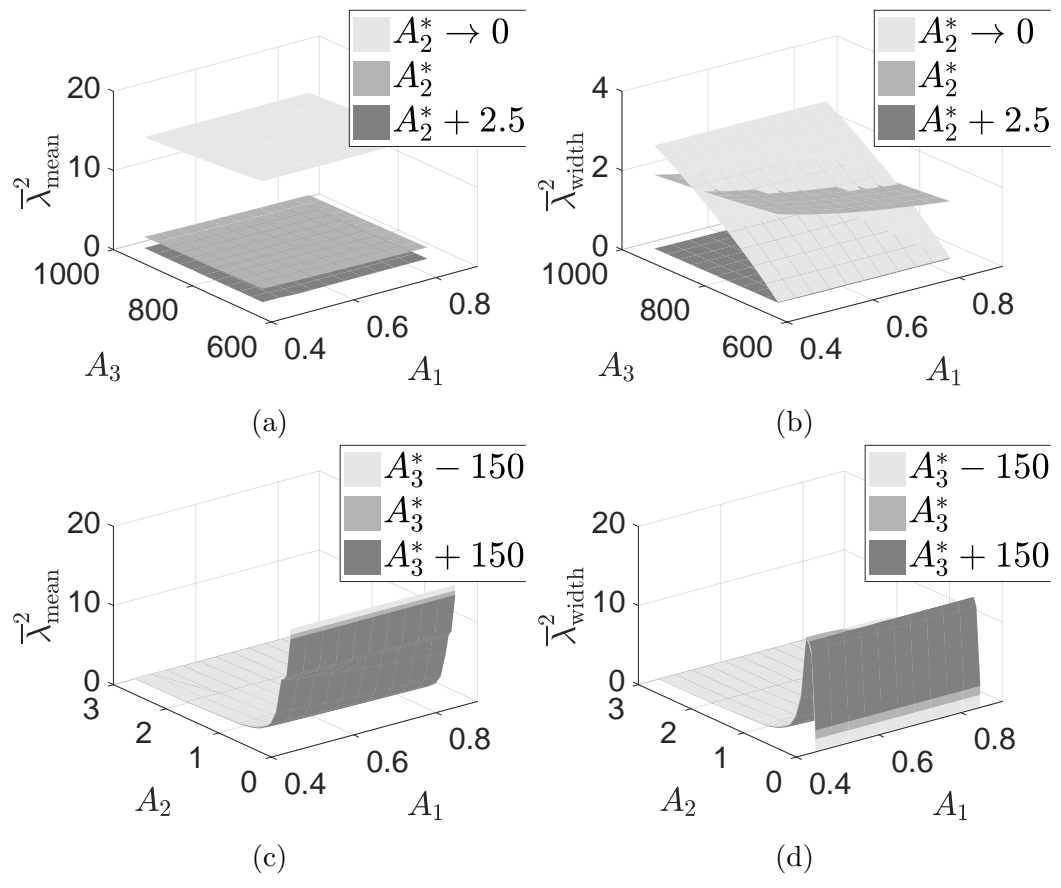


Figure 13: Square configuration: Influence of dimensionless groups on location and bandwidth.

1  
2  
3  
4  
5  
6  
7  
8  
9  
10  
11  
12  
13  
14  
15  
16  
17  
18  
19  
20  
21  
22  
23  
24  
25  
26  
27  
28  
29  
30  
31  
32  
33  
34  
35  
36  
37  
38  
39  
40  
41  
42  
43  
44  
45  
46  
47  
48  
49  
50  
51  
52  
53  
54  
55  
56  
57  
58  
59  
60  
61  
62  
63  
64  
65

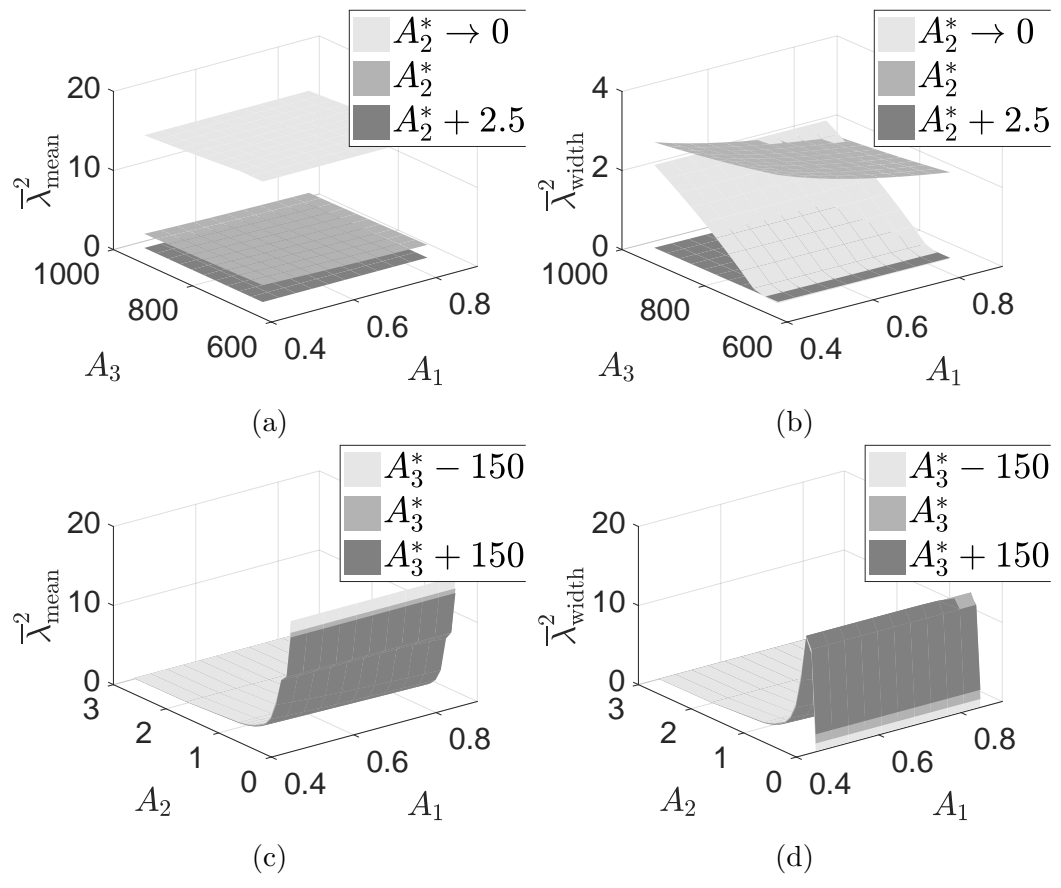


Figure 14: Triangular configuration: Influence of dimensionless groups on location and bandwidth.

1  
2  
3  
4  
5  
6  
7  
8  
9  
10  
11  
12  
13  
14  
15  
16  
17  
18  
19  
20  
21  
22  
23  
24  
25  
26  
27  
28  
29  
30  
31  
32  
33  
34  
35  
36  
37  
38  
39  
40  
41  
42  
43  
44  
45  
46  
47  
48  
49  
50  
51  
52  
53  
54  
55  
56  
57  
58  
59  
60  
61  
62  
63  
64  
65

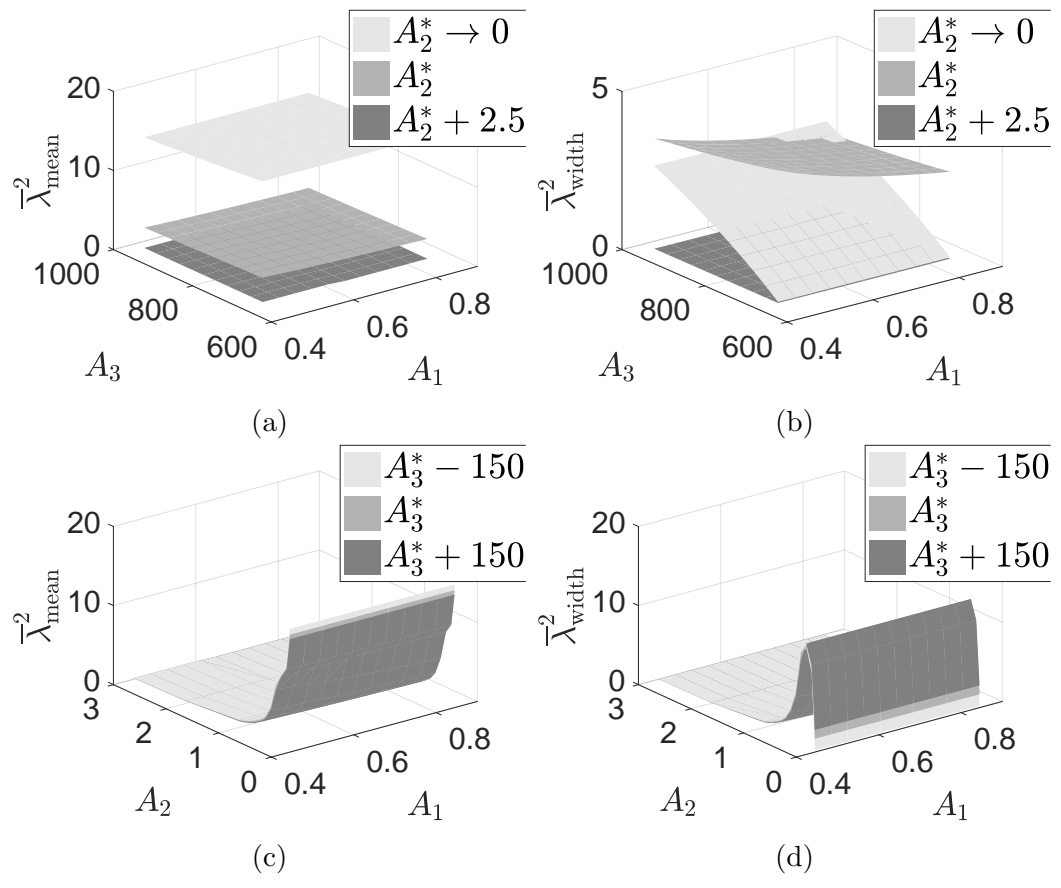


Figure 15: Hexagonal configuration: Influence of dimensionless groups on location and bandwidth.

1  
2  
3  
4  
5  
6  
7  
8  
9  
10  
11  
12  
13  
14  
15  
16  
17  
18  
19  
20  
21  
22  
23  
24  
25  
26  
27  
28  
29  
30  
31  
32  
33  
34  
35  
36  
37  
38  
39  
40  
41  
42  
43  
44  
45  
46  
47  
48  
49  
50  
51  
52  
53  
54  
55  
56  
57  
58  
59  
60  
61  
62  
63  
64  
65

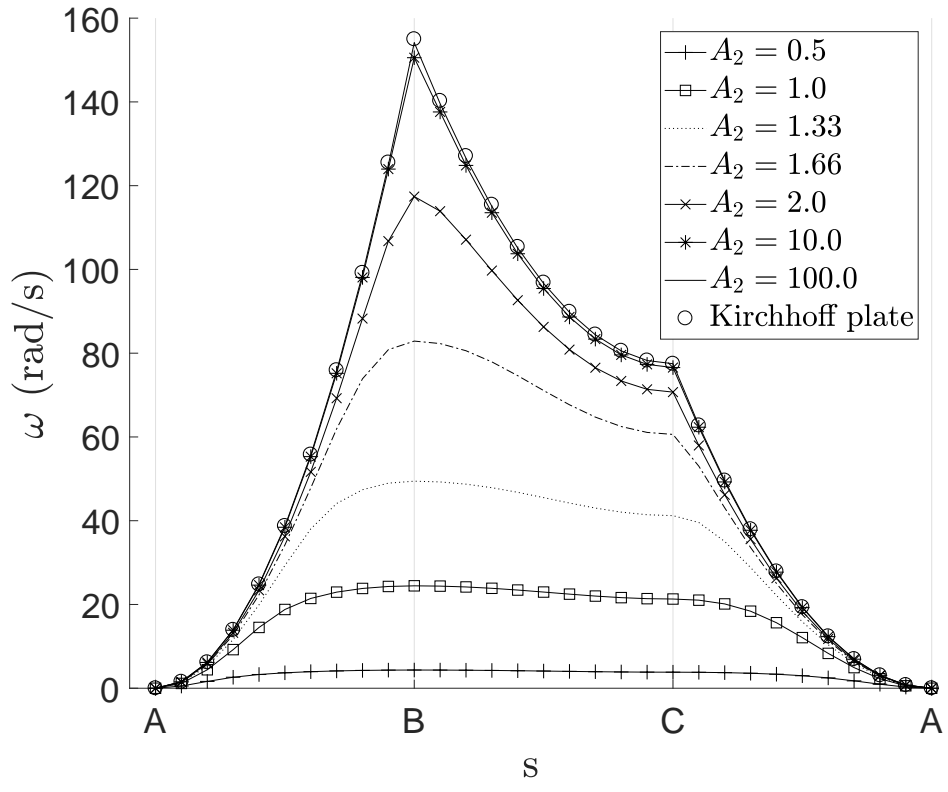


Figure 16: Dispersion curve of a Kirchhoff plate and 1st modes of different values of  $l$  for a lattice with square configuration.

### 7. Conclusions

This work analyzes the band structures and directivity of wave propagation in systems composed of a periodic arrangement of vertical beams rigidly joined to a thin plate.

Three different configurations for the distribution of the beams were analyzed: square, triangular, and hexagonal. Due to the periodicity of the system, it can be treated as a lattice structure and thus the main features of the wave propagation have been determined using Bloch's methodology combined with numerical procedures based on the Finite Element Method.

The main findings of the work are:

- 1  
2  
3  
4  
5  
6  
7  
8  
9  
10  
11  
12  
13  
14  
15  
16  
17  
18  
19  
20  
21  
22  
23  
24  
25  
26  
27  
28  
29  
30  
31  
32
- The lattice composed of a periodic hexagonal arrangement of slender beams clamped on a plate presents three wide band gaps, this being the best system in terms of the insulation behavior at low frequencies.
  - The velocity plots have shown the shift from isotropic behavior to anisotropic one depending on the excitation frequency, as well as the evidence of caustics for the three configurations studied.
  - A dimensional analysis reveals three independent dimensionless groups of variables governing the dynamic response of the lattice. The dimensionless groups relate the plate to beam density, the cell dimension to beam length, and the beam to plate stiffness, respectively.
  - A parametric study on the effect of the dimensionless groups on the position and width of the first band gap has been conducted. The same trends have been found in the three configurations considered. For the range of values presented, the ratio of cell dimension to beam length ( $A_2$ ) is the most affected dimensionless group.

33  
34  
35  
36  
37  
38

This work has evidenced the existence of band gaps for a thin plate with periodic arrangements of slender beams, showing the ability of these structures to stop wave propagation for certain frequencies. The study of the dimensionless groups provides valuable insights for the design of these kinds of systems with the required features.

### 39 40 41 42 43 44 45

### Acknowledgments

This work was supported by the Ministerio de Economía y Competitividad de España (grant number DPI2014-57989-P).

### 46 47 48 49 50 51 52 53

### References

- 54  
55  
56  
57  
58  
59  
60  
61  
62  
63  
64  
65
- [1] G. Mor, O. Varghese, M. Paulose, K. Shankar, C. Grimes, A review on highly ordered, vertically oriented TiO<sub>2</sub> nanotube arrays: Fabrication, material properties, and solar energy applications, *Solar Energy Materials and Solar Cells* 90 (14) (2006) 2011 – 2075.
  - [2] V. Vayssieres, K. Keis, A. Hagfeldt, S. Lindquist, Three-Dimensional Array of Highly Oriented Crystalline ZnO Microtubes, *Chemistry of Materials* 13 (12) (2001) 4395–4398.



- 1  
2  
3  
4  
5  
6  
7  
8  
9  
10  
11  
12  
13  
14  
15  
16  
17  
18  
19  
20  
21  
22  
23  
24  
25  
26  
27  
28  
29  
30  
31  
32  
33  
34  
35  
36  
37  
38  
39  
40  
41  
42  
43  
44  
45  
46  
47  
48  
49  
50  
51  
52  
53  
54  
55  
56  
57  
58  
59  
60  
61  
62  
63  
64  
65
- [3] M. Collet, M. Ouisse, M. Ruzzene, M. Ichchou, Floquet–Bloch decomposition for the computation of dispersion of two-dimensional periodic, damped mechanical systems, *International Journal of Solids and Structures* 48 (20) (2011) 2837 – 2848.
  - [4] W. Tsung-Tsong, H. Zi-Gui, T. Tzu-Chin, W. Tzung-Chen, Evidence of complete band gap and resonances in a plate with periodic stubbed surface, *Applied Physics Letters* 93 (11) (2008) 111902.
  - [5] W. Tzung-Chen, W. Tsung-Tsong, H. Jin-Chen, Waveguiding and frequency selection of Lamb waves in a plate with a periodic stubbed surface, *Physical Review B* 79 (2009) 104306.
  - [6] H. Zi-Gui, Analysis of frequency band gaps in a plate with periodic stubbed surface, in: *ASME 2010 International Mechanical Engineering Congress and Exposition*, American Society of Mechanical Engineers, Vancouver, Canada, 2010, pp. 409–412.
  - [7] Y. Tanaka, S. Tamura, Acoustic stop bands of surface and bulk modes in two-dimensional phononic lattices consisting of aluminum and a polymer, *Physical Review B* 60 (1999) 13294–13297.
  - [8] V. Eremeyev, E. Ivanova, N. Morozov, A. Soloviev, Method of determining the eigenfrequencies of an ordered system of nanoobjects, *Technical Physics* 52 (1) (2007) 1–6.
  - [9] V. Eremeyev, E. Ivanova, D. Indeitsev, Wave processes in nanostructures formed by nanotube arrays or nanosize crystals, *Journal of Applied Mechanics and Technical Physics* 51 (4) (2010) 569–578.
  - [10] C. Sugino, Y. Xia, S. Leadenham, M. Ruzzene, A. Erturk, A general theory for bandgap estimation in locally resonant metastructures, *Journal of Sound and Vibration* 406 (2017) 104 – 123.
  - [11] O. Sigmund, J. Jensen, Topology optimization of phononic band gap materials and structures, in: *Proc. 5th World Congress on Computational Mechanics*, Vienna, Austria, 2002.
  - [12] O. Sigmund, J. Jensen, Systematic design of phononic band-gap materials and structures by topology optimization, *Philosophical Transactions*

1  
2  
3  
4  
5  
6  
7  
8  
9 of the Royal Society A: Mathematical, Physical and Engineering Sci-  
10 ences 361 (2003) 1001–1019.  
11

- 12 [13] P. Atkins, R. Friedman, *Molecular Quantum Mechanics*, Oxford, Eng-  
13 land, 2005.  
14  
15 [14] J. Joannopoulos, S. Johnson, J. Winn, R. Meade, *Photonic crystals:*  
16 *molding the flow of light*, Princeton university press, 2011.  
17  
18 [15] S. Gonella, M. Ruzzene, Analysis of in-plane wave propagation in hexag-  
19 onal and re-entrant lattices, *Journal of Sound and Vibration* 312 (1)  
20 (2008) 125–139.  
21  
22 [16] A. Phani, J. Woodhouse, N. Fleck, Wave propagation in two-dimensional  
23 periodic lattices, *The Journal of the Acoustical Society of America*  
24 119 (4) (2006) 1995–2005.  
25  
26 [17] B. Tie, B. Tian, D. Aubry, Theoretical and numerical investigation of  
27 HF elastic wave propagation in two-dimensional periodic beam lattices,  
28 *Acta Mechanica Sinica* 29 (6) (2013) 783–798.  
29  
30 [18] W. Liu, J. Chen, X. Su, Local resonance phononic band gaps in modified  
31 two-dimensional lattice materials, *Acta Mechanica Sinica*.  
32  
33 [19] C. Kittel, *Elementary solid state physics: a short course*, Wiley, 1962.  
34  
35 [20] *Structural analysis with the finite element method. Linear statics: vol-*  
36 *ume 2: beams, plates and shells*, Springer Science & Business Media,  
37 Barcelona, Spain, 2013.  
38  
39 [21] F. Farzbod, M. Leamy, The treatment of forces in Bloch analysis, *Jour-*  
40 *nal of Sound and Vibration* 325 (3) (2009) 545 – 551.  
41  
42 [22] A. Spadoni, M. Ruzzene, S. Gonella, F. Scarpa, Phononic properties of  
43 hexagonal chiral lattices, *Wave Motion* 46 (7) (2009) 435 – 450.  
44  
45  
46  
47  
48  
49  
50  
51  
52  
53  
54  
55  
56  
57  
58  
59  
60  
61  
62  
63  
64  
65

1  
2  
3  
4  
5  
6  
7  
8

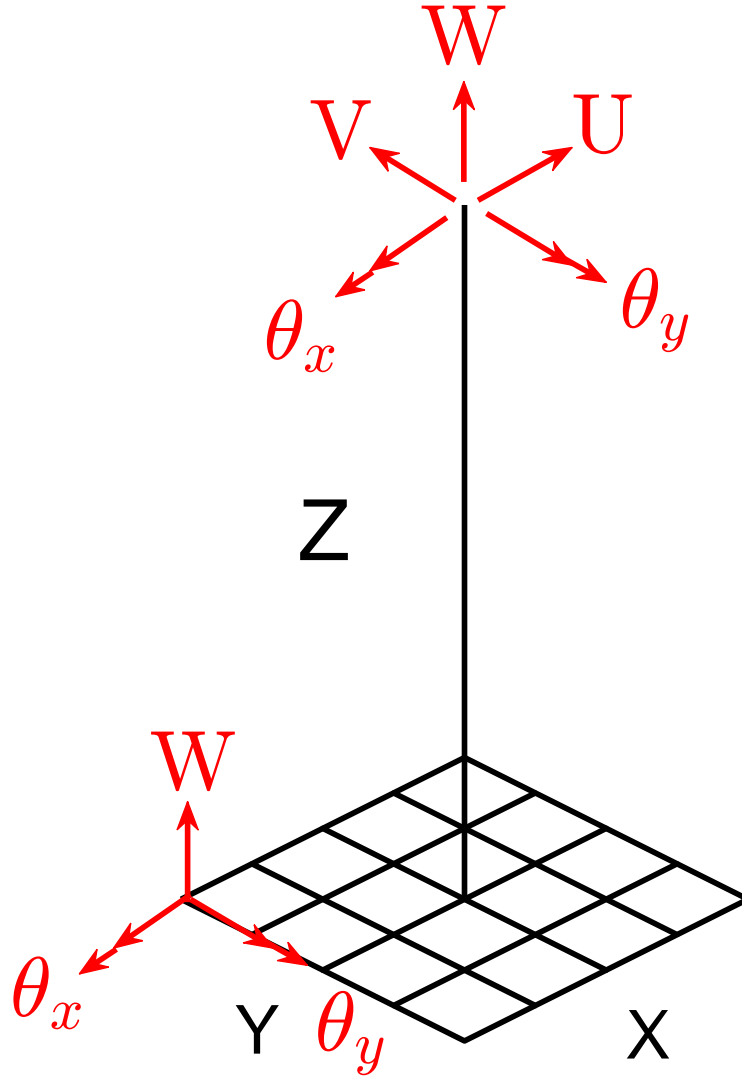
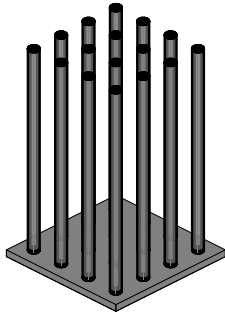


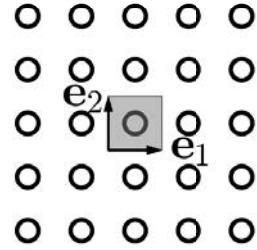
Figure 1: Scheme of a lattice structure with the degrees of freedom considered.

49  
50  
51  
52  
53  
54  
55  
56  
57  
58  
59  
60  
61  
62  
63  
64  
65

1  
2  
3  
4  
5  
6  
7  
8  
9  
10  
11  
12  
13  
14  
15  
16  
17  
18  
19  
20  
21  
22  
23  
24  
25  
26  
27  
28  
29  
30  
31  
32  
33  
34  
35  
36  
37  
38  
39  
40  
41  
42  
43  
44  
45  
46  
47  
48  
49  
50  
51  
52  
53  
54  
55  
56  
57  
58  
59  
60  
61  
62  
63  
64  
65



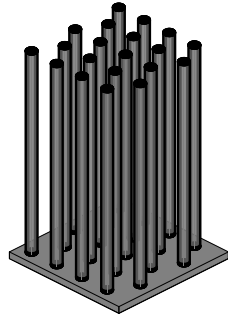
(a)



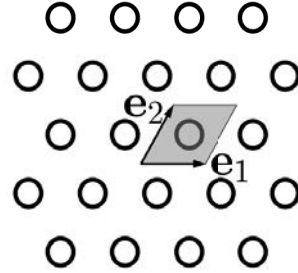
(b)

Figure 2: Lattice structure with square configuration: (a) Isometric view, (b) Top view with primitive unit cell.

1  
2  
3  
4  
5  
6  
7  
8  
9  
10  
11  
12  
13  
14  
15  
16  
17  
18  
19  
20  
21  
22  
23  
24  
25  
26  
27  
28  
29  
30  
31  
32  
33  
34  
35  
36  
37  
38  
39  
40  
41  
42  
43  
44  
45  
46  
47  
48  
49  
50  
51  
52  
53  
54  
55  
56  
57  
58  
59  
60  
61  
62  
63  
64  
65



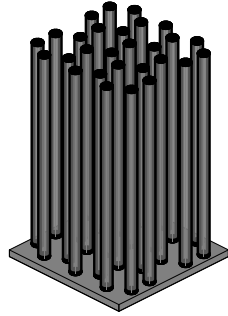
(a)



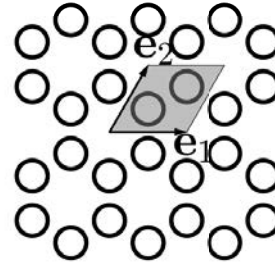
(b)

Figure 3: Lattice structure with triangular configuration: (a) Isometric view, (b) Top view with primitive unit cell.

1  
2  
3  
4  
5  
6  
7  
8  
9  
10  
11  
12  
13  
14  
15  
16  
17  
18  
19  
20  
21  
22  
23  
24  
25  
26  
27  
28  
29  
30  
31  
32  
33  
34  
35  
36  
37  
38  
39  
40  
41  
42  
43  
44  
45  
46  
47  
48  
49  
50  
51  
52  
53  
54  
55  
56  
57  
58  
59  
60  
61  
62  
63  
64  
65



(a)



(b)

Figure 4: Lattice structure with hexagonal configuration: (a) Isometric view, (b) Top view with primitive unit cell.

1  
2  
3  
4  
5  
6  
7  
8  
9  
10  
11  
12  
13  
14  
15  
16  
17  
18  
19  
20  
21  
22  
23  
24  
25  
26  
27  
28  
29  
30  
31  
32  
33  
34  
35  
36  
37  
38  
39  
40  
41  
42  
43  
44  
45  
46  
47  
48  
49  
50  
51  
52  
53  
54  
55  
56  
57  
58  
59  
60  
61  
62  
63  
64  
65

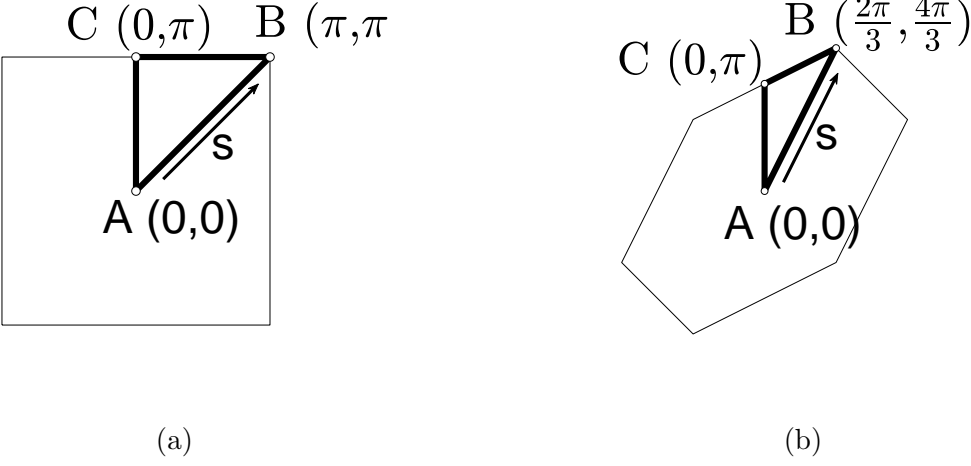


Figure 5: Reciprocal lattice in  $k_1$ - $k_2$  space: (a) Square configuration, (b) Triangular and hexagonal configurations.

1  
2  
3  
4  
5  
6  
7  
8  
9  
10  
11  
12  
13  
14  
15  
16  
17  
18  
19  
20  
21  
22  
23  
24  
25  
26  
27  
28  
29  
30  
31  
32  
33  
34  
35  
36  
37  
38  
39  
40  
41  
42  
43  
44  
45  
46  
47  
48  
49  
50  
51  
52  
53  
54  
55  
56  
57  
58  
59  
60  
61  
62  
63  
64  
65

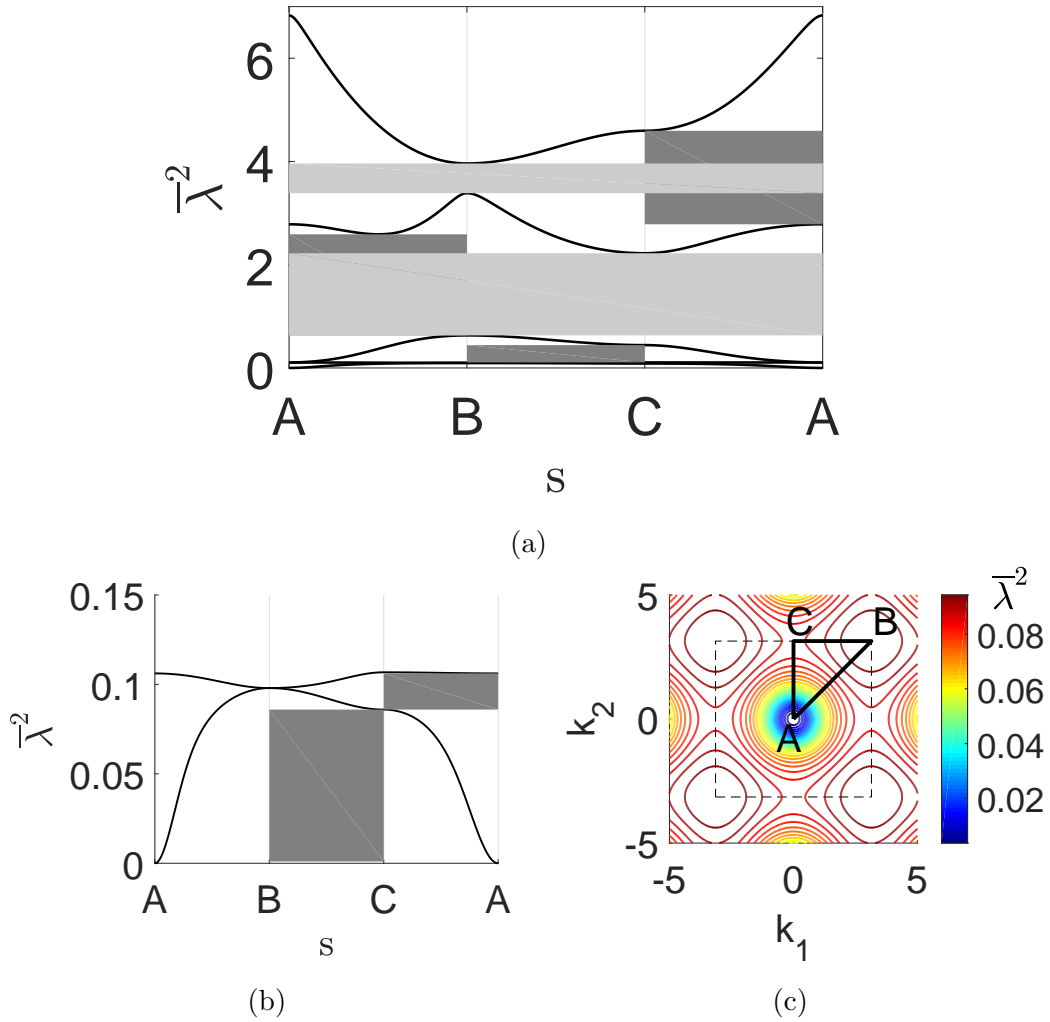


Figure 6: Square configuration: (a) Band structure: 1st to 5th modes, (b) Detail of band structure: 1st and 2nd modes, (c) 1st mode dispersion surface presented in the contour plot.



1  
2  
3  
4  
5  
6  
7  
8  
9  
10  
11  
12  
13  
14  
15  
16  
17  
18  
19  
20  
21  
22  
23  
24  
25  
26  
27  
28  
29  
30  
31  
32  
33  
34  
35  
36  
37  
38  
39  
40  
41  
42  
43  
44  
45  
46  
47  
48  
49  
50  
51  
52  
53  
54  
55  
56  
57  
58  
59  
60  
61  
62  
63  
64  
65

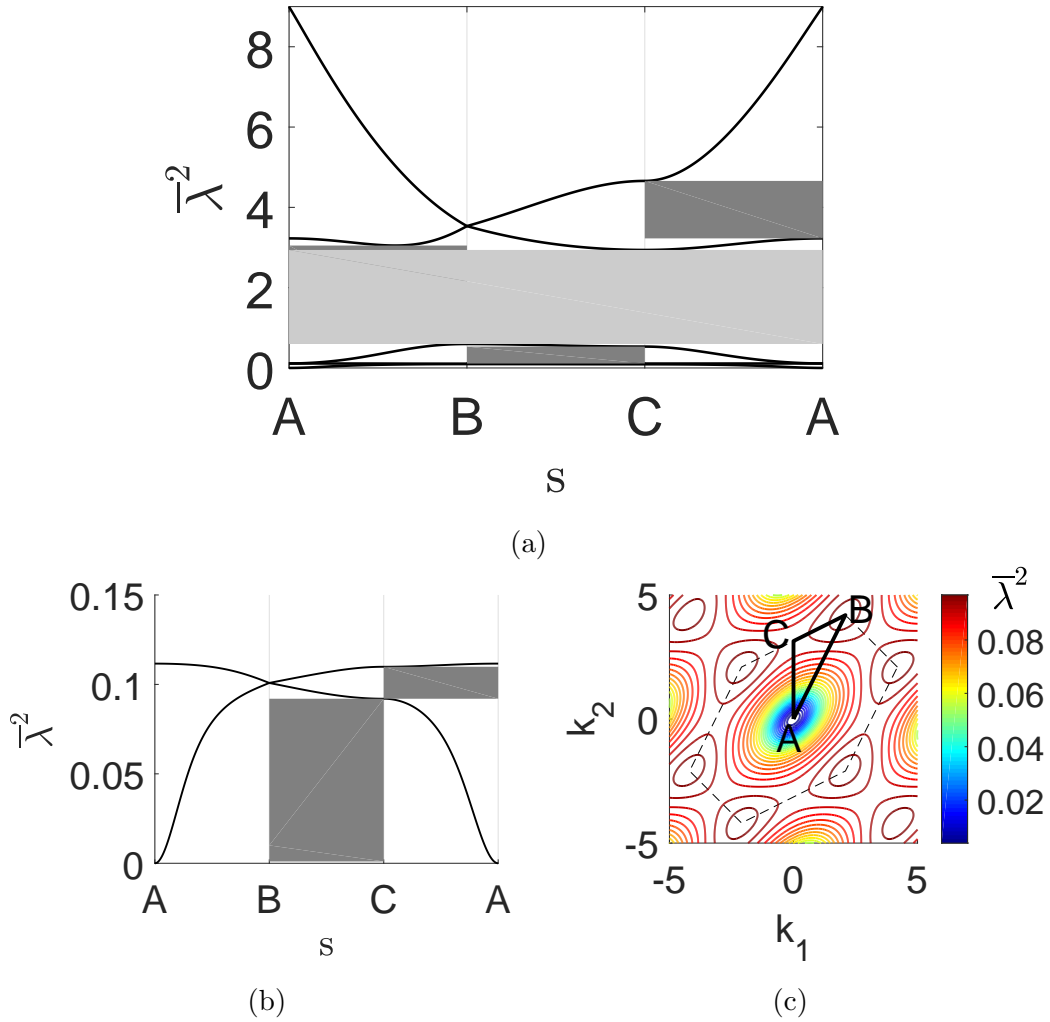


Figure 7: Triangular configuration: (a) Band structure: 1st to 5th modes, (b) Detail of band structure: 1st and 2nd modes, (c) 1st mode dispersion surface presented in the contour plot.

1  
2  
3  
4  
5  
6  
7  
8  
9  
10  
11  
12  
13  
14  
15  
16  
17  
18  
19  
20  
21  
22  
23  
24  
25  
26  
27  
28  
29  
30  
31  
32  
33  
34  
35  
36  
37  
38  
39  
40  
41  
42  
43  
44  
45  
46  
47  
48  
49  
50  
51  
52  
53  
54  
55  
56  
57  
58  
59  
60  
61  
62  
63  
64  
65

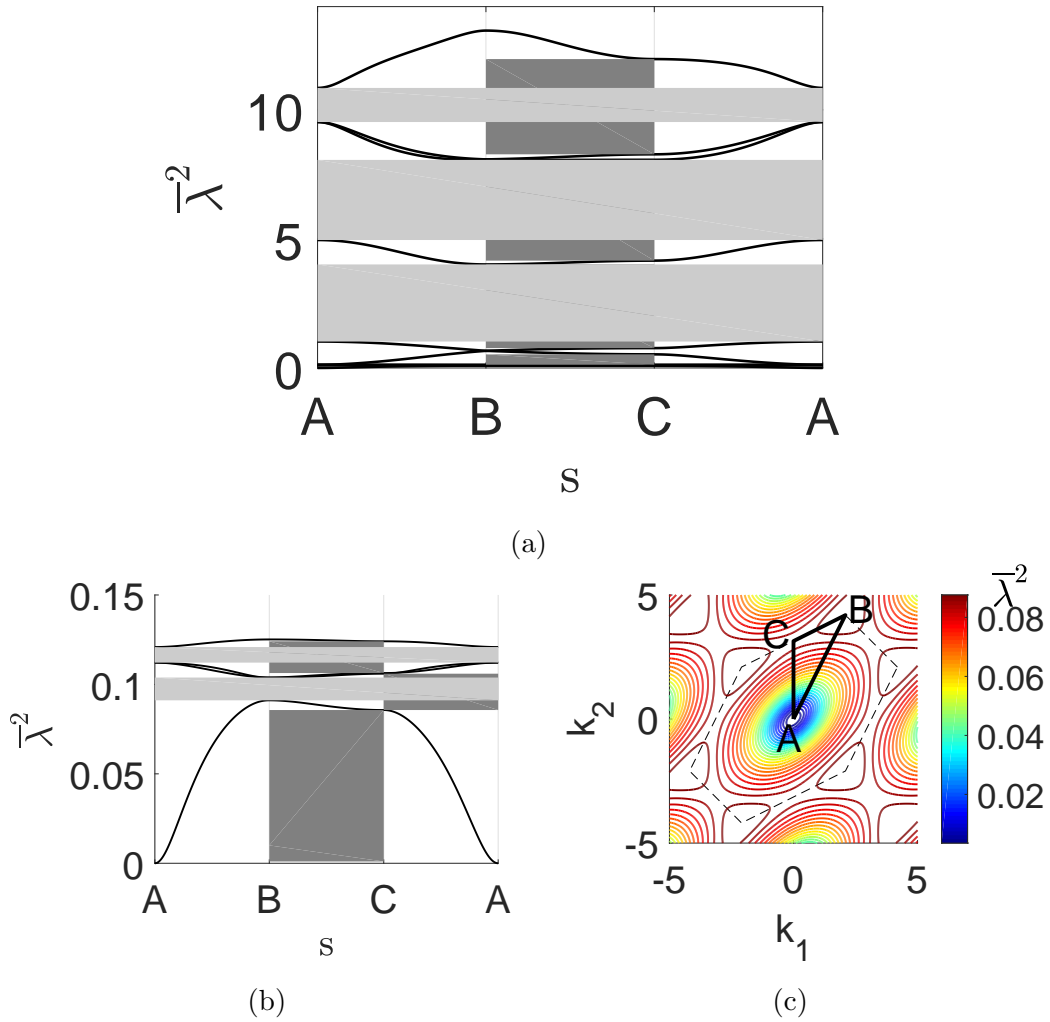


Figure 8: Hexagonal configuration: (a) Band structure: 1st to 10th modes, (b) Detail of band structure: 1st and 4th modes, (c) 1st mode dispersion surface presented in the contour plot.

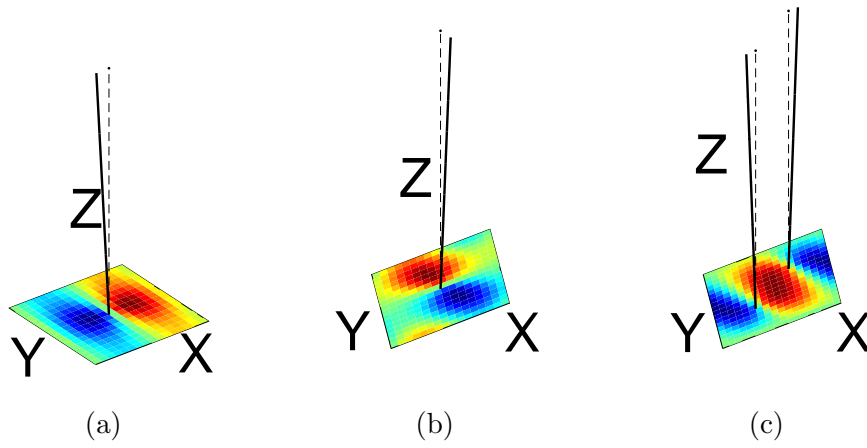


Figure 9: Example of mode shape in problem Type 2 (Mode 2, Point A): (a) Square configuration, (b) Triangular configuration, (c) Hexagonal configuration.

1  
2  
3  
4  
5  
6  
7  
8  
9  
10  
11  
12  
13  
14  
15  
16  
17  
18  
19  
20  
21  
22  
23  
24  
25  
26  
27  
28  
29  
30  
31  
32  
33  
34  
35  
36  
37  
38  
39  
40  
41  
42  
43  
44  
45  
46  
47  
48  
49  
50  
51  
52  
53  
54  
55  
56  
57  
58  
59  
60  
61  
62  
63  
64  
65

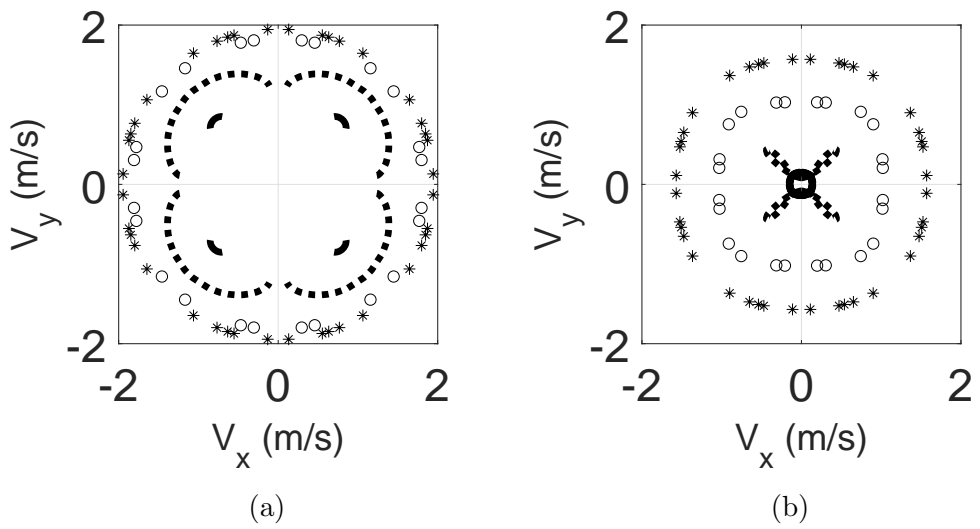


Figure 10: Square configuration: (a) Phase velocity, (b) Group velocity. 1st mode at various frequencies: '\*'  $\omega = 0.65 \cdot \omega_{max}$ , 'o'  $\omega = 0.75 \cdot \omega_{max}$ , 'dashed line'  $\omega = 0.88 \cdot \omega_{max}$ , 'solid line'  $\omega = 0.99 \cdot \omega_{max}$ .  $\omega_{max}$  = maximum value of  $\omega$  for the 1st mode.

1  
2  
3  
4  
5  
6  
7  
8  
9  
10  
11  
12  
13  
14  
15  
16  
17  
18  
19  
20  
21  
22  
23  
24  
25  
26  
27  
28  
29  
30  
31  
32  
33  
34  
35  
36  
37  
38  
39  
40  
41  
42  
43  
44  
45  
46  
47  
48  
49  
50  
51  
52  
53  
54  
55  
56  
57  
58  
59  
60  
61  
62  
63  
64  
65

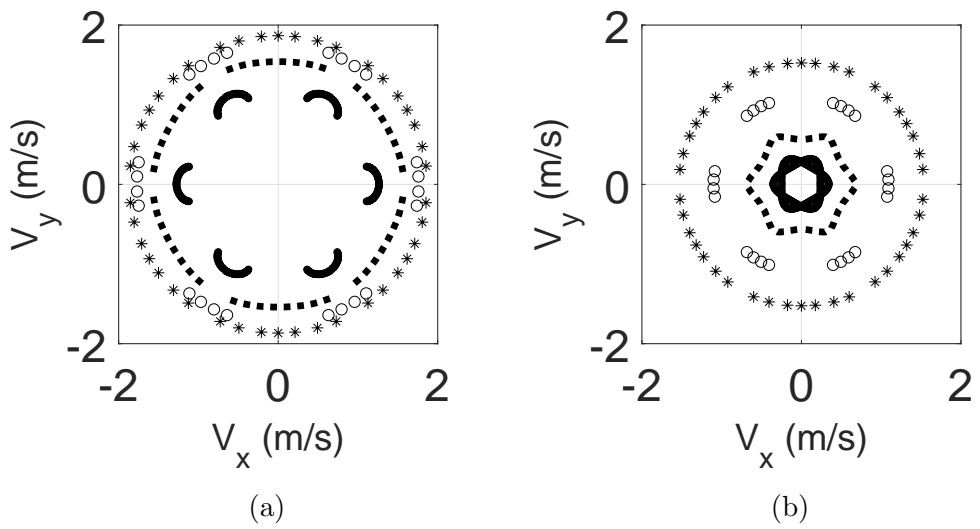


Figure 11: Triangular configuration: (a) Phase velocity, (b) Group velocity. 1st mode at various frequencies: ‘\*’  $\omega = 0.65 \cdot \omega_{max}$ , ‘o’  $\omega = 0.75 \cdot \omega_{max}$ , ‘dashed line’  $\omega = 0.85 \cdot \omega_{max}$ , ‘solid line’  $\omega = 0.95 \cdot \omega_{max}$ .  $\omega_{max}$  = maximum value of  $\omega$  for the 1st mode.

1  
2  
3  
4  
5  
6  
7  
8  
9  
10  
11  
12  
13  
14  
15  
16  
17  
18  
19  
20  
21  
22  
23  
24  
25  
26  
27  
28  
29  
30  
31  
32  
33  
34  
35  
36  
37  
38  
39  
40  
41  
42  
43  
44  
45  
46  
47  
48  
49  
50  
51  
52  
53  
54  
55  
56  
57  
58  
59  
60  
61  
62  
63  
64  
65

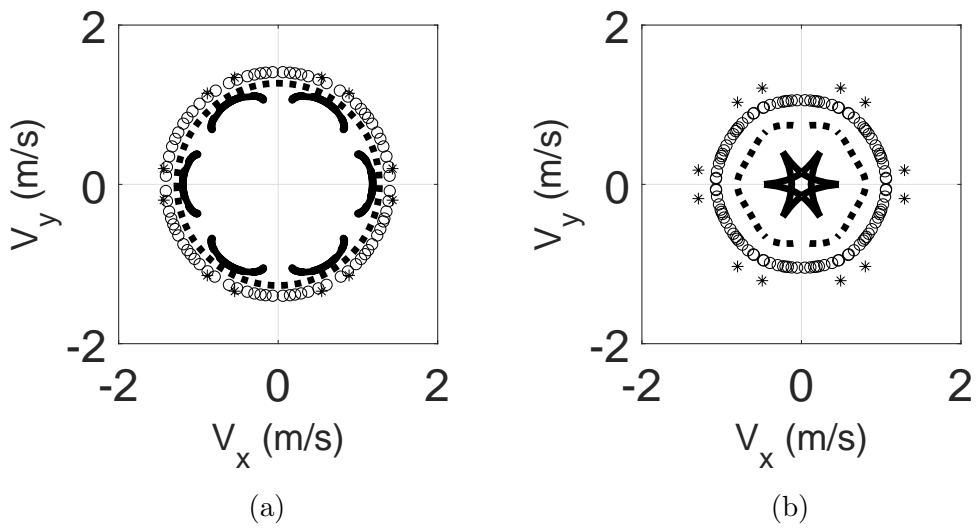


Figure 12: Hexagonal configuration: (a) Phase velocity, (b) Group velocity. 1st mode at various frequencies: '\*'  $\omega = 0.65 \cdot \omega_{max}$ , 'o'  $\omega = 0.75 \cdot \omega_{max}$ , 'dashed line'  $\omega = 0.85 \cdot \omega_{max}$ , 'solid line'  $\omega = 0.95 \cdot \omega_{max}$ .  $\omega_{max}$  = maximum value of  $\omega$  for the 1st mode.

1  
2  
3  
4  
5  
6  
7  
8  
9  
10  
11  
12  
13  
14  
15  
16  
17  
18  
19  
20  
21  
22  
23  
24  
25  
26  
27  
28  
29  
30  
31  
32  
33  
34  
35  
36  
37  
38  
39  
40  
41  
42  
43  
44  
45  
46  
47  
48  
49  
50  
51  
52  
53  
54  
55  
56  
57  
58  
59  
60  
61  
62  
63  
64  
65

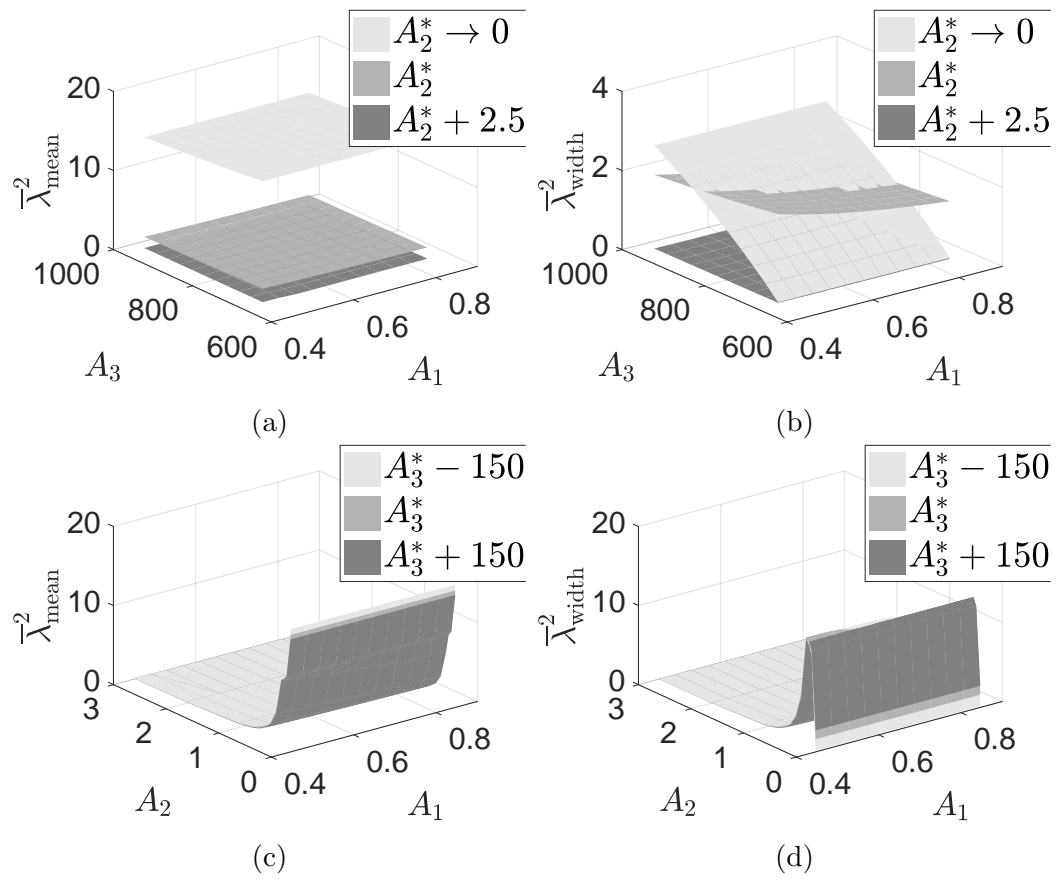


Figure 13: Square configuration: Influence of dimensionless groups on location and bandwidth.

1  
2  
3  
4  
5  
6  
7  
8  
9  
10  
11  
12  
13  
14  
15  
16  
17  
18  
19  
20  
21  
22  
23  
24  
25  
26  
27  
28  
29  
30  
31  
32  
33  
34  
35  
36  
37  
38  
39  
40  
41  
42  
43  
44  
45  
46  
47  
48  
49  
50  
51  
52  
53  
54  
55  
56  
57  
58  
59  
60  
61  
62  
63  
64  
65

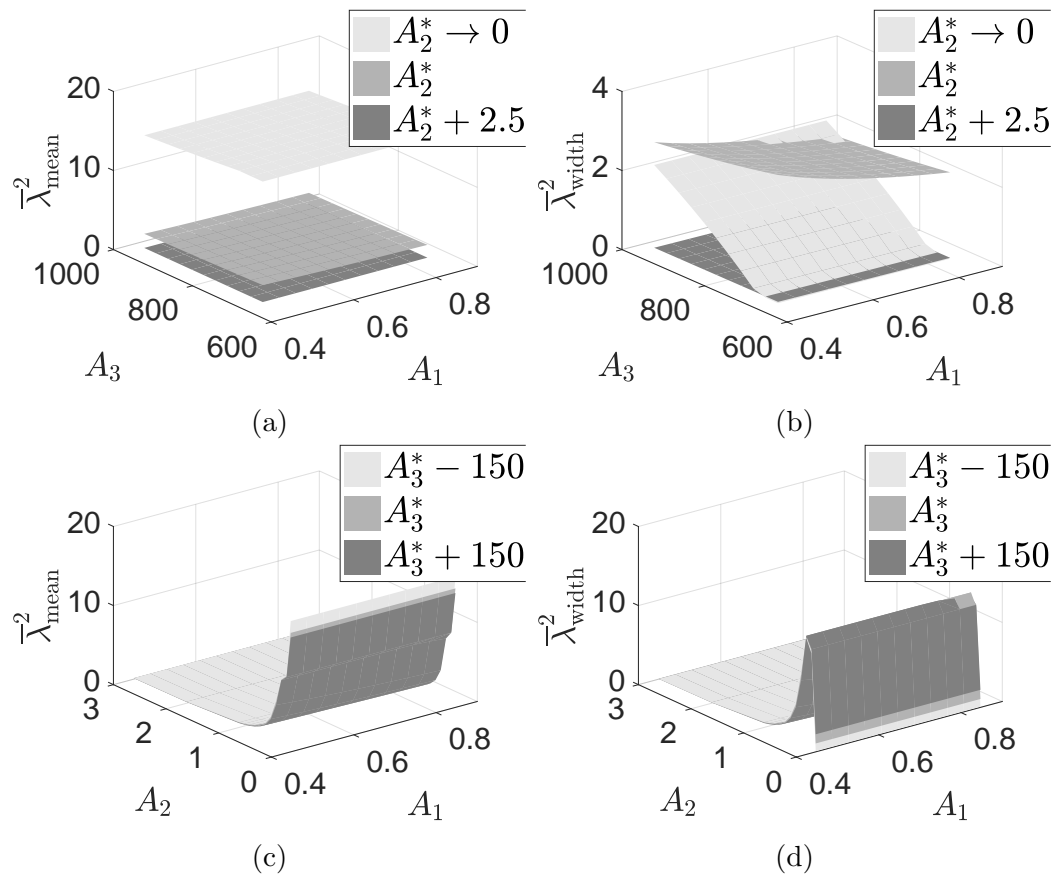


Figure 14: Triangular configuration: Influence of dimensionless groups on location and bandwidth.



1  
2  
3  
4  
5  
6  
7  
8  
9  
10  
11  
12  
13  
14  
15  
16  
17  
18  
19  
20  
21  
22  
23  
24  
25  
26  
27  
28  
29  
30  
31  
32  
33  
34  
35  
36  
37  
38  
39  
40  
41  
42  
43  
44  
45  
46  
47  
48  
49  
50  
51  
52  
53  
54  
55  
56  
57  
58  
59  
60  
61  
62  
63  
64  
65

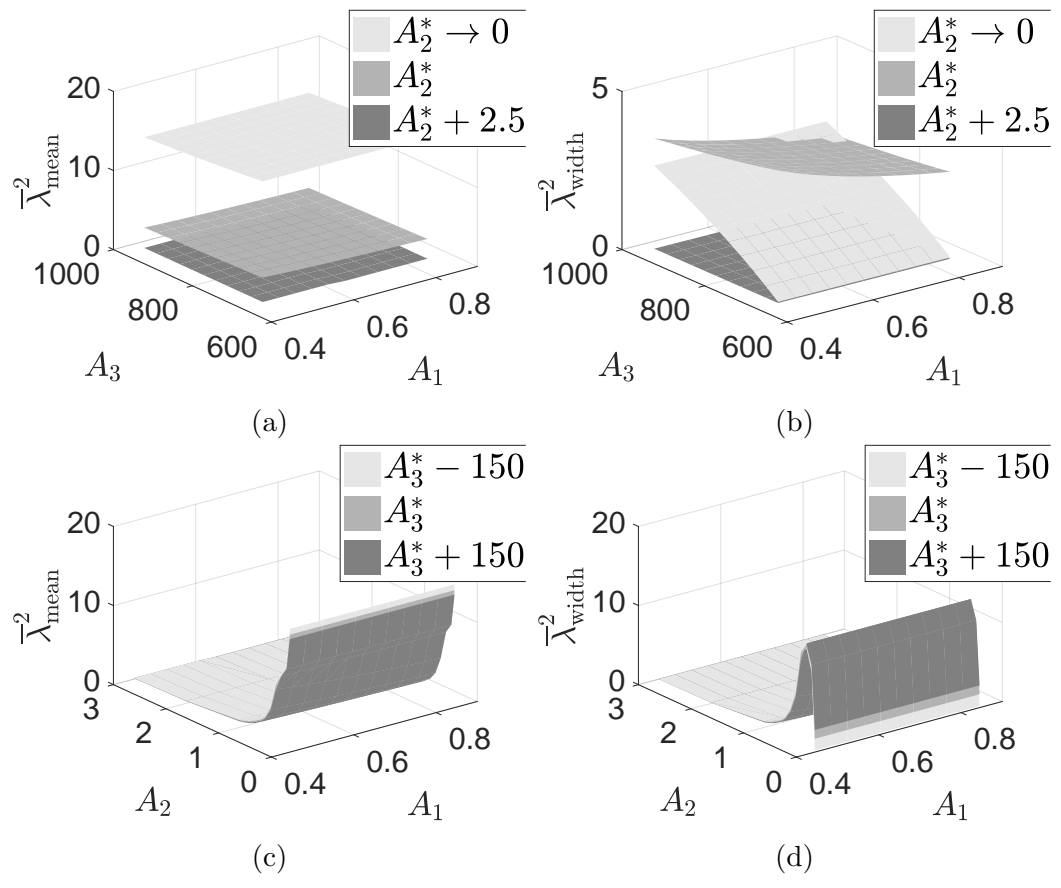


Figure 15: Hexagonal configuration: Influence of dimensionless groups on location and bandwidth.

1  
2  
3  
4  
5  
6  
7  
8  
9  
10  
11  
12  
13  
14  
15  
16  
17  
18  
19  
20  
21  
22  
23  
24  
25  
26  
27  
28  
29  
30  
31  
32  
33  
34  
35  
36  
37  
38  
39  
40  
41  
42  
43  
44  
45  
46  
47  
48  
49  
50  
51  
52  
53  
54  
55  
56  
57  
58  
59  
60  
61  
62  
63  
64  
65

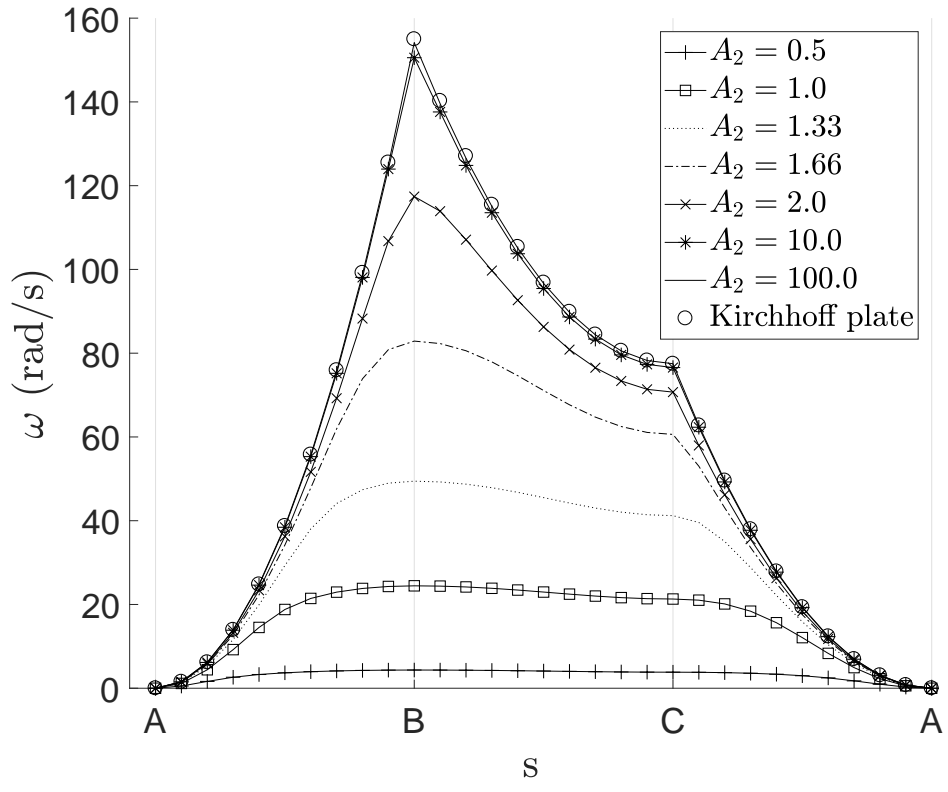


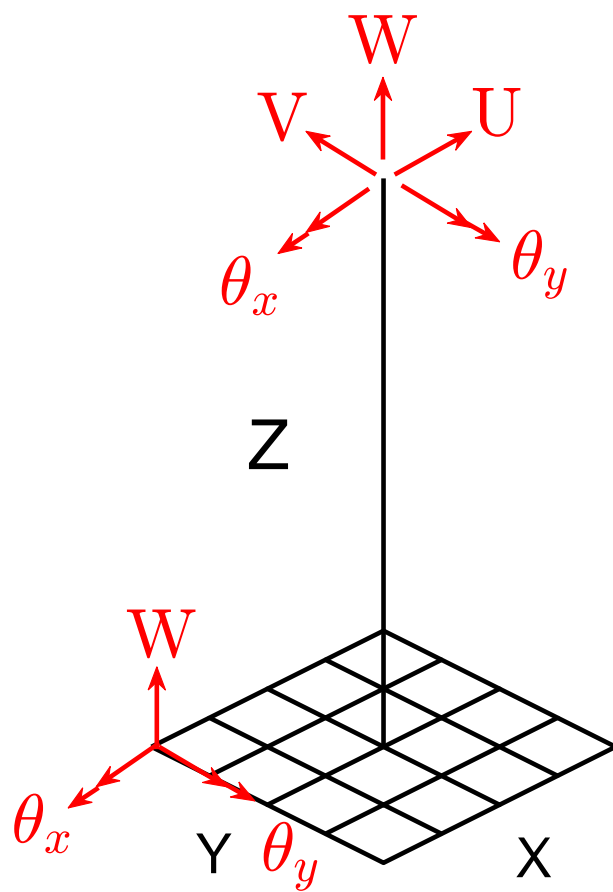
Figure 16: Dispersion curve of a Kirchhoff plate and 1st modes of different values of  $l$  for a lattice with square configuration.

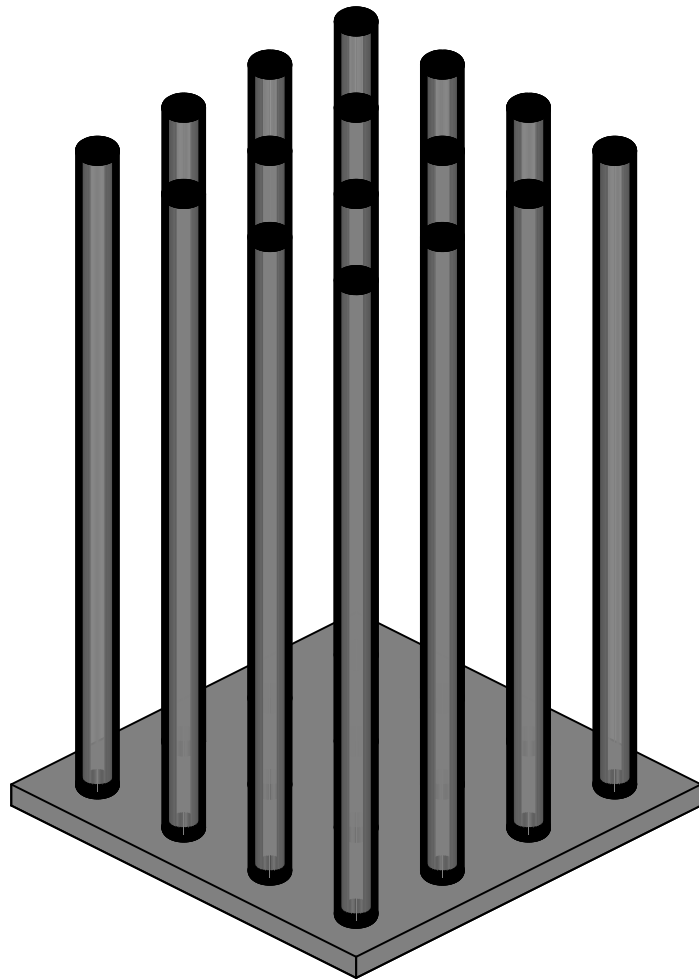
**LaTeX Source Files**

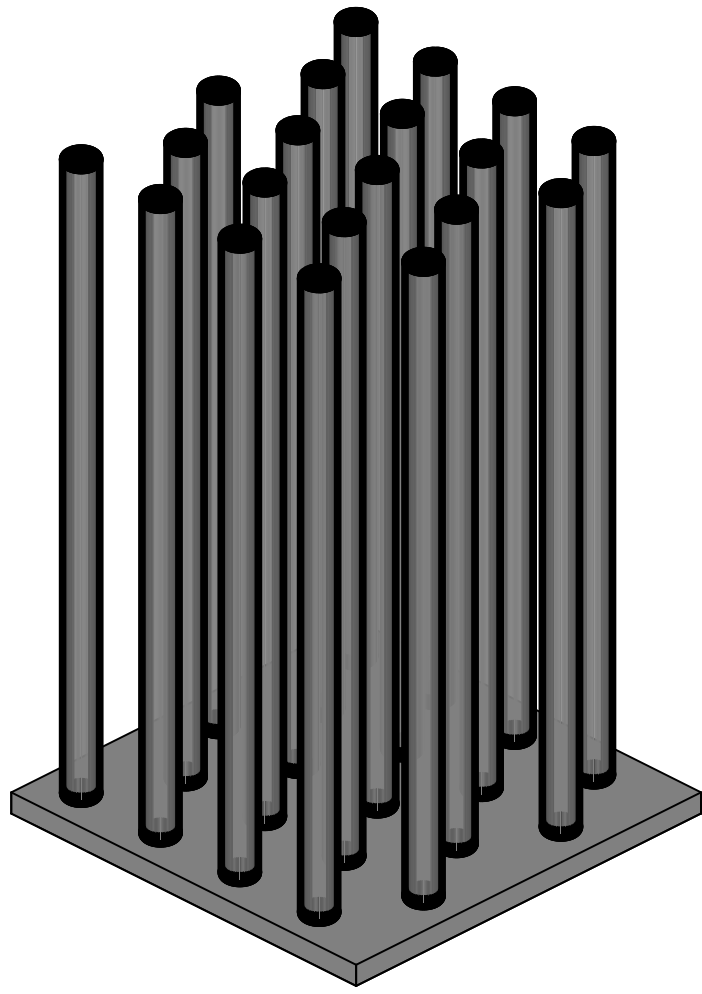
[Click here to download LaTeX Source Files: refs.bib](#)

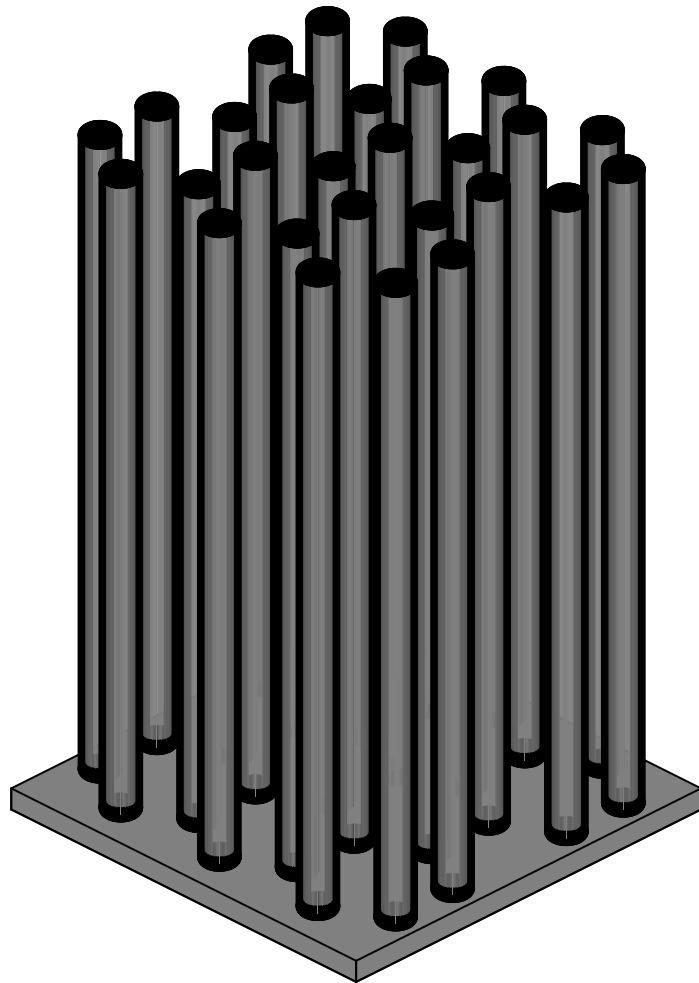
**LaTeX Source Files**

[Click here to download LaTeX Source Files: Paper\\_2.tex](#)

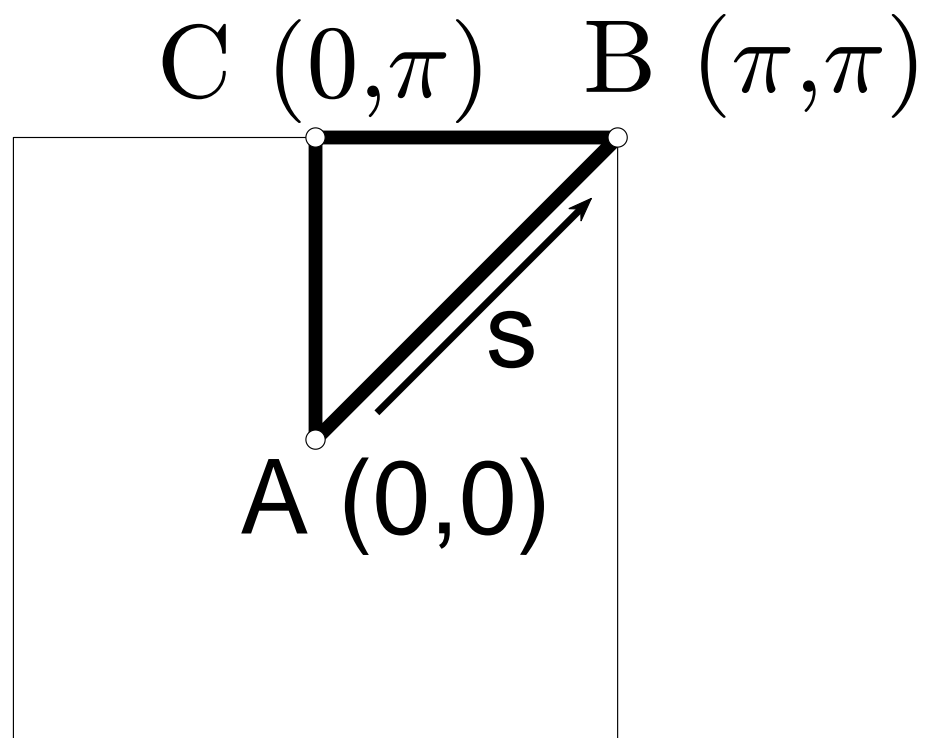


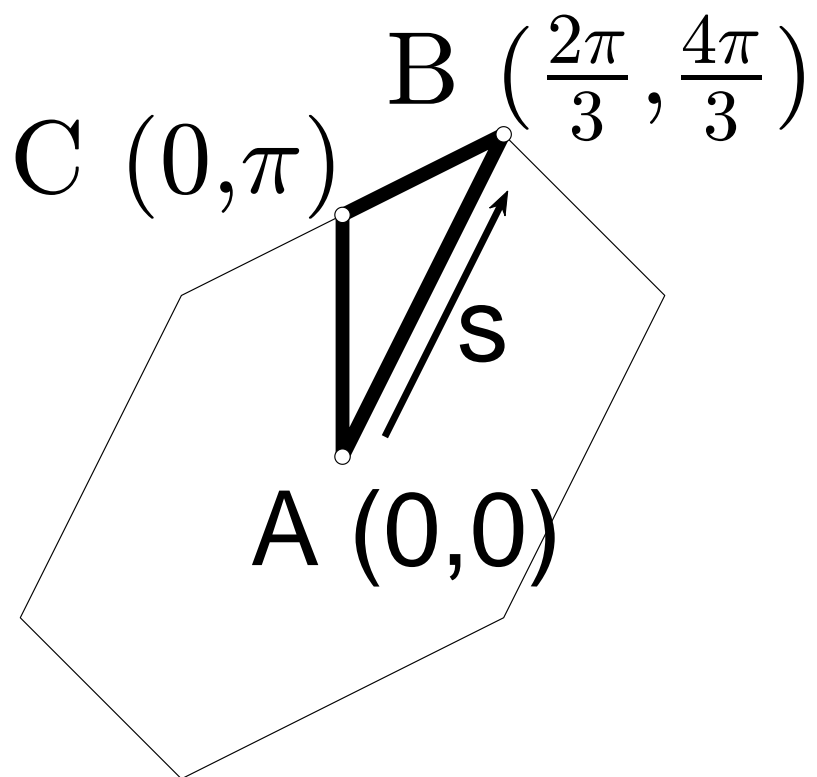




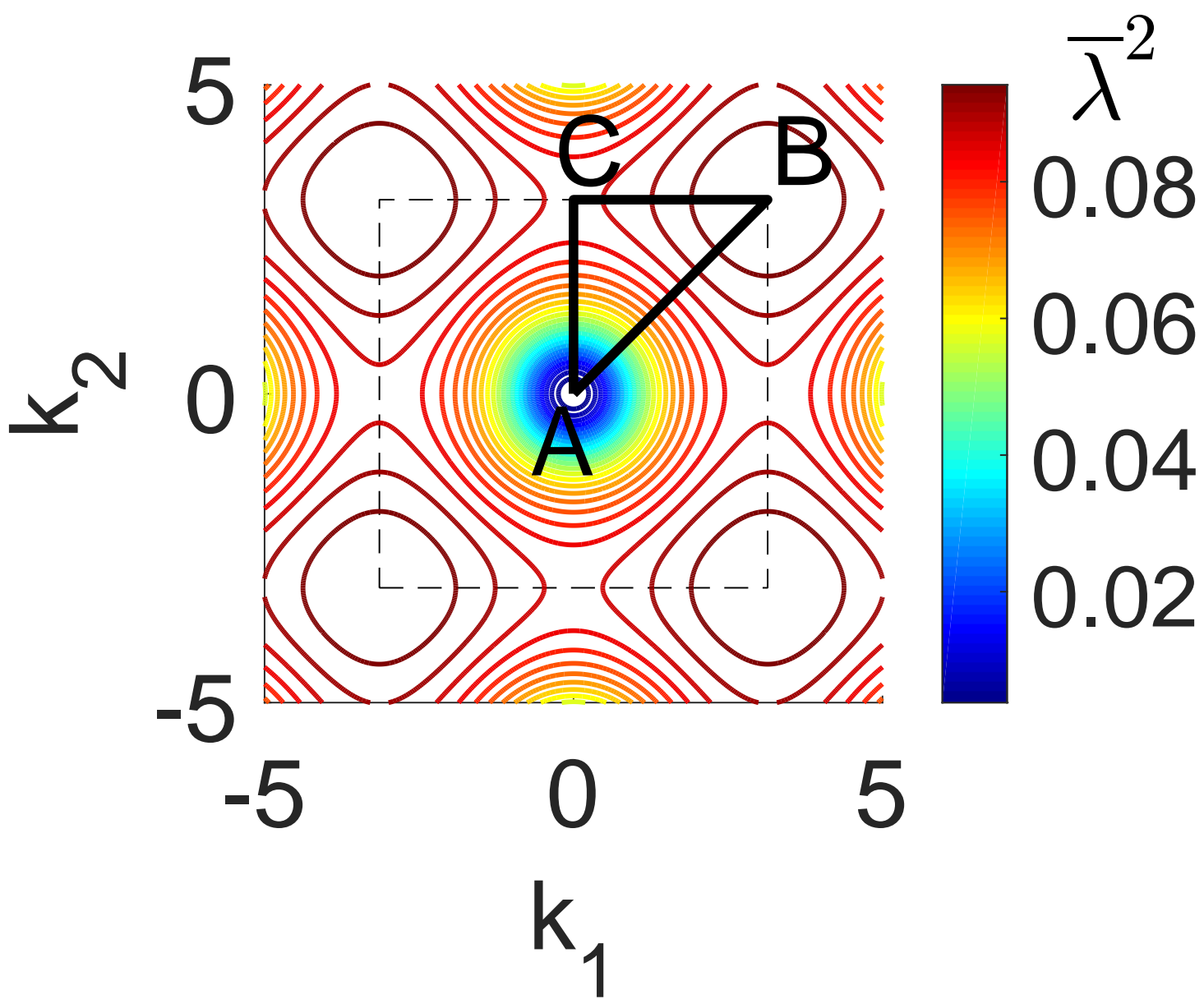




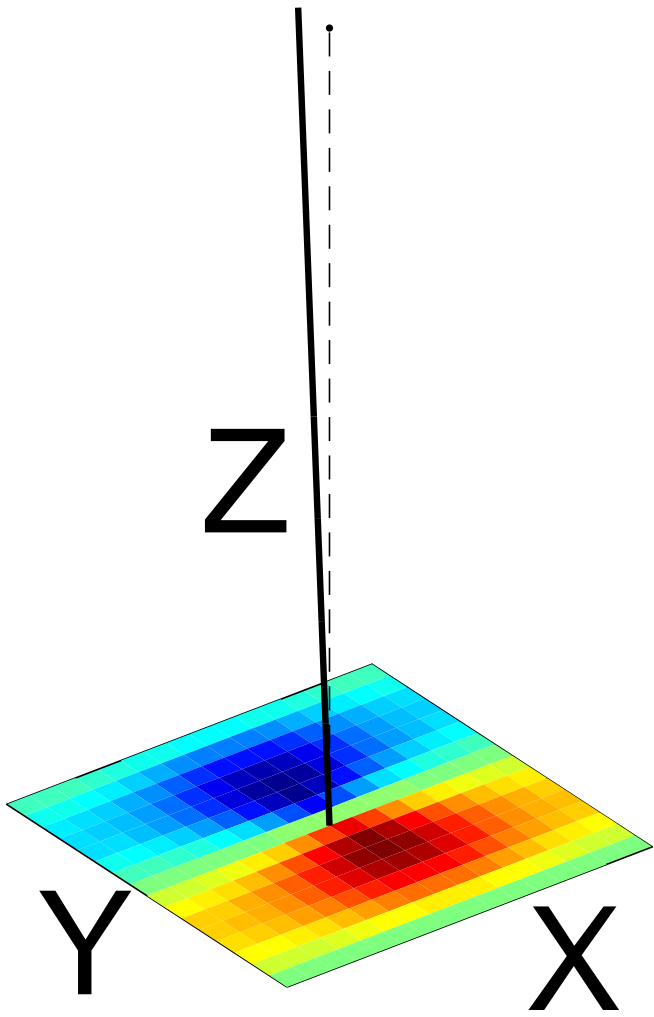




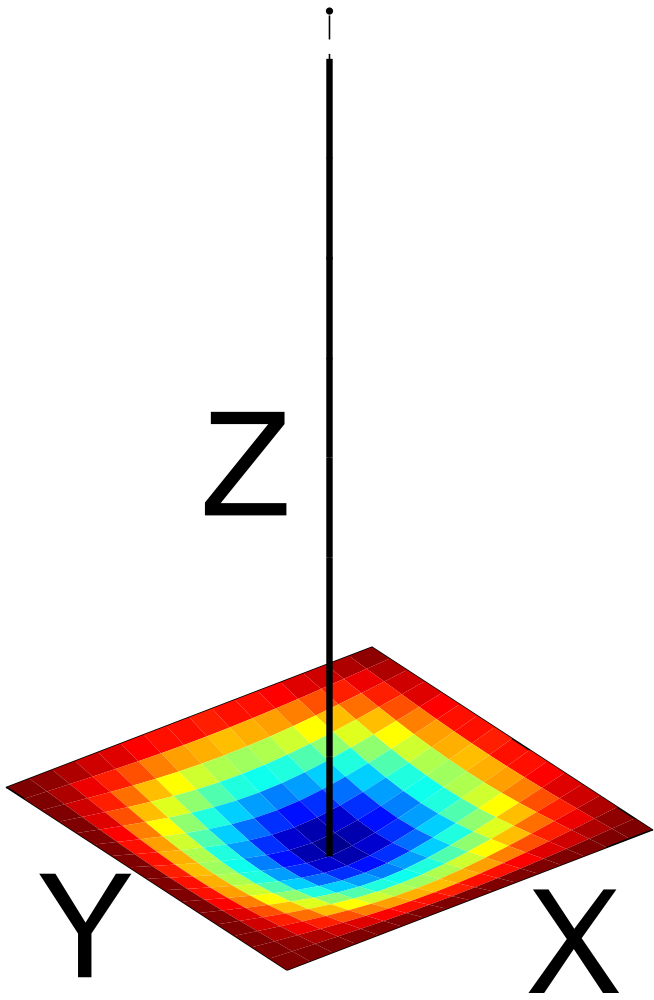
Figure(s)



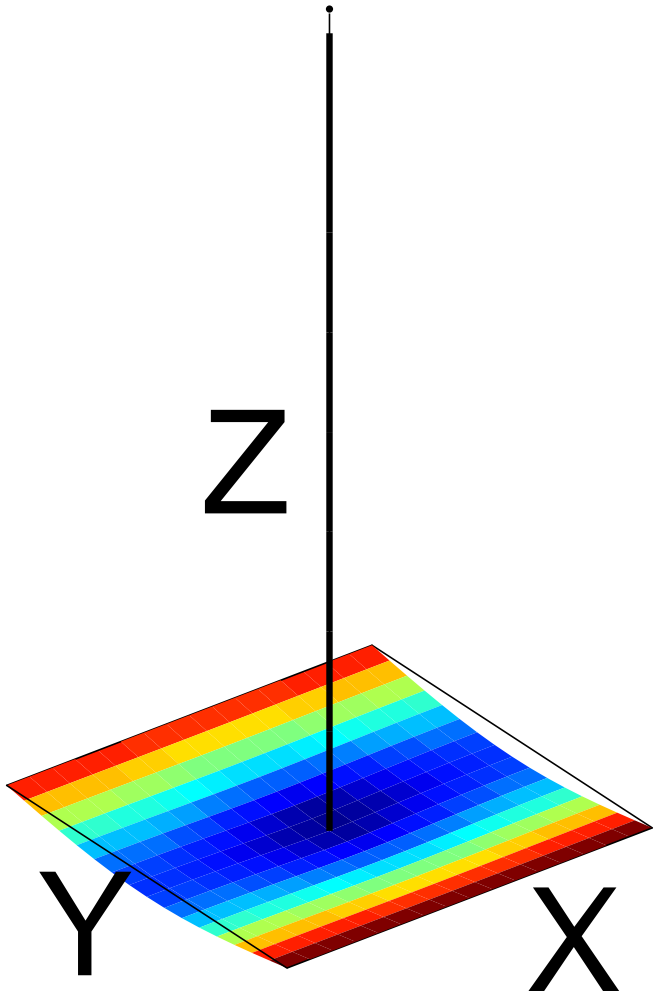
Figure(s)



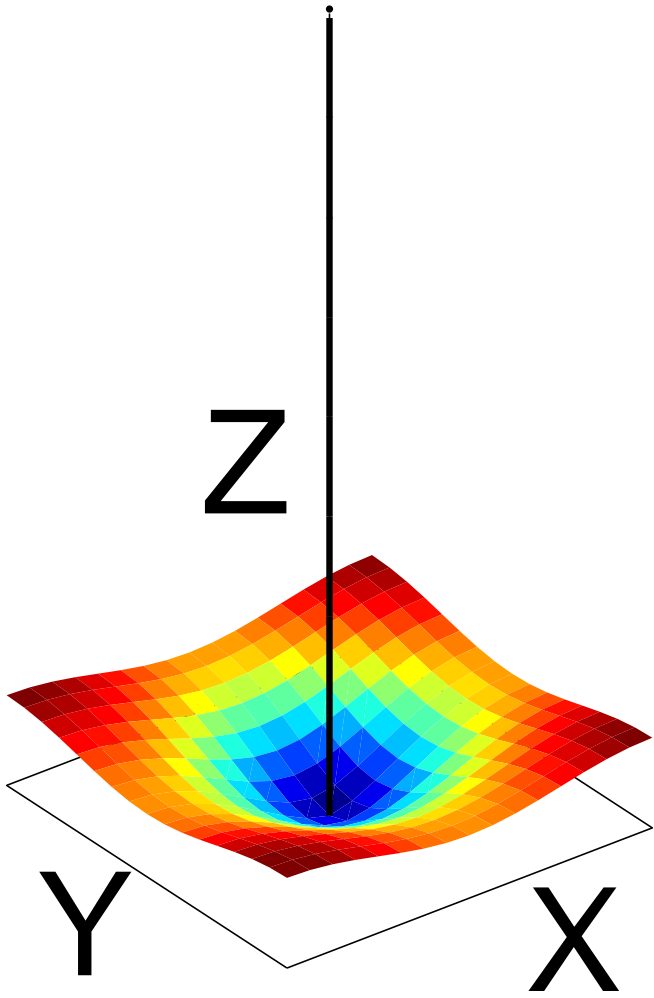
Figure(s)



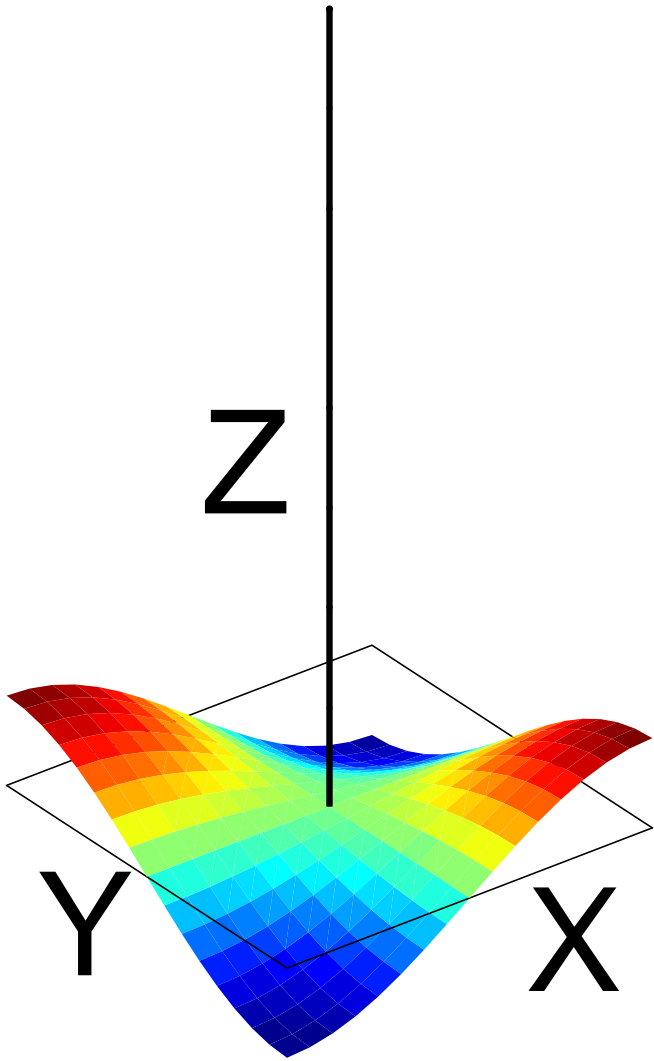
Figure(s)



Figure(s)

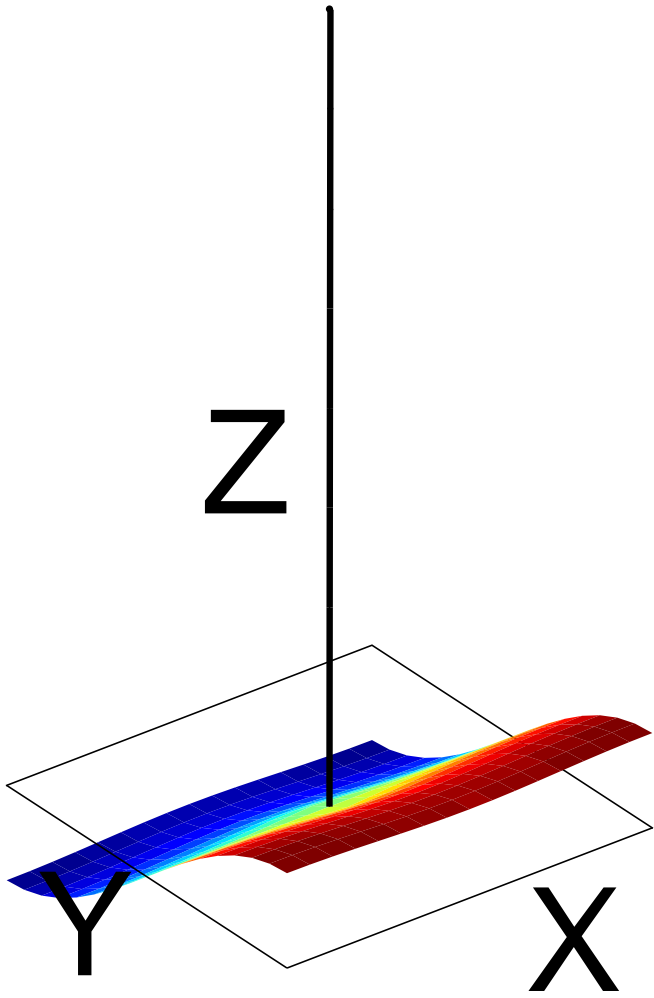


Figure(s)

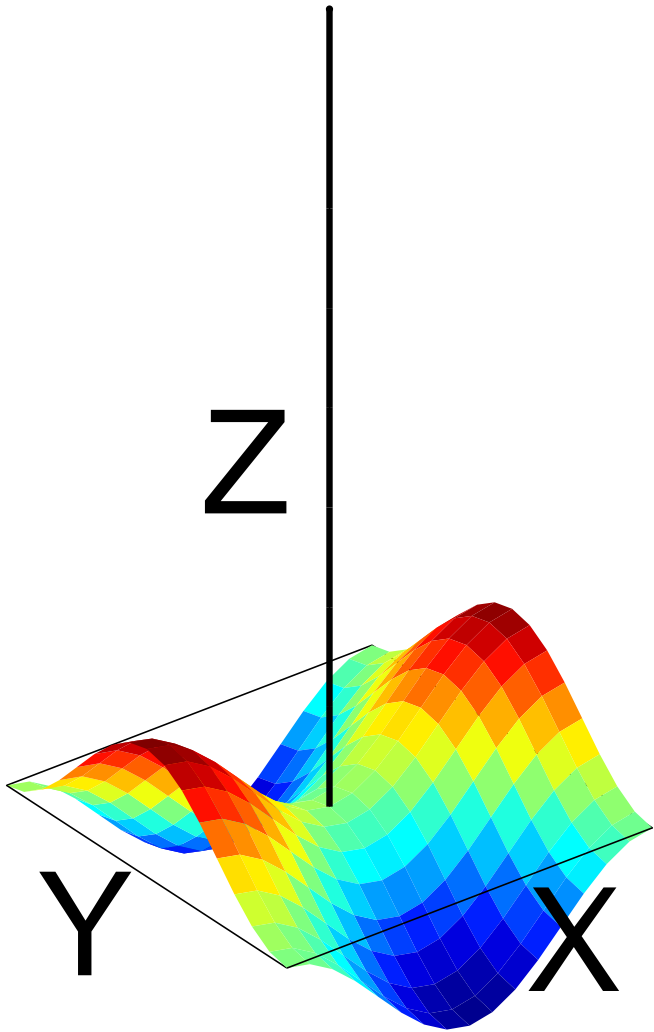




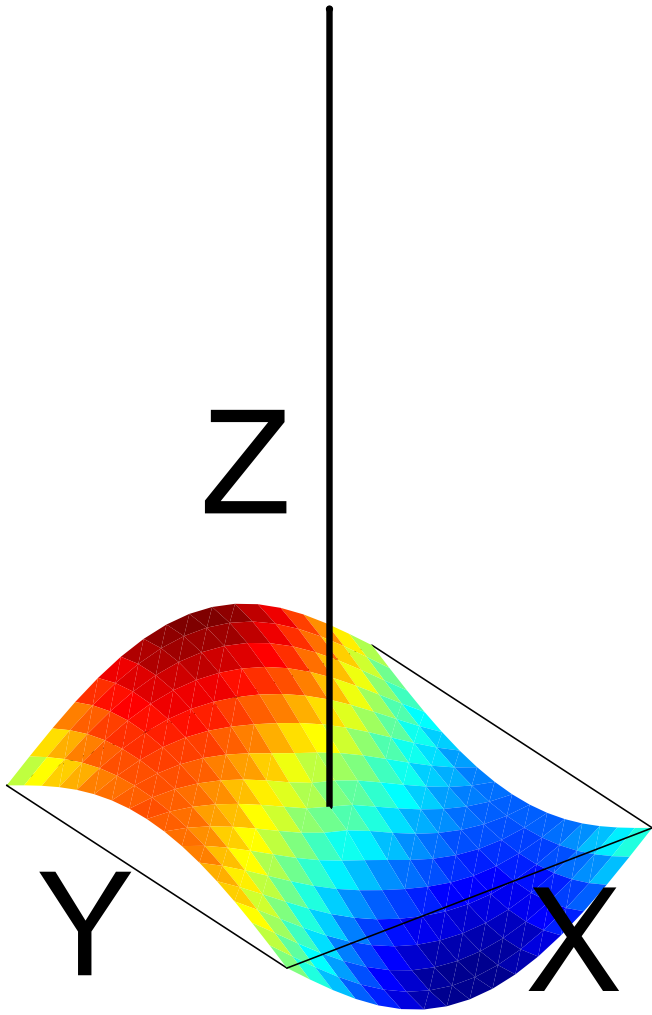
Figure(s)



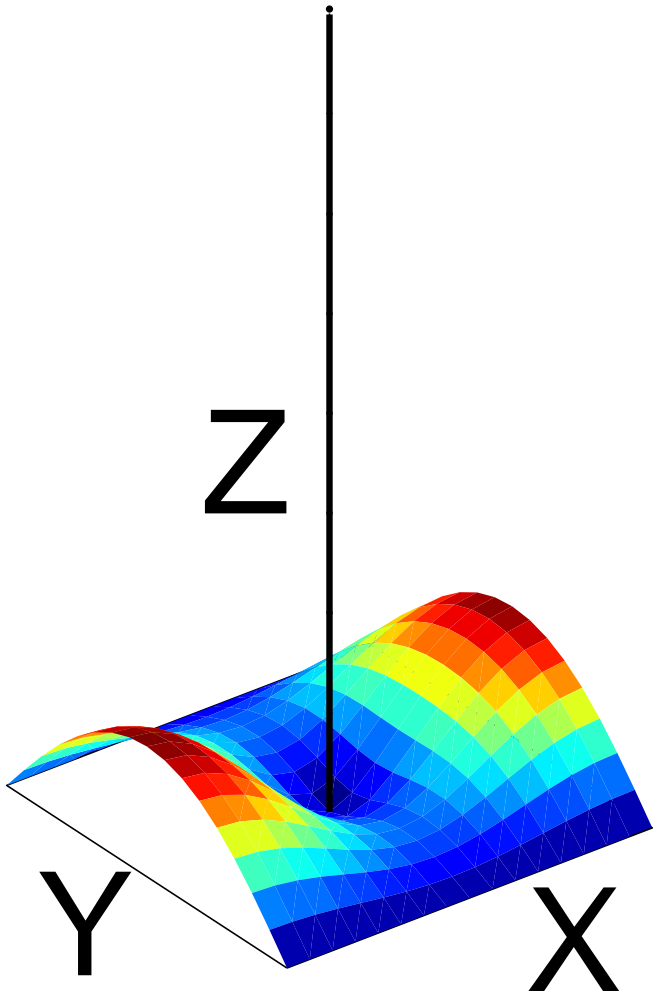
Figure(s)



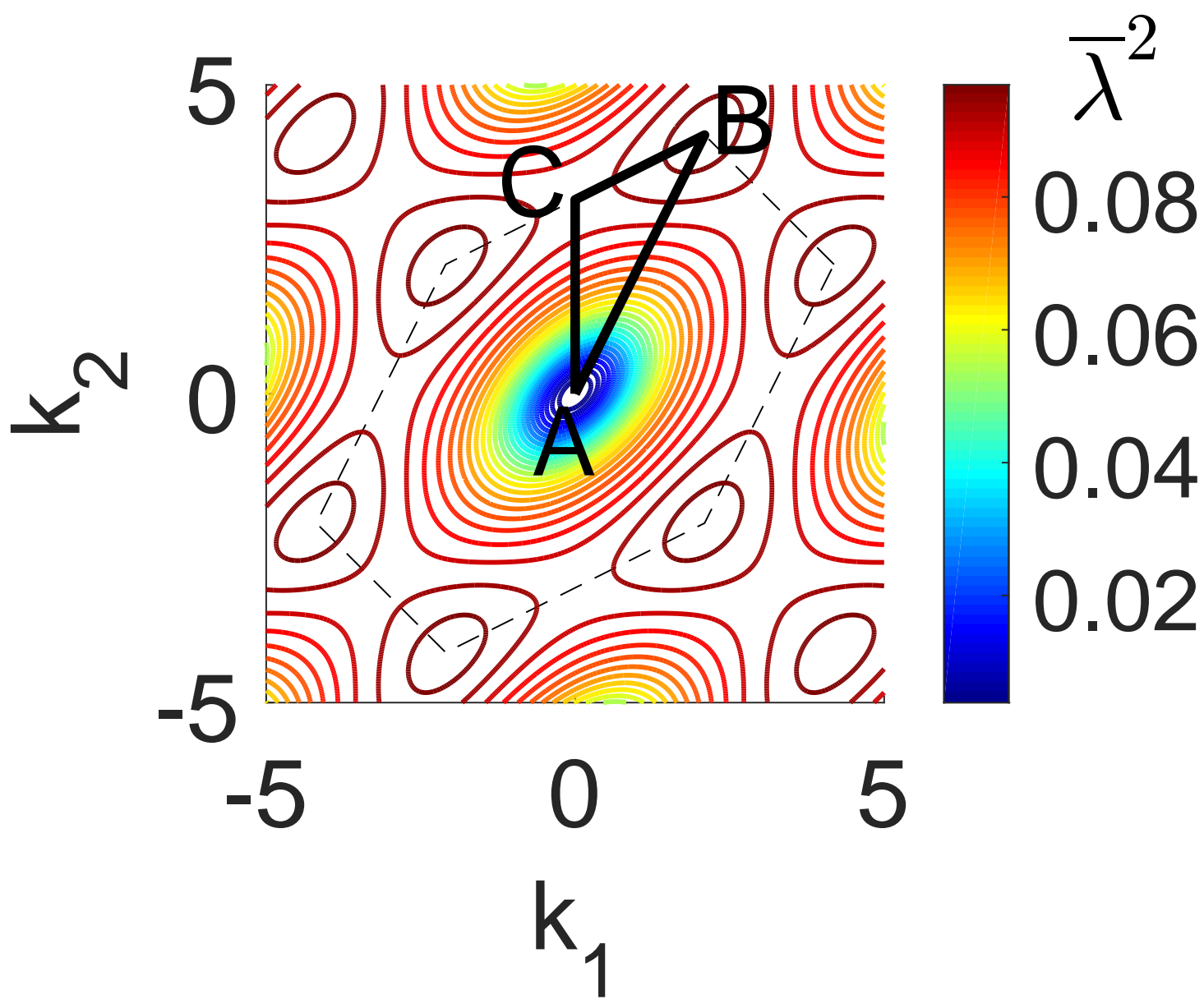
Figure(s)



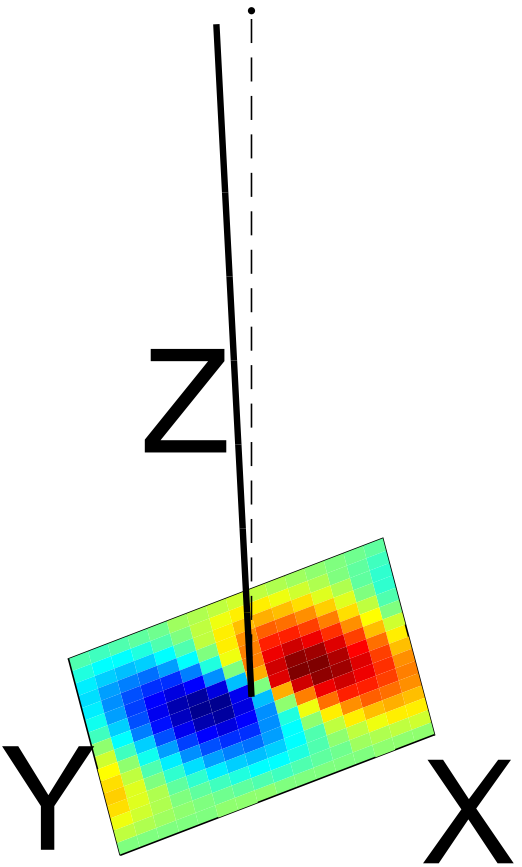
Figure(s)



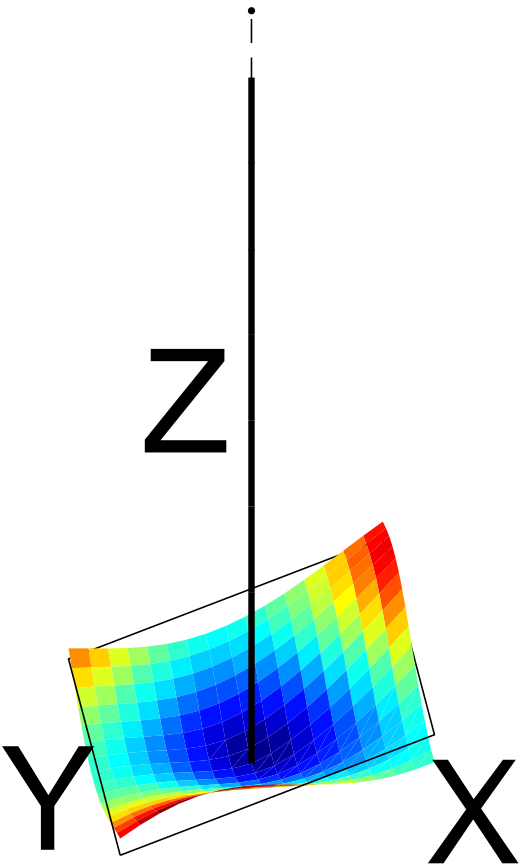
Figure(s)



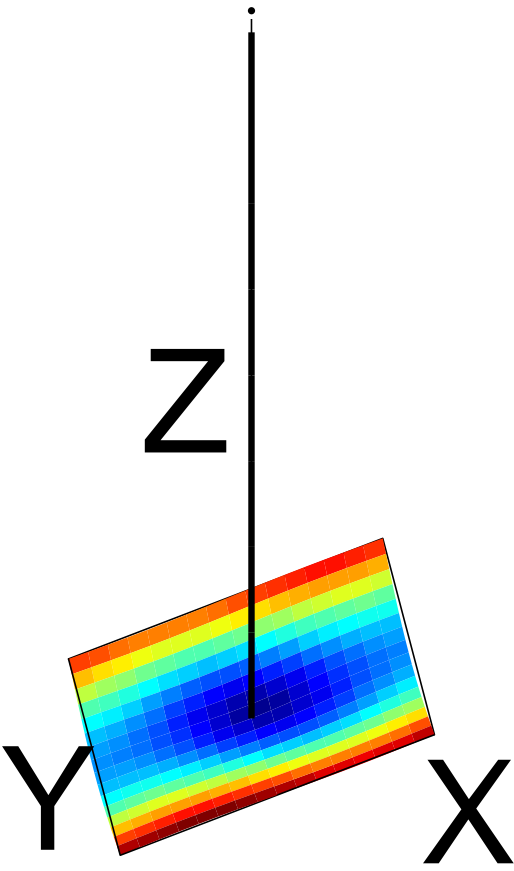
Figure(s)



Figure(s)

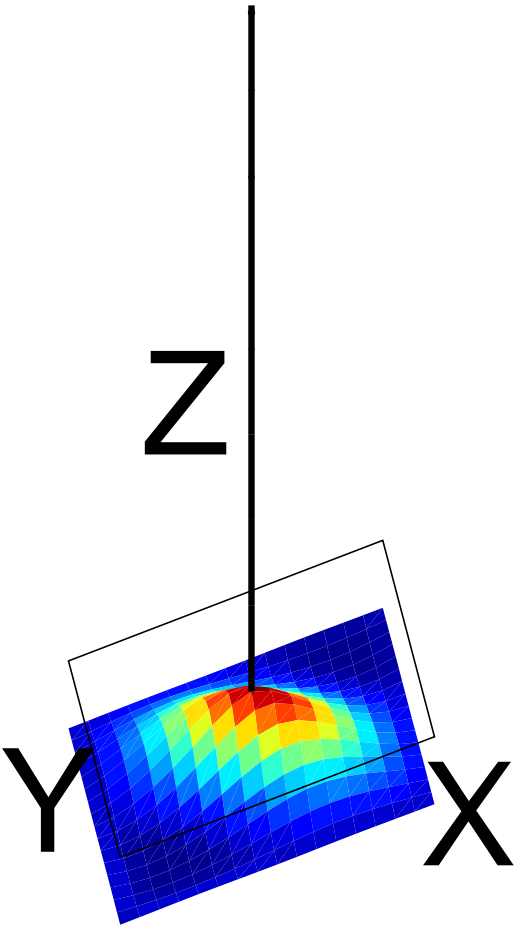


Figure(s)

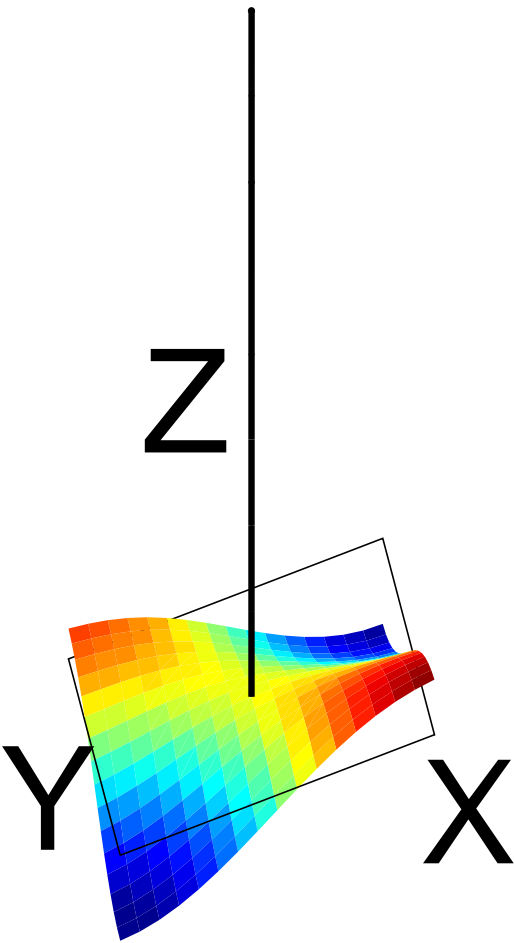




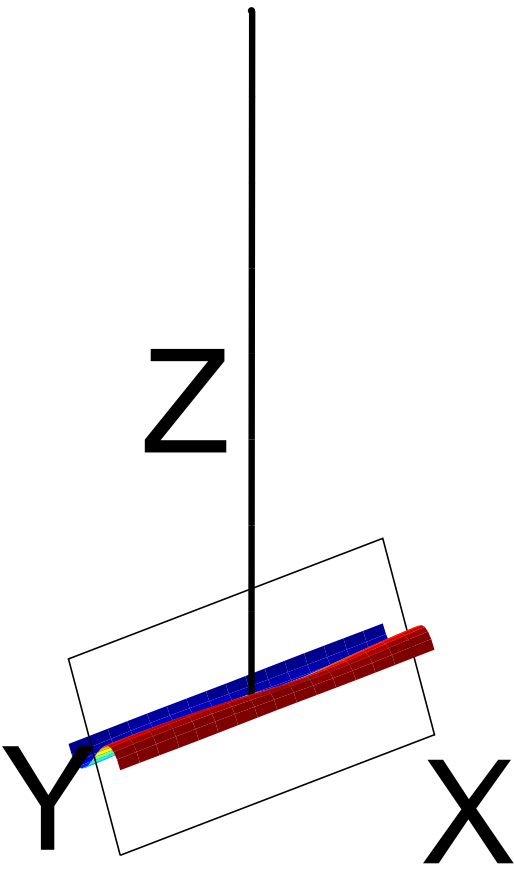
Figure(s)



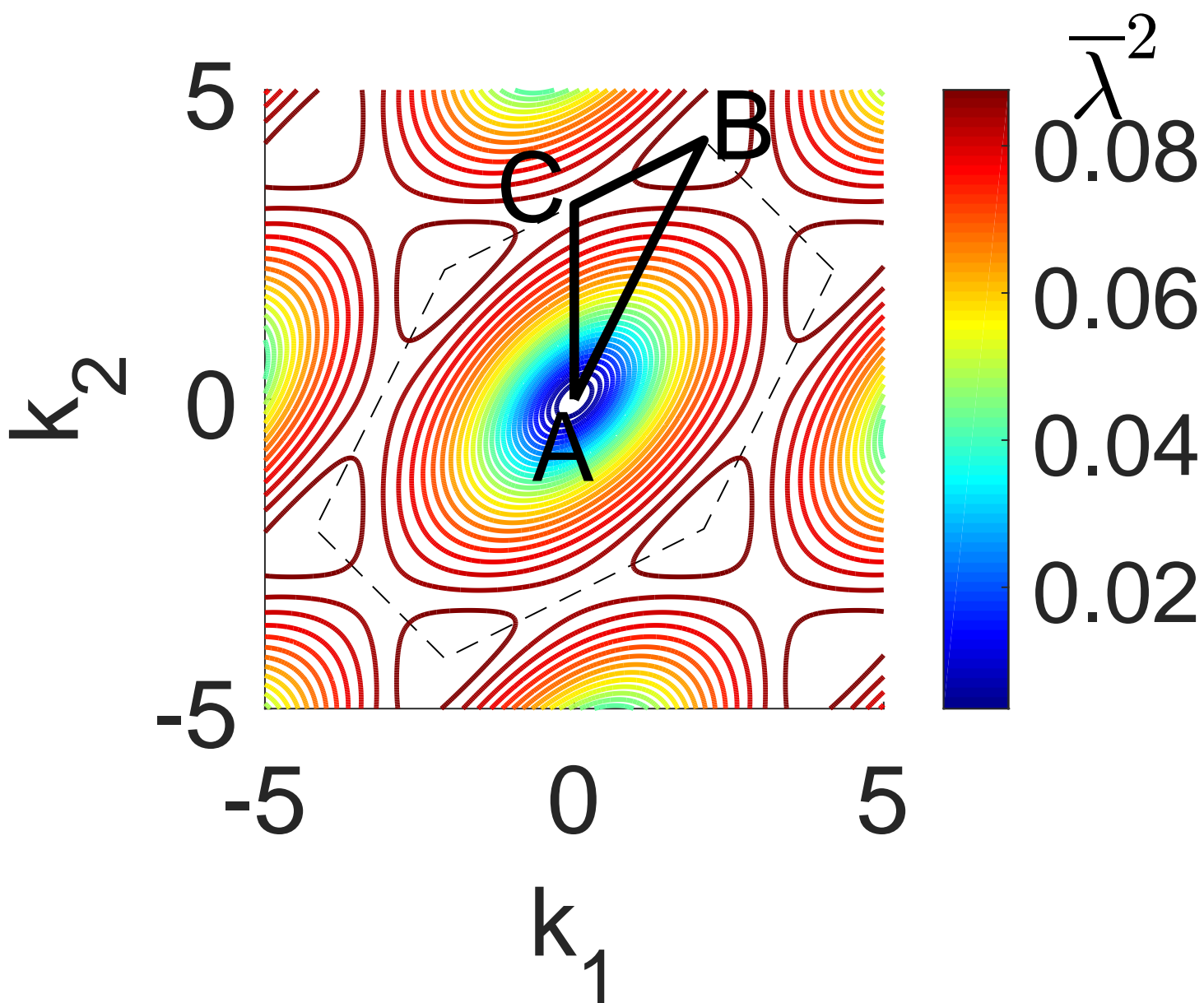
Figure(s)



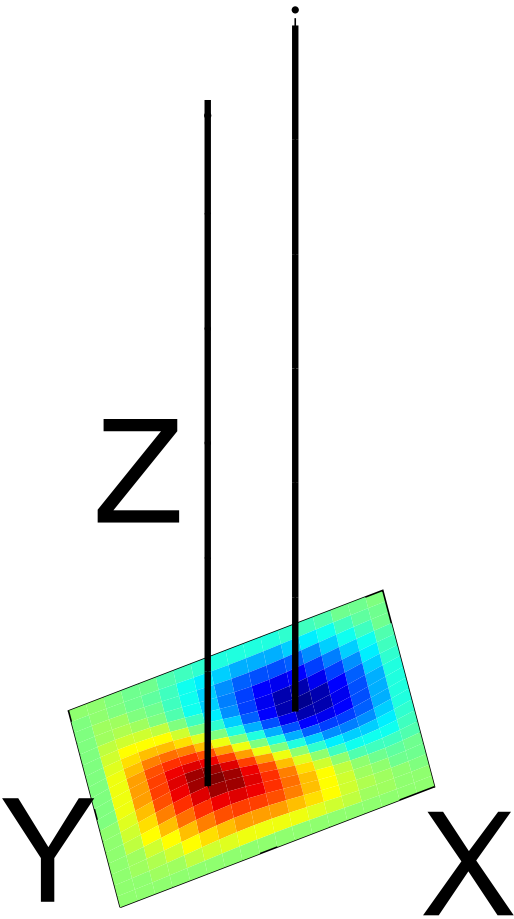
Figure(s)



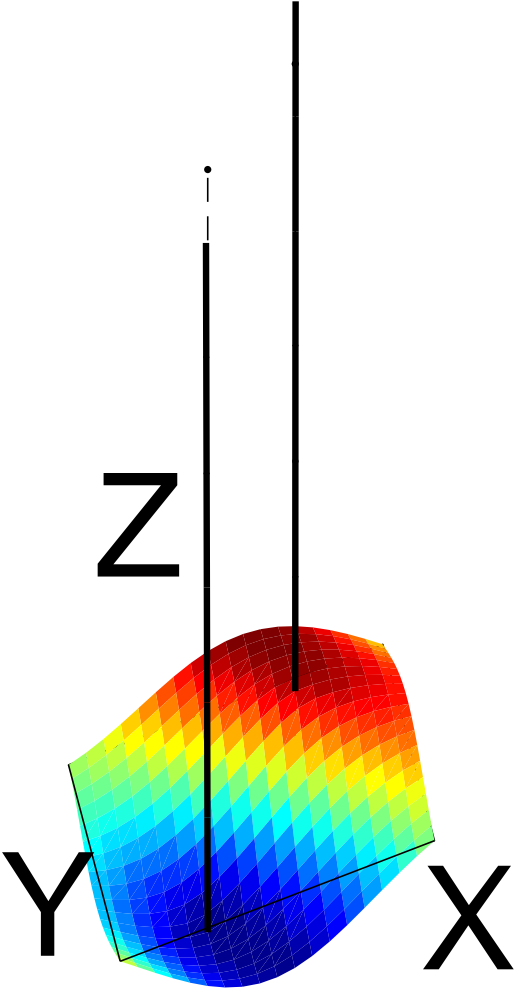
Figure(s)



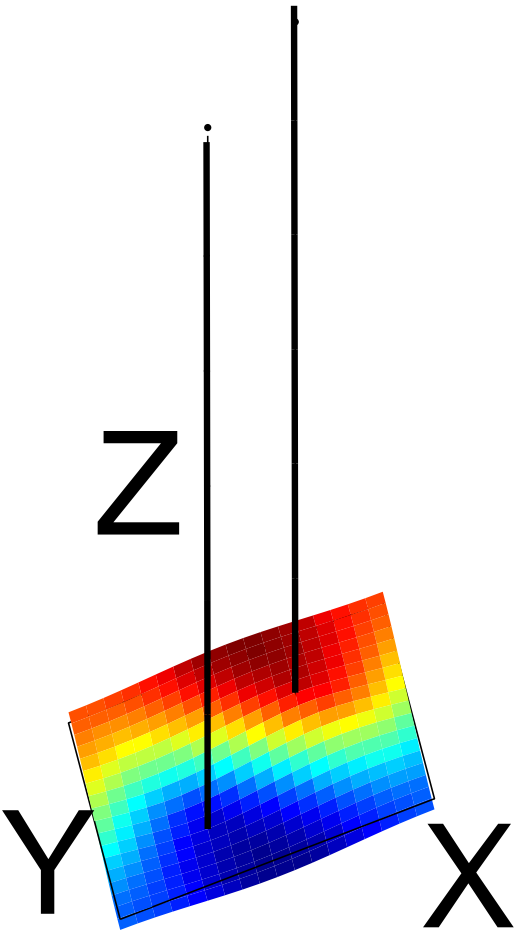
Figure(s)



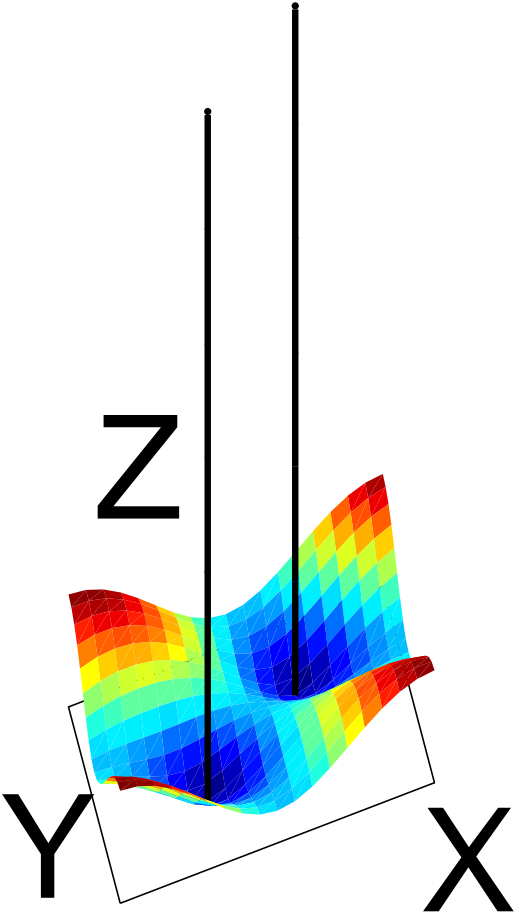
Figure(s)



Figure(s)

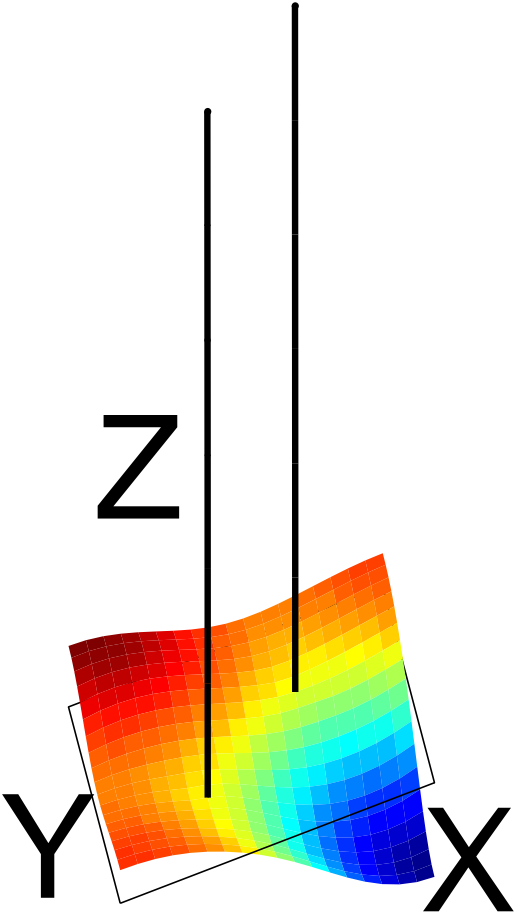


Figure(s)

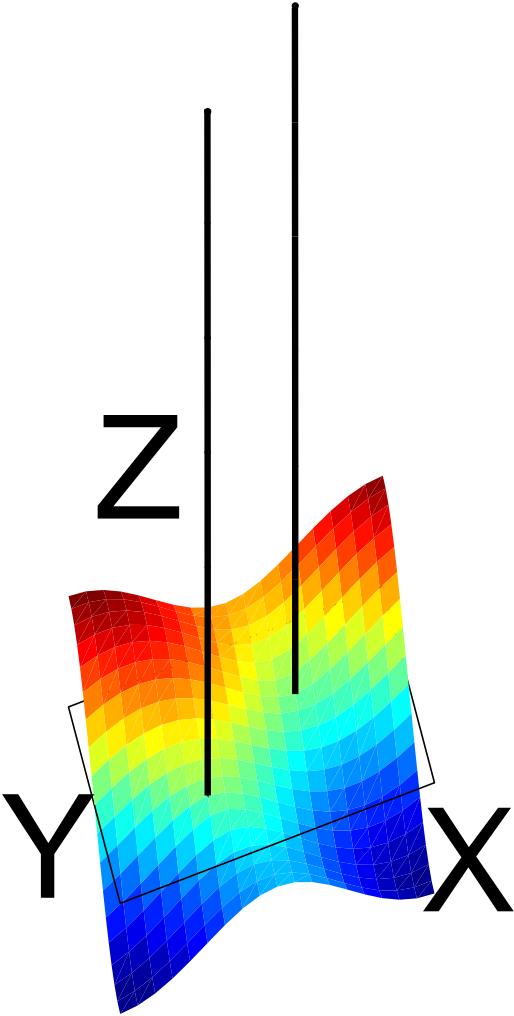




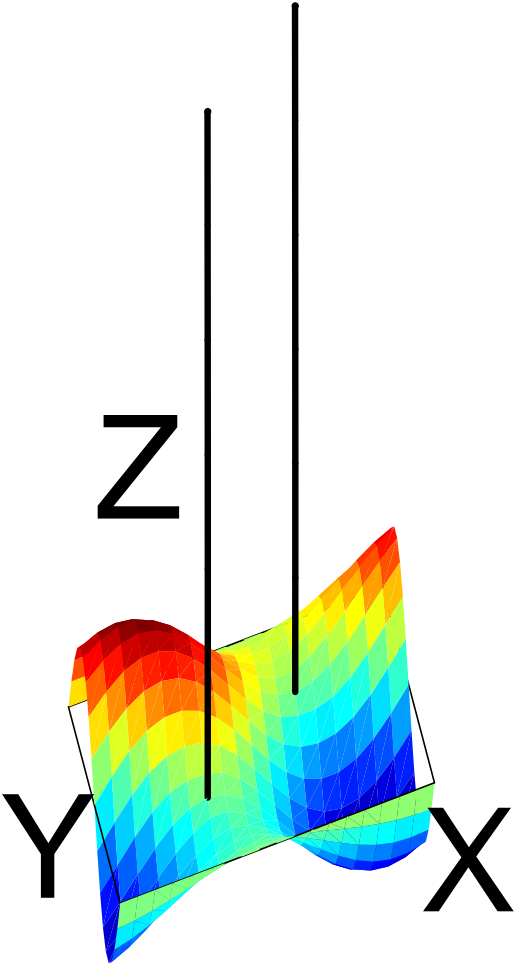
Figure(s)



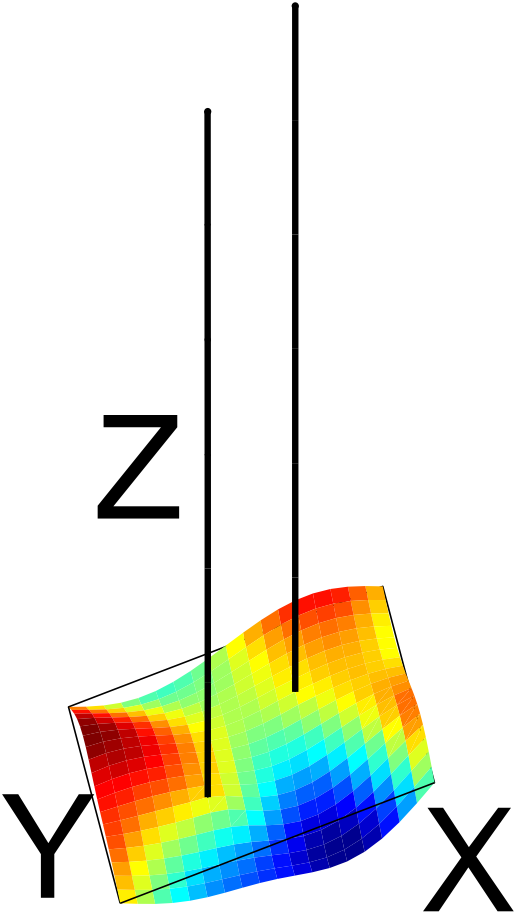
Figure(s)



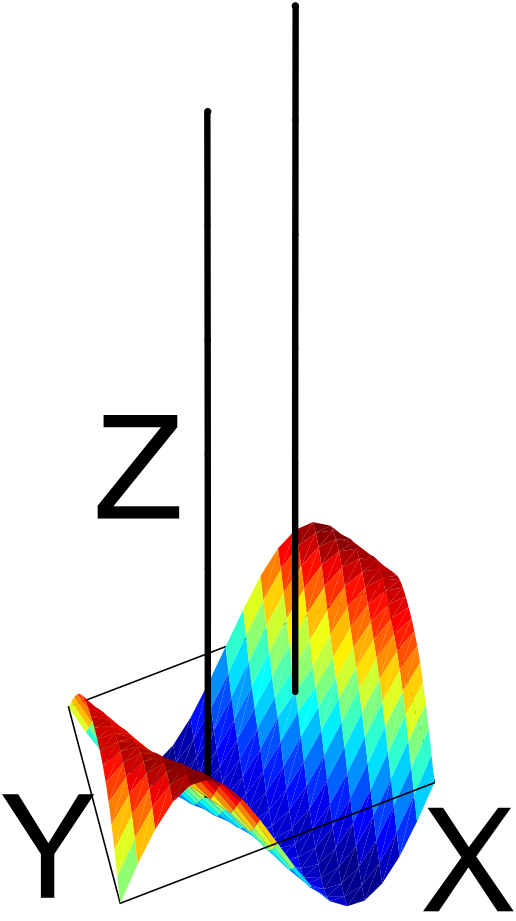
Figure(s)



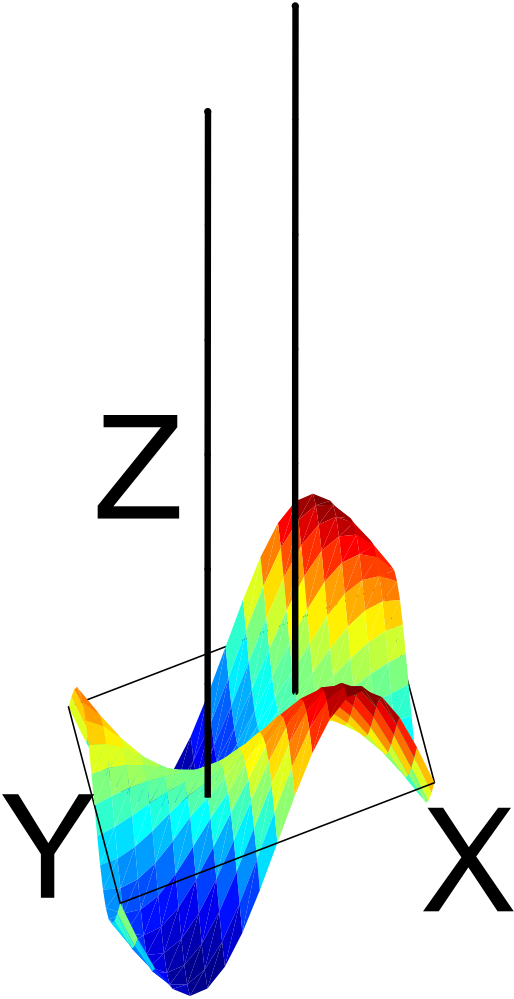
Figure(s)



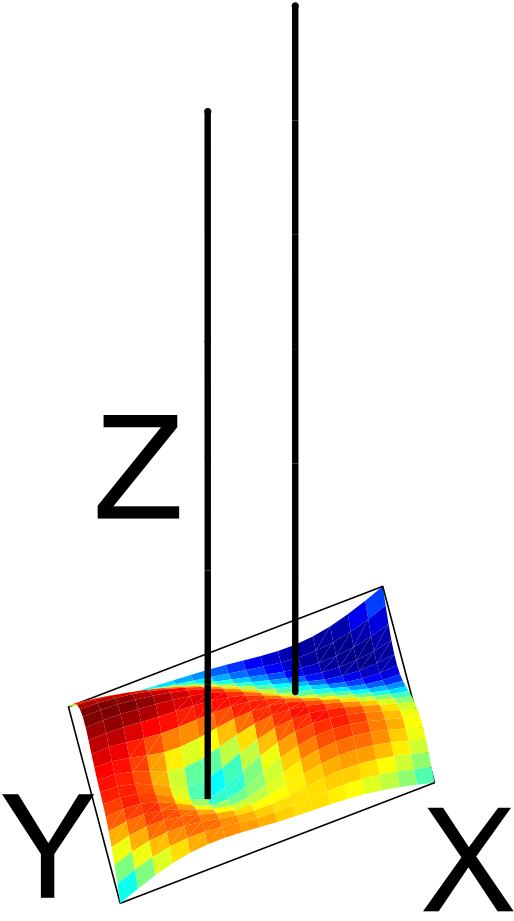
Figure(s)



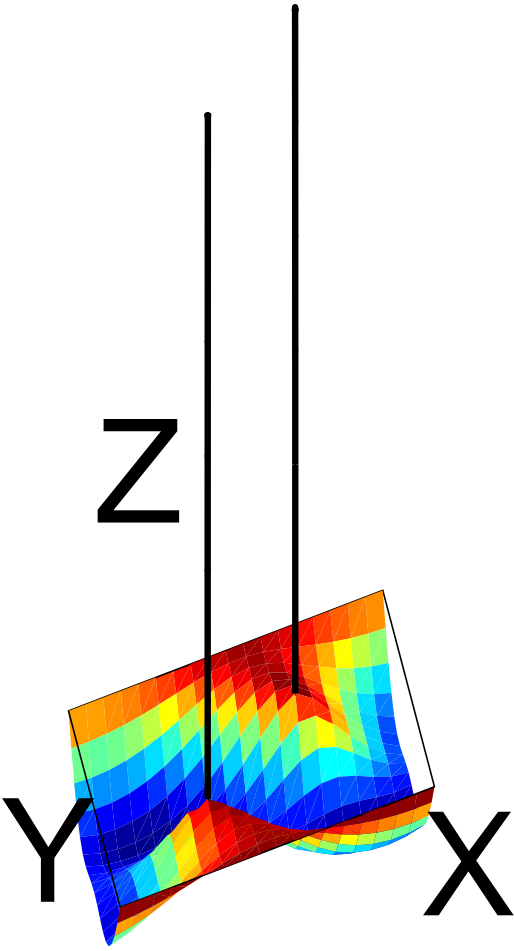
Figure(s)



Figure(s)

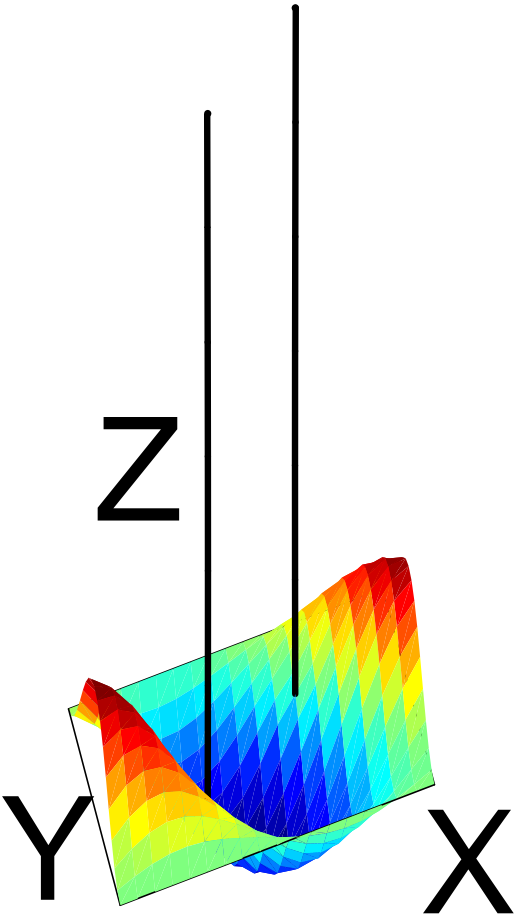


Figure(s)

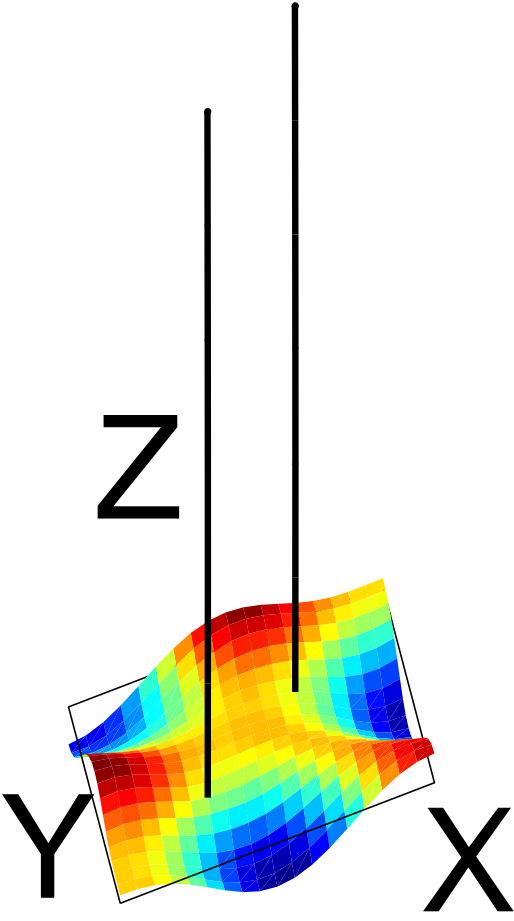




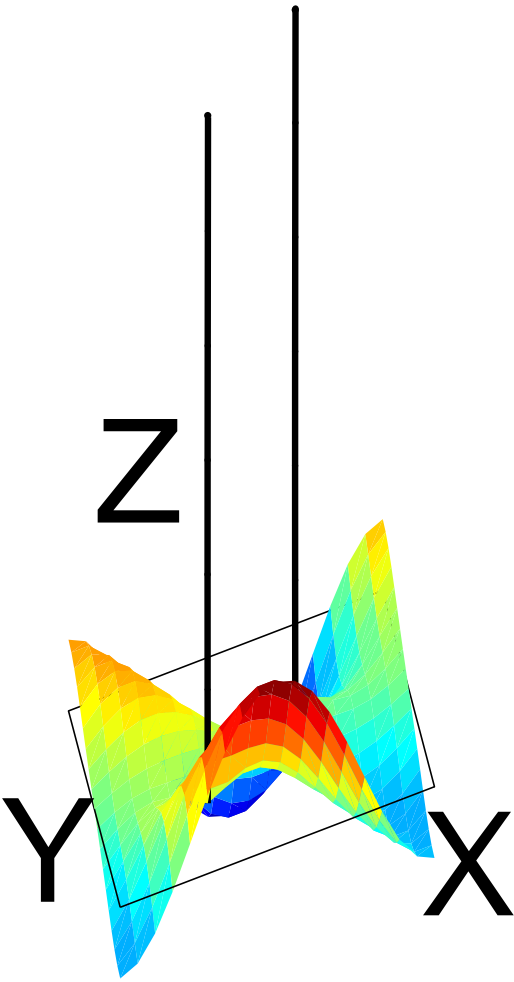
Figure(s)



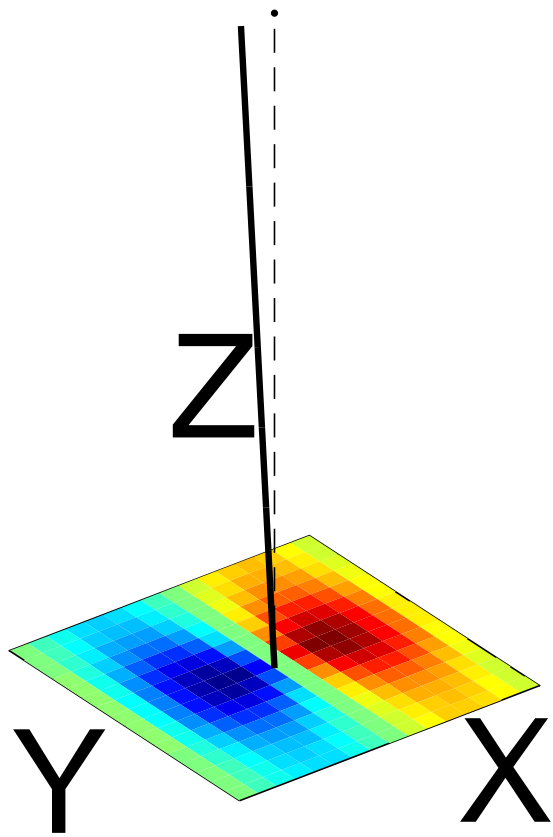
Figure(s)



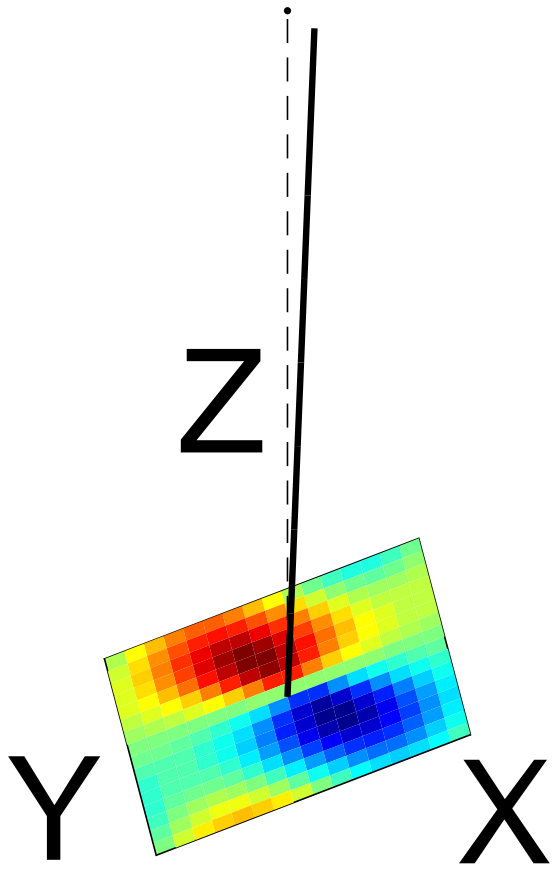
Figure(s)



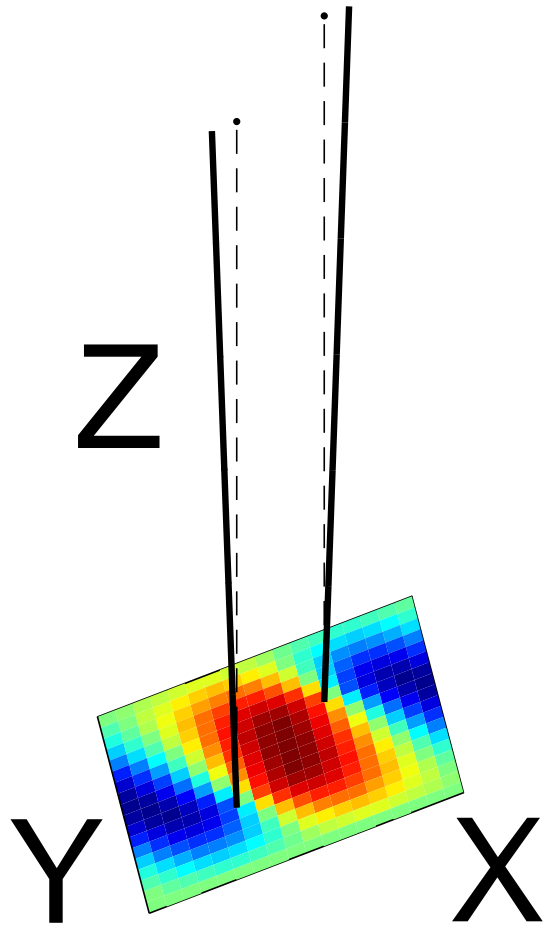
Figure(s)

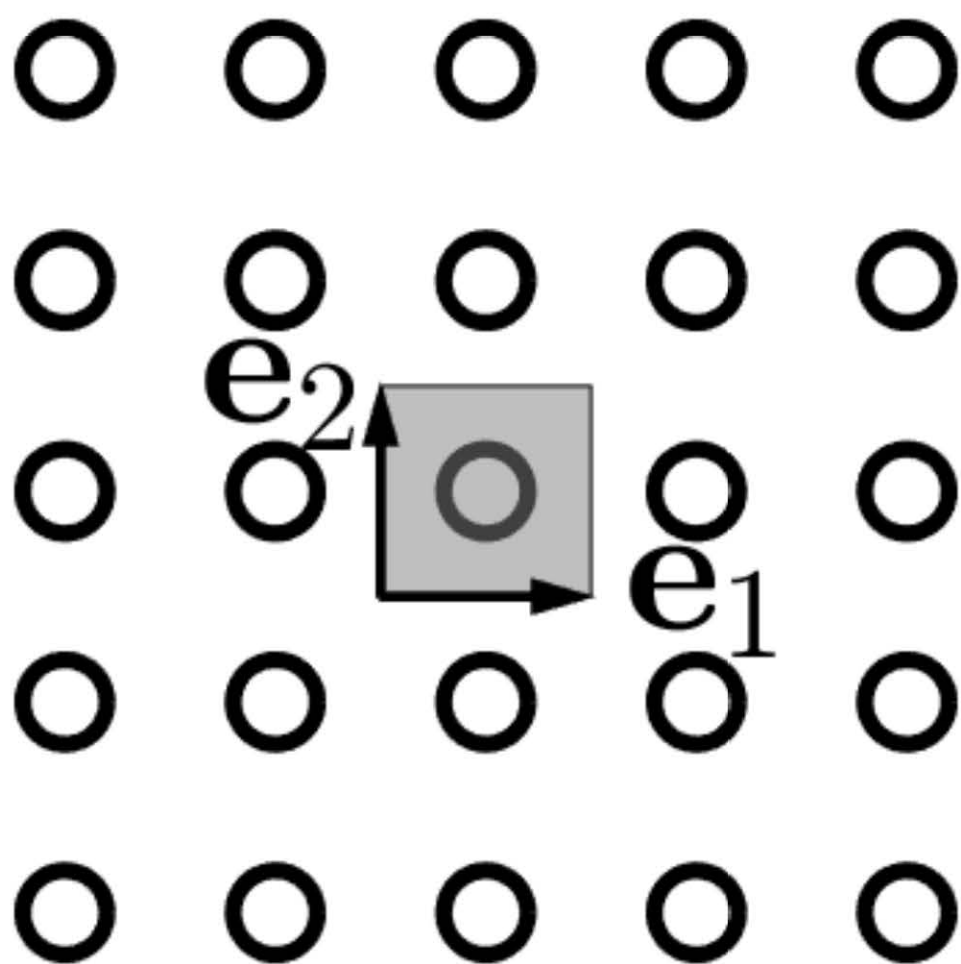


Figure(s)

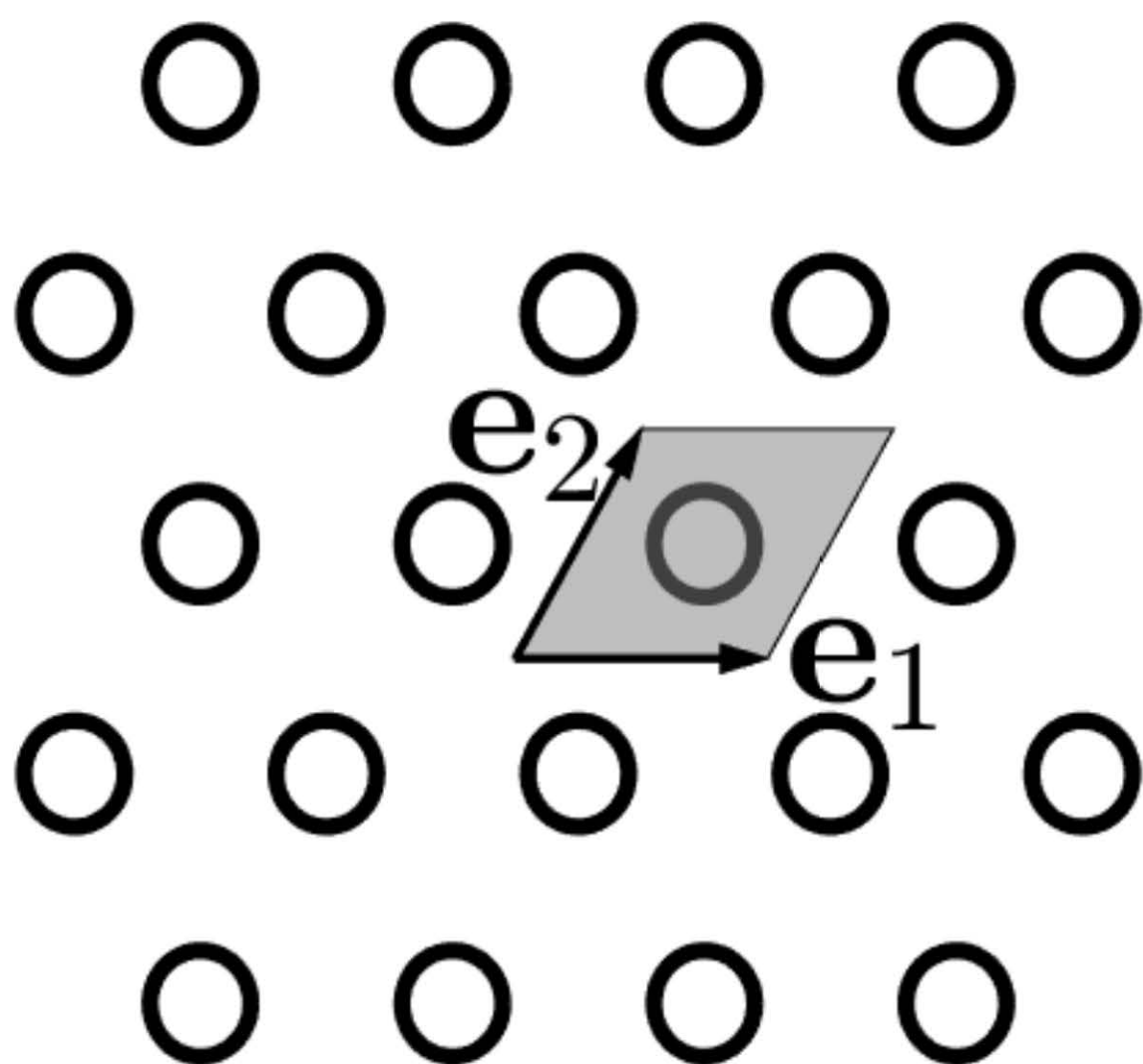


Figure(s)

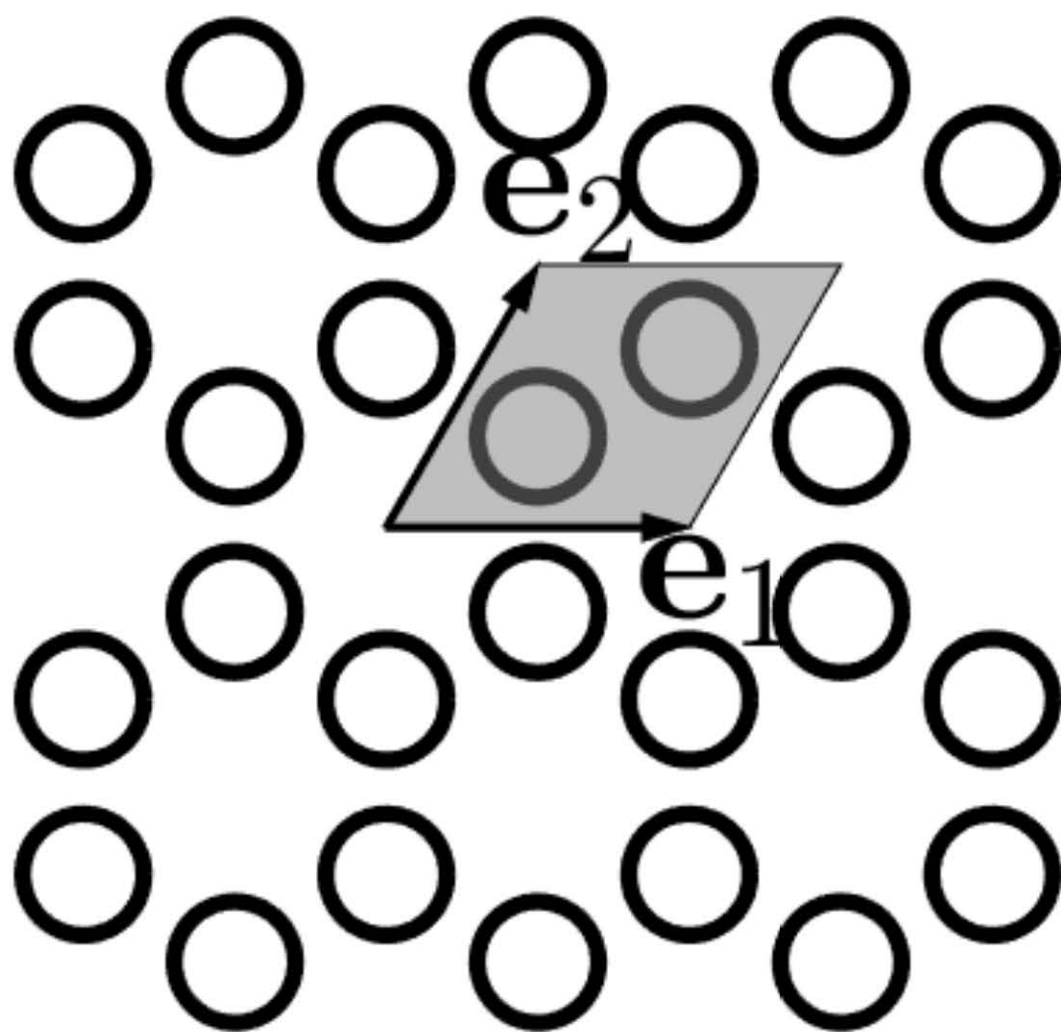




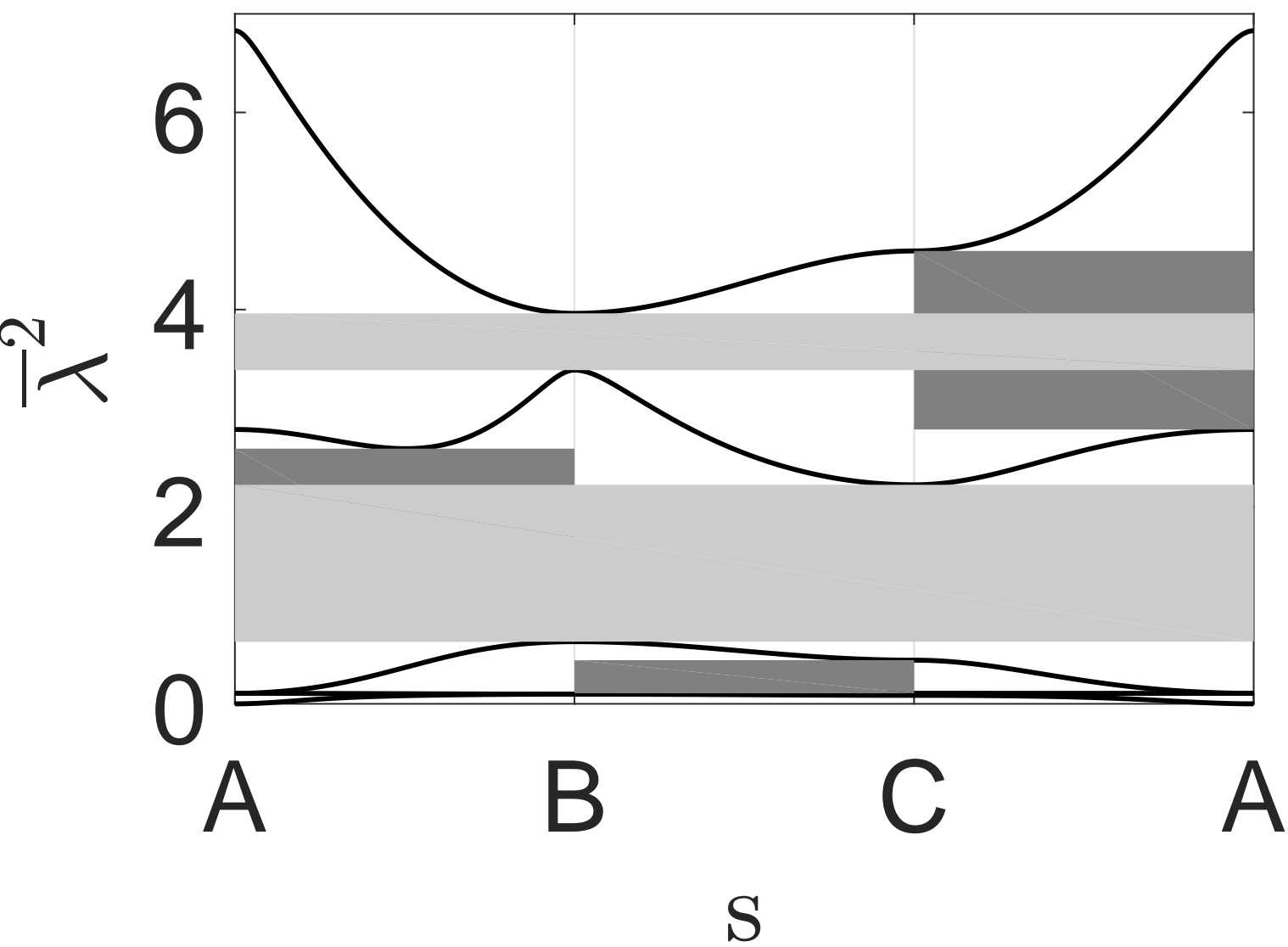
Figure(s)



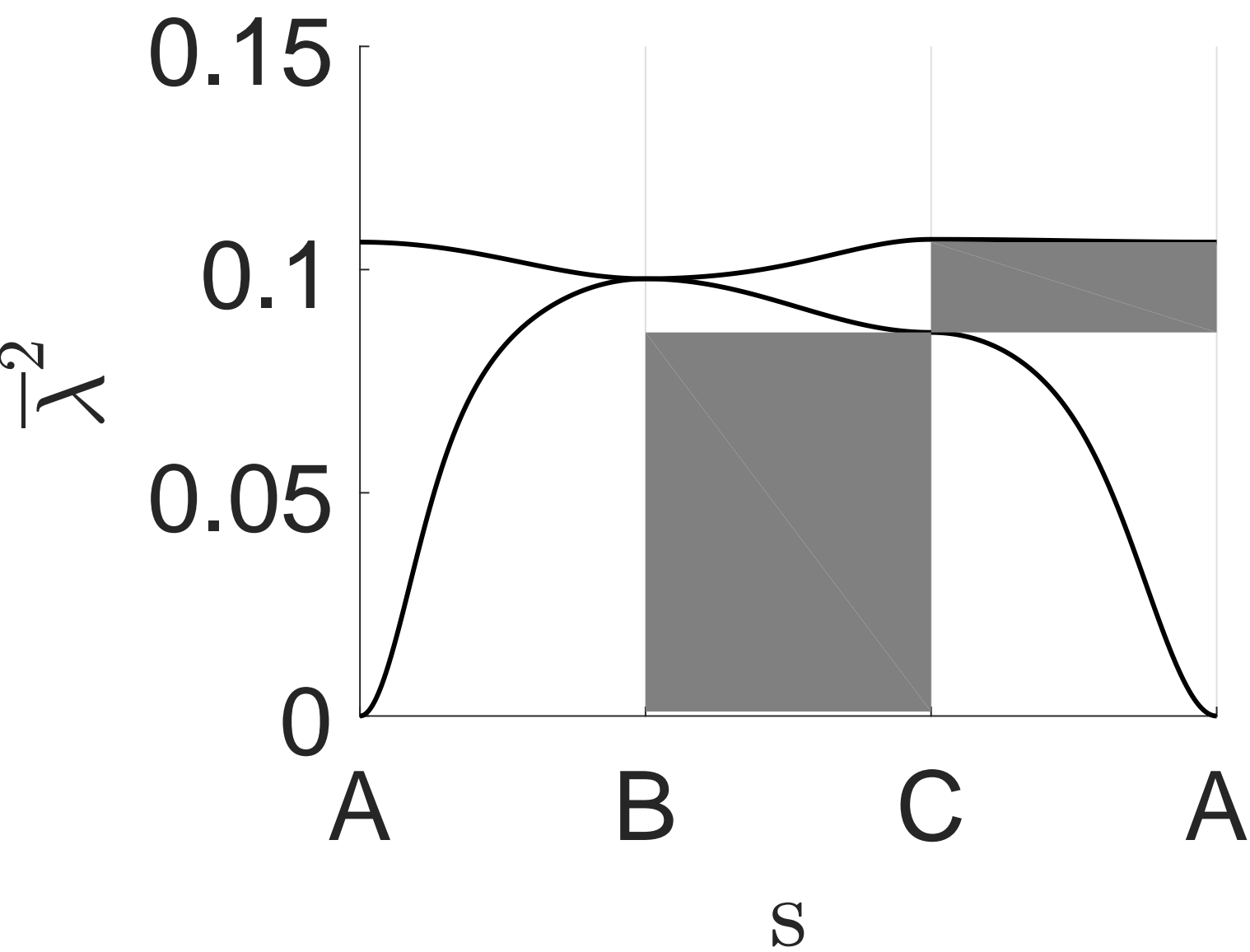




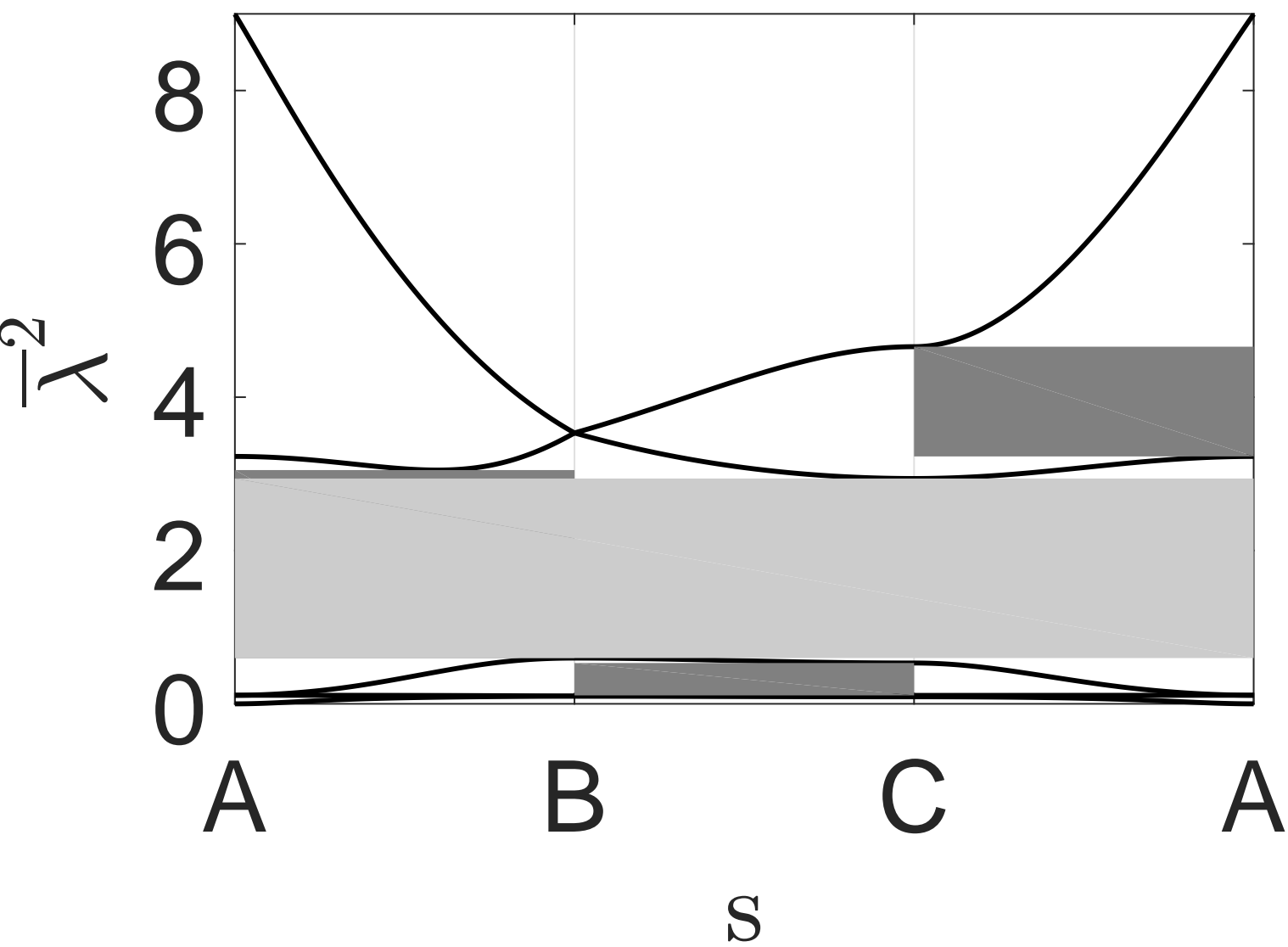
Figure(s)



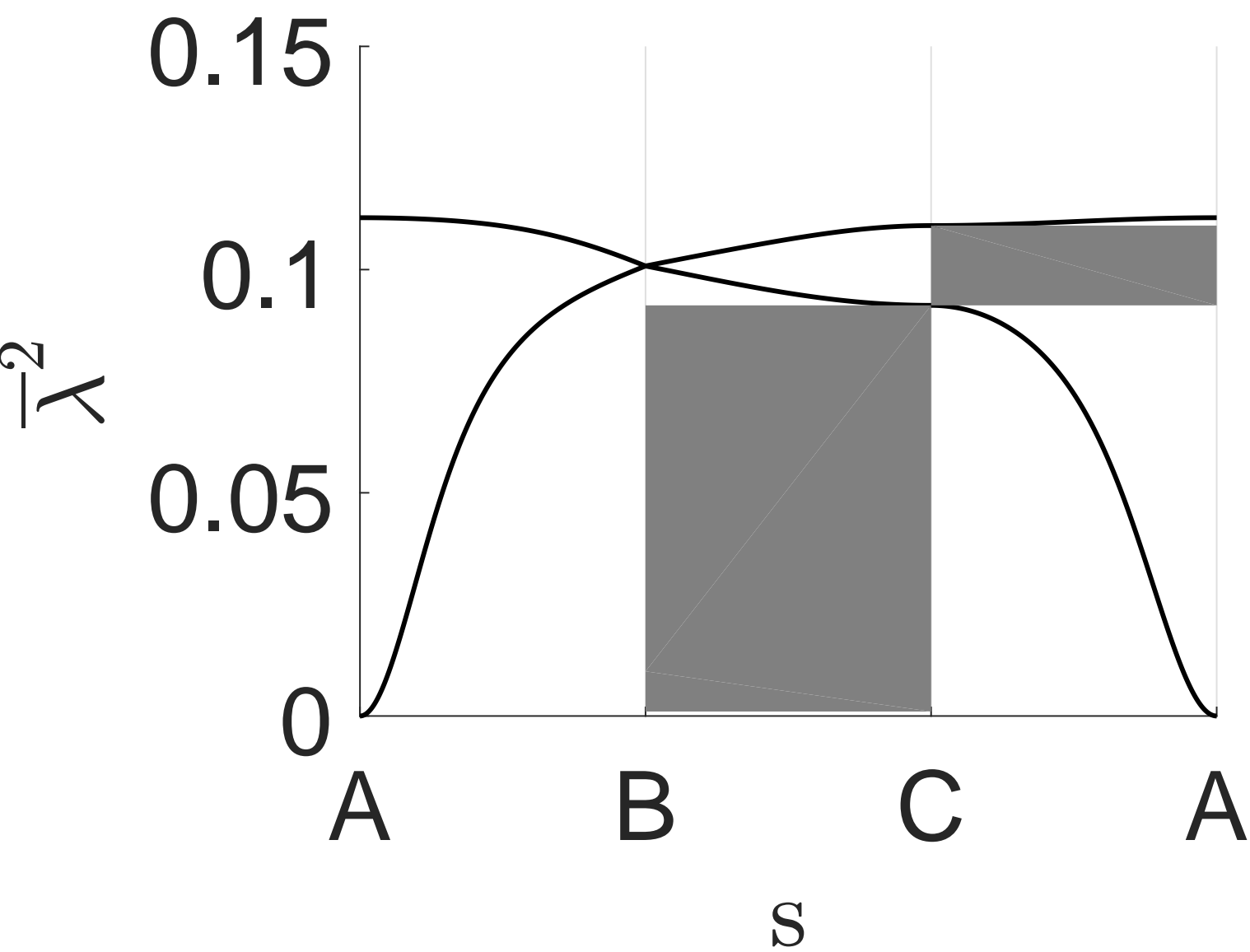
Figure(s)



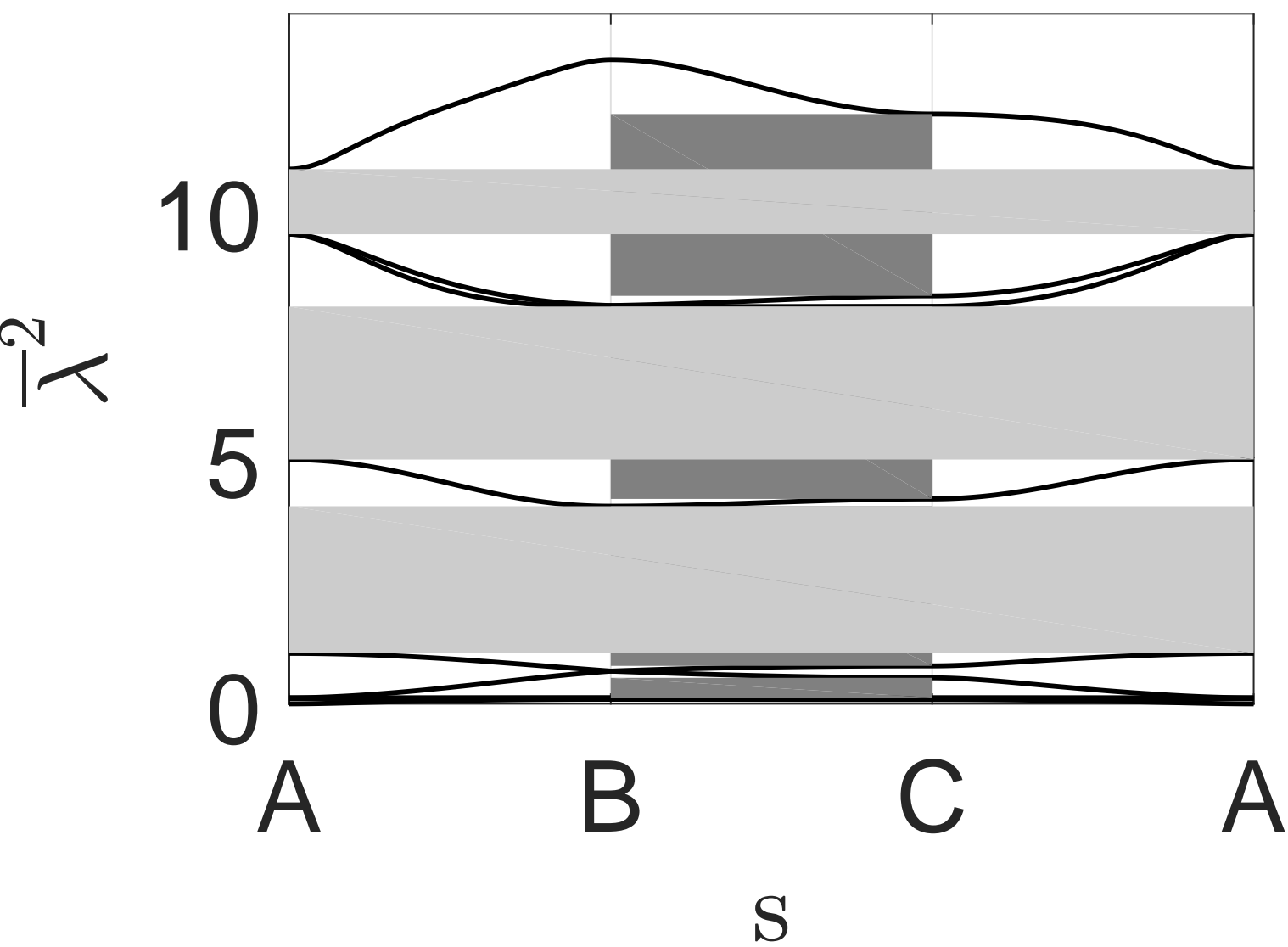
Figure(s)



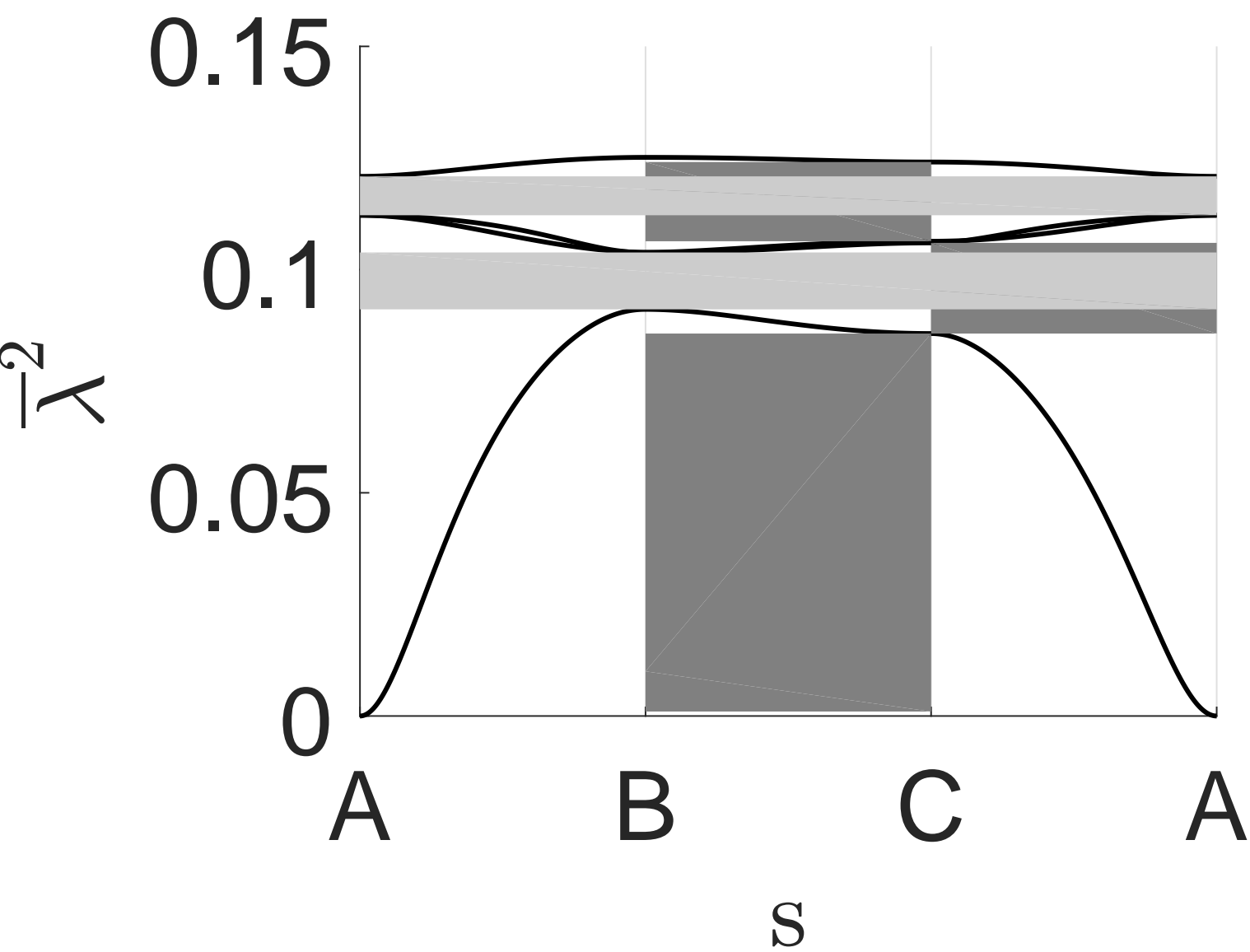
Figure(s)



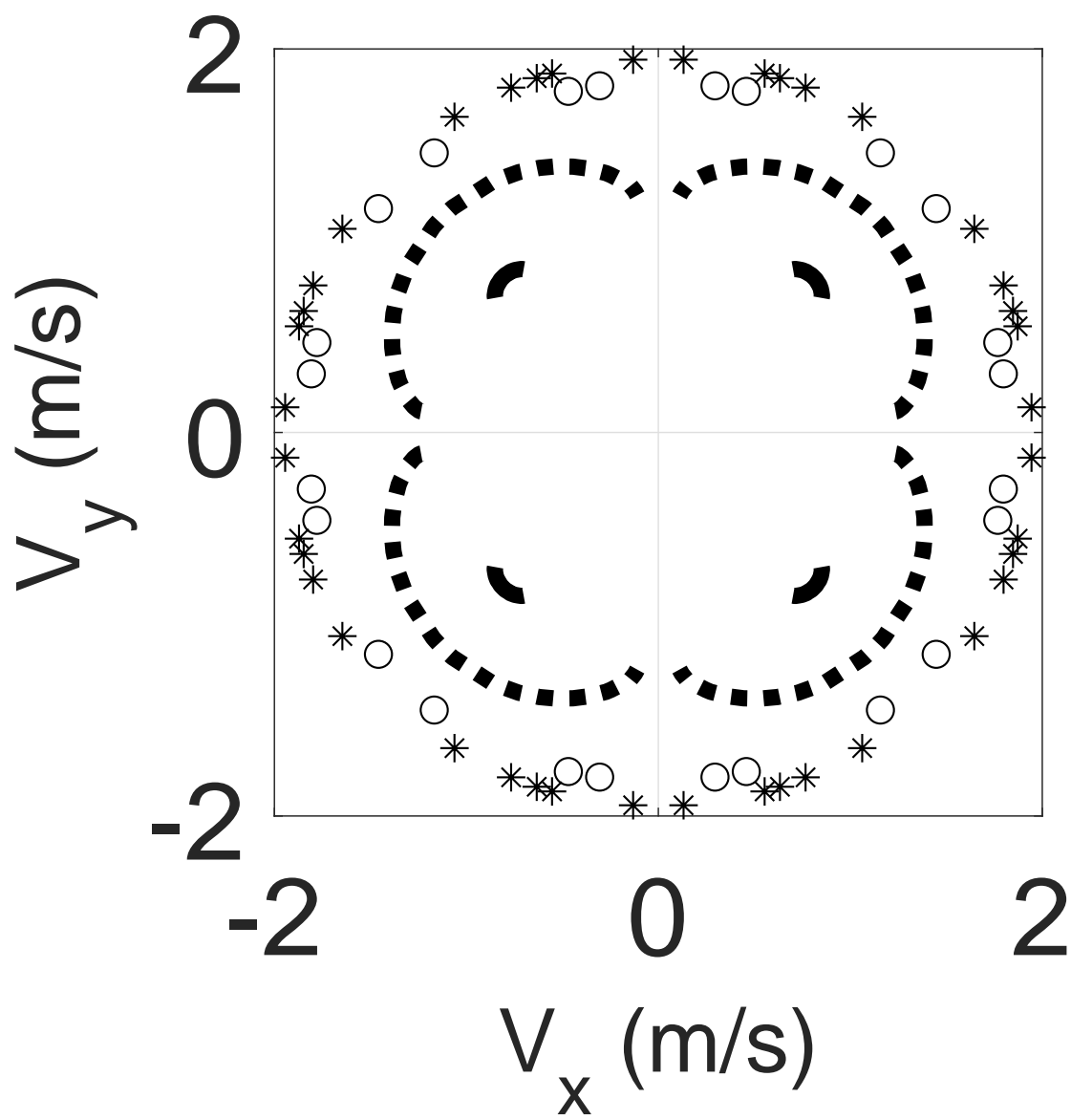
Figure(s)



Figure(s)

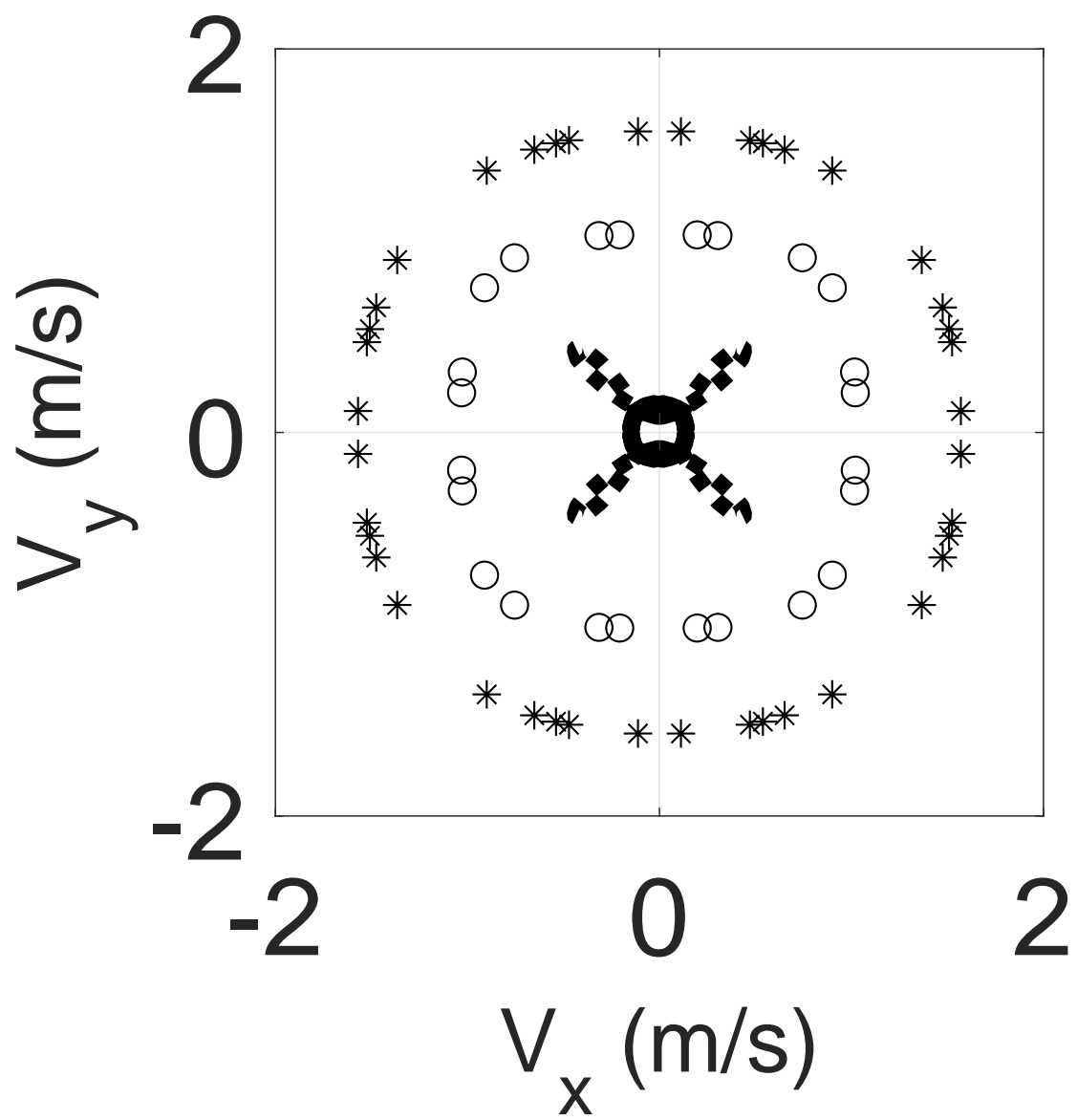


Figure(s)

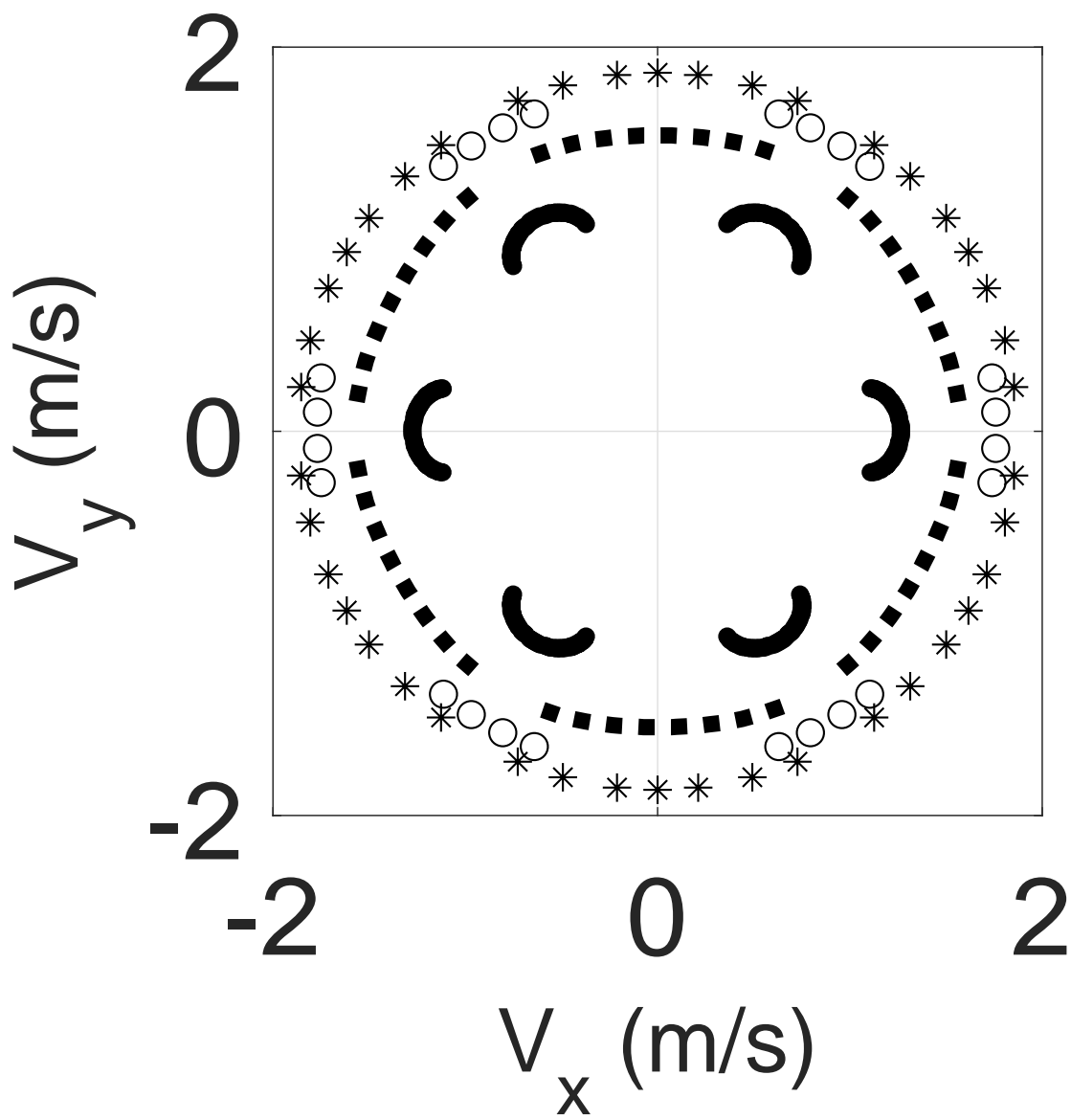




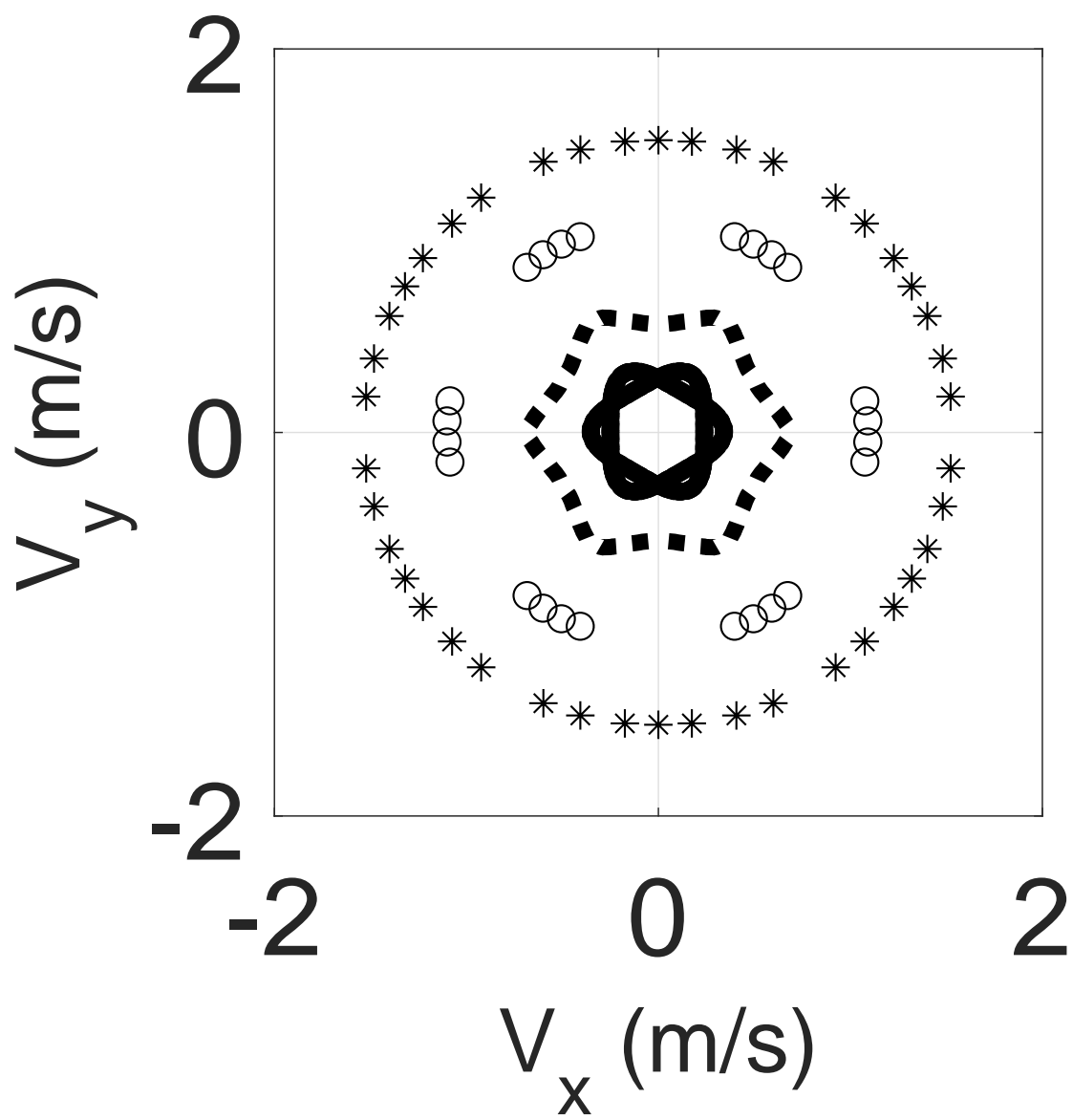
Figure(s)



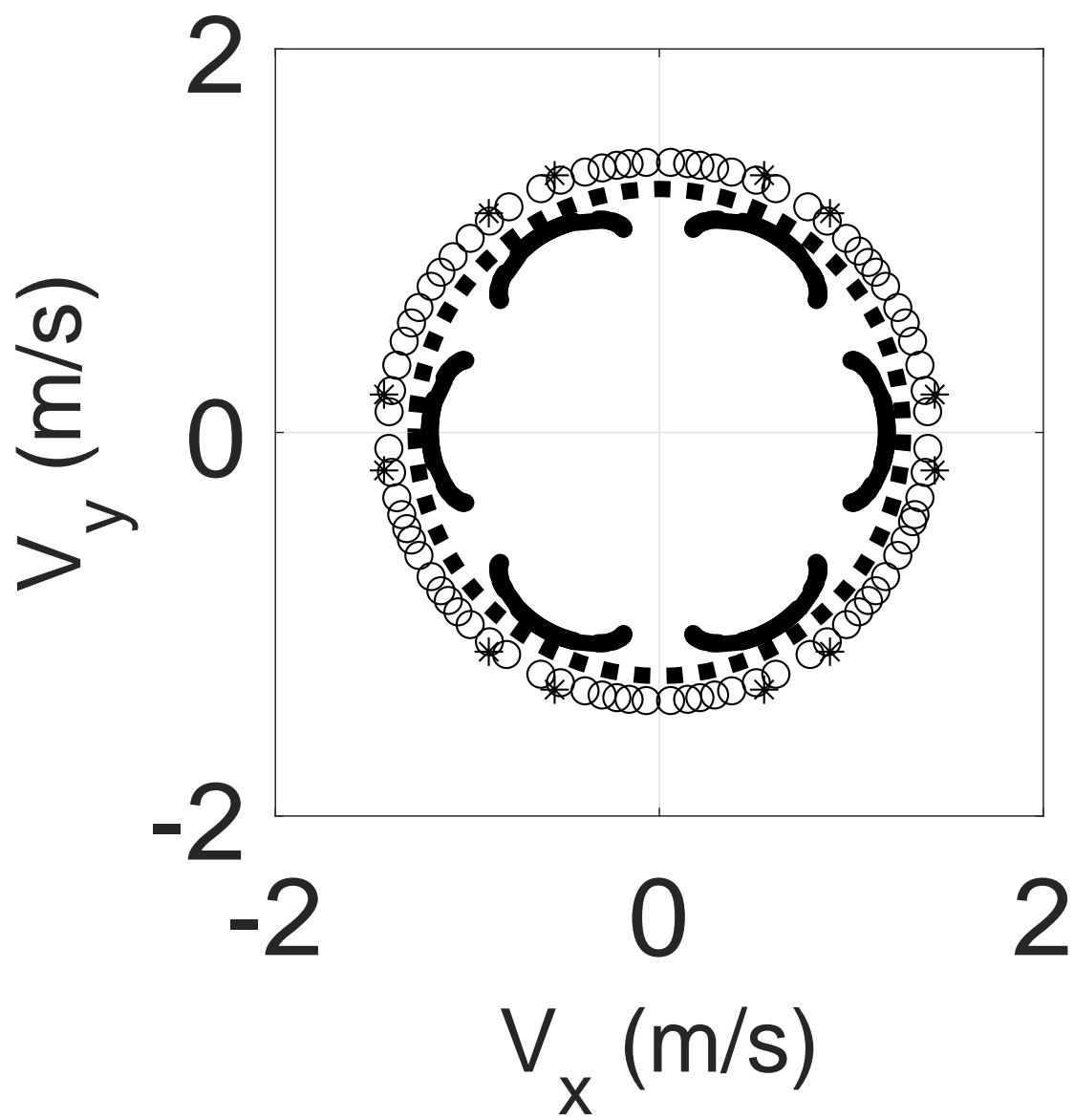
Figure(s)



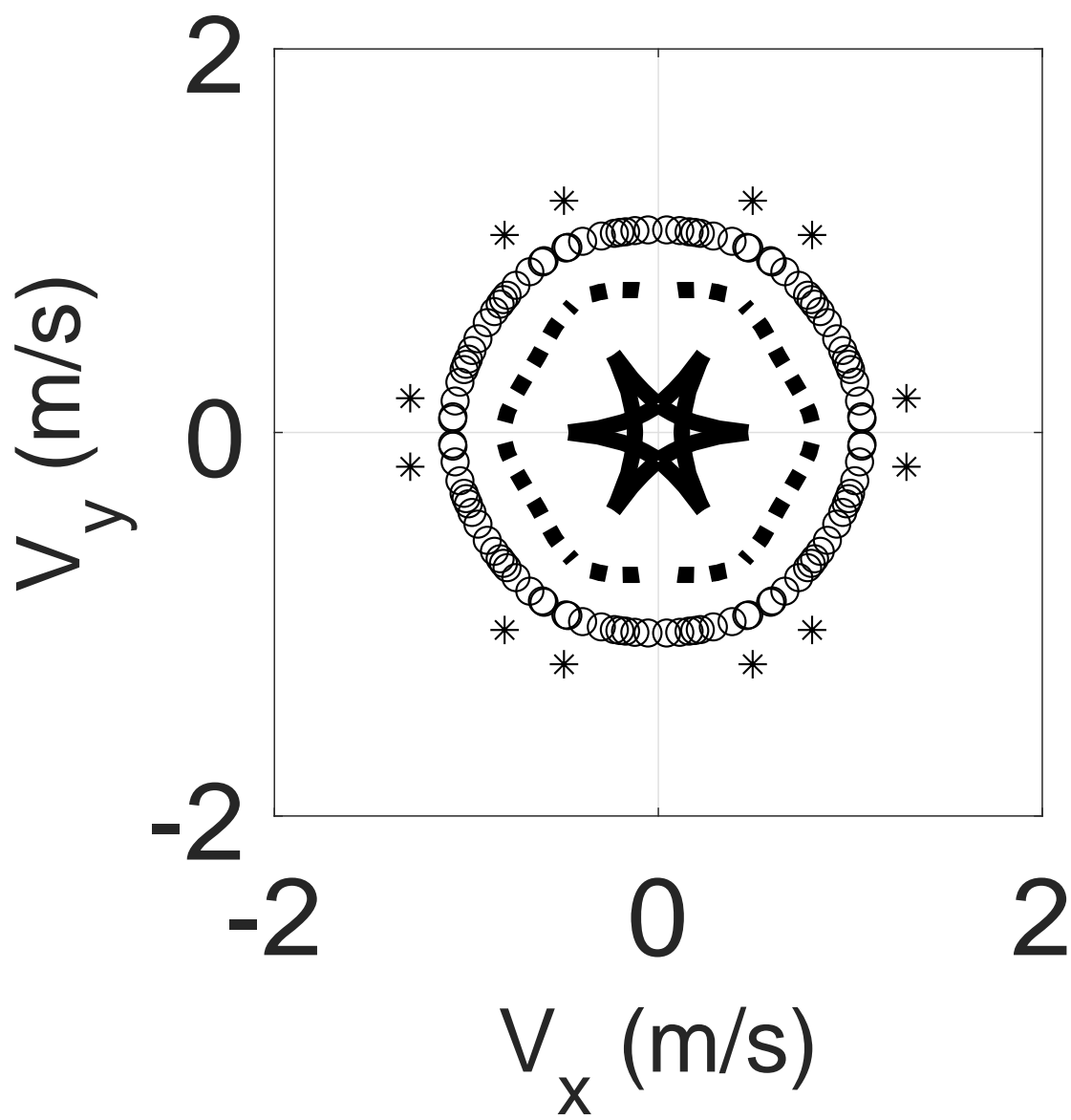
Figure(s)



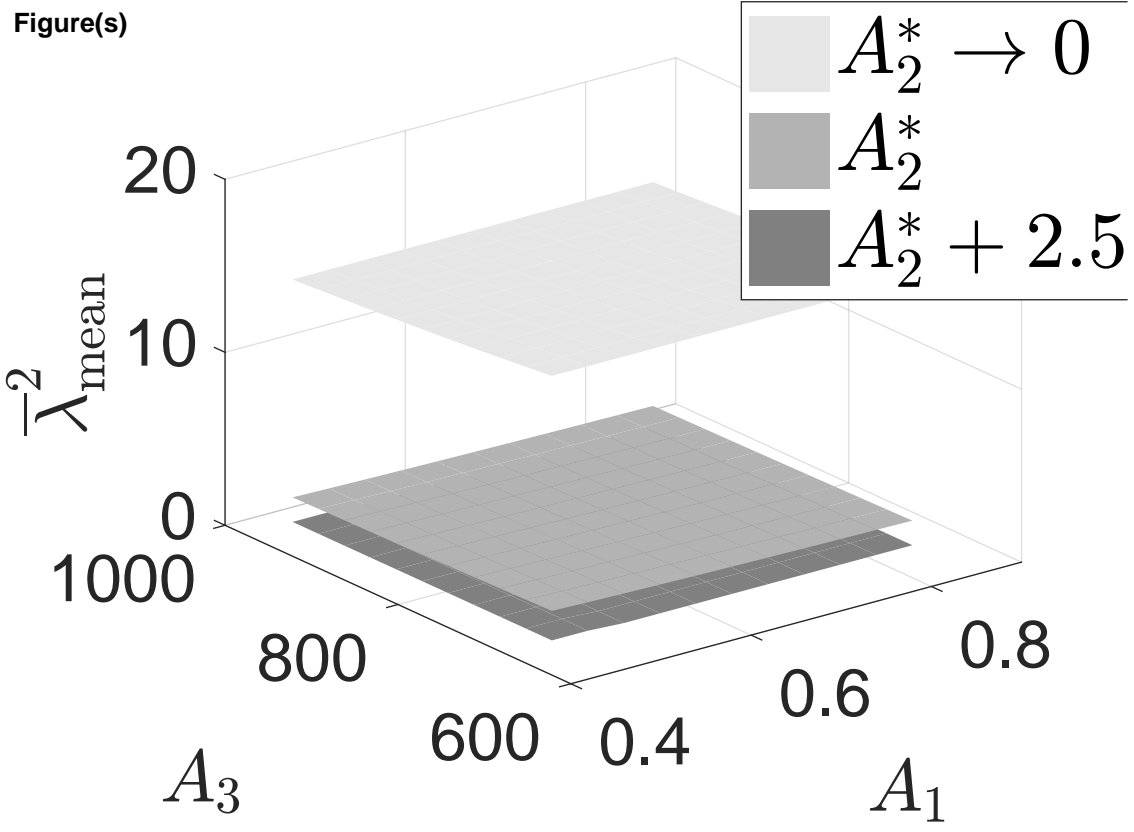
Figure(s)



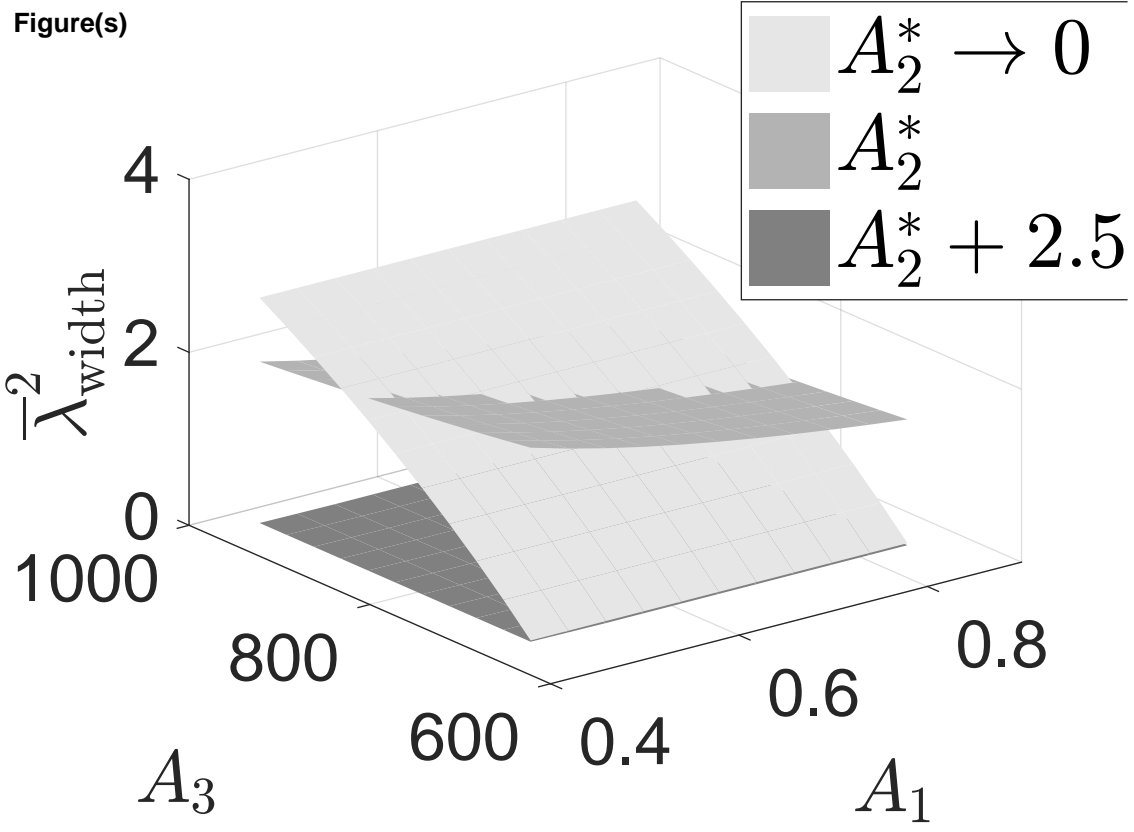
Figure(s)



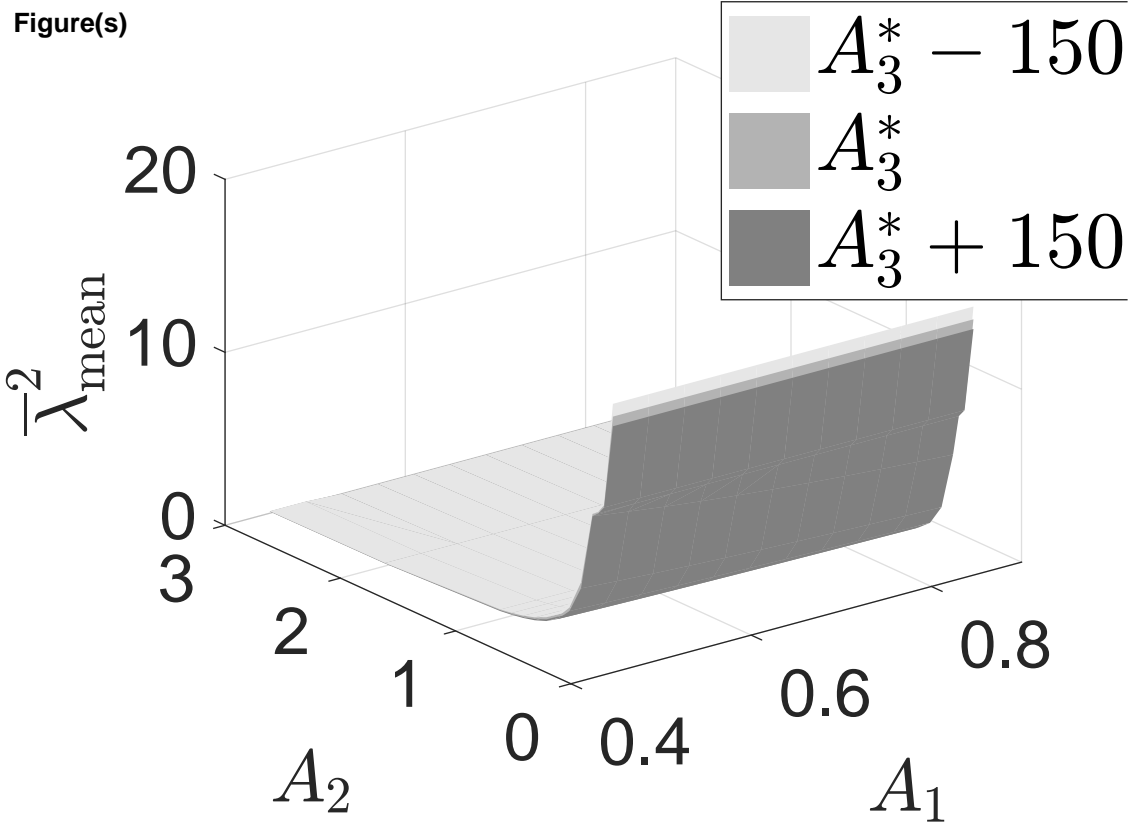
Figure(s)



Figure(s)

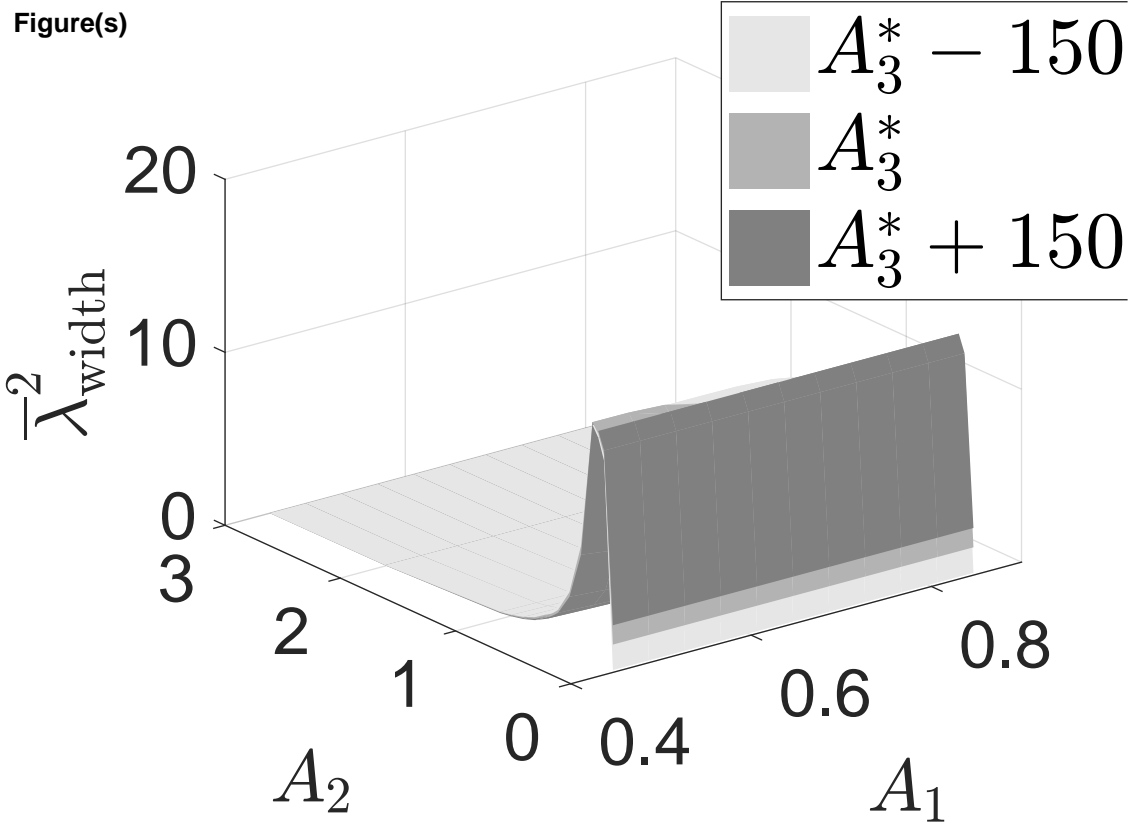


Figure(s)

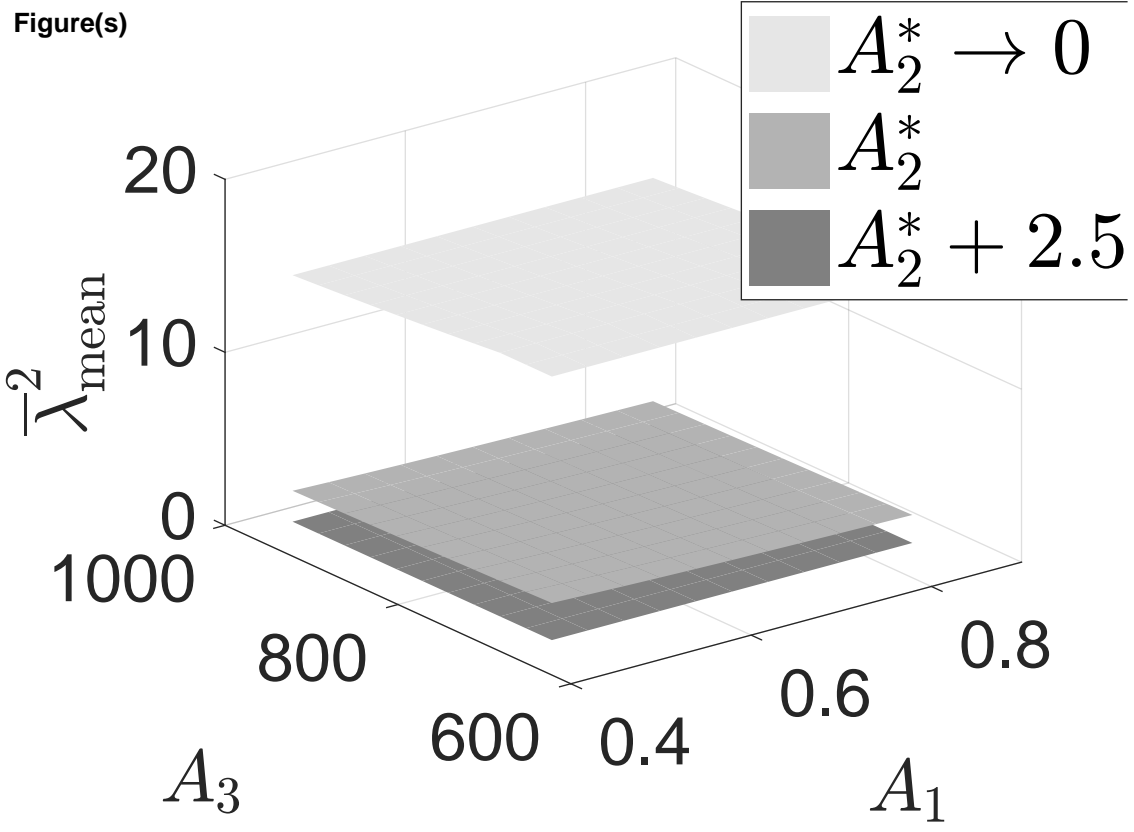




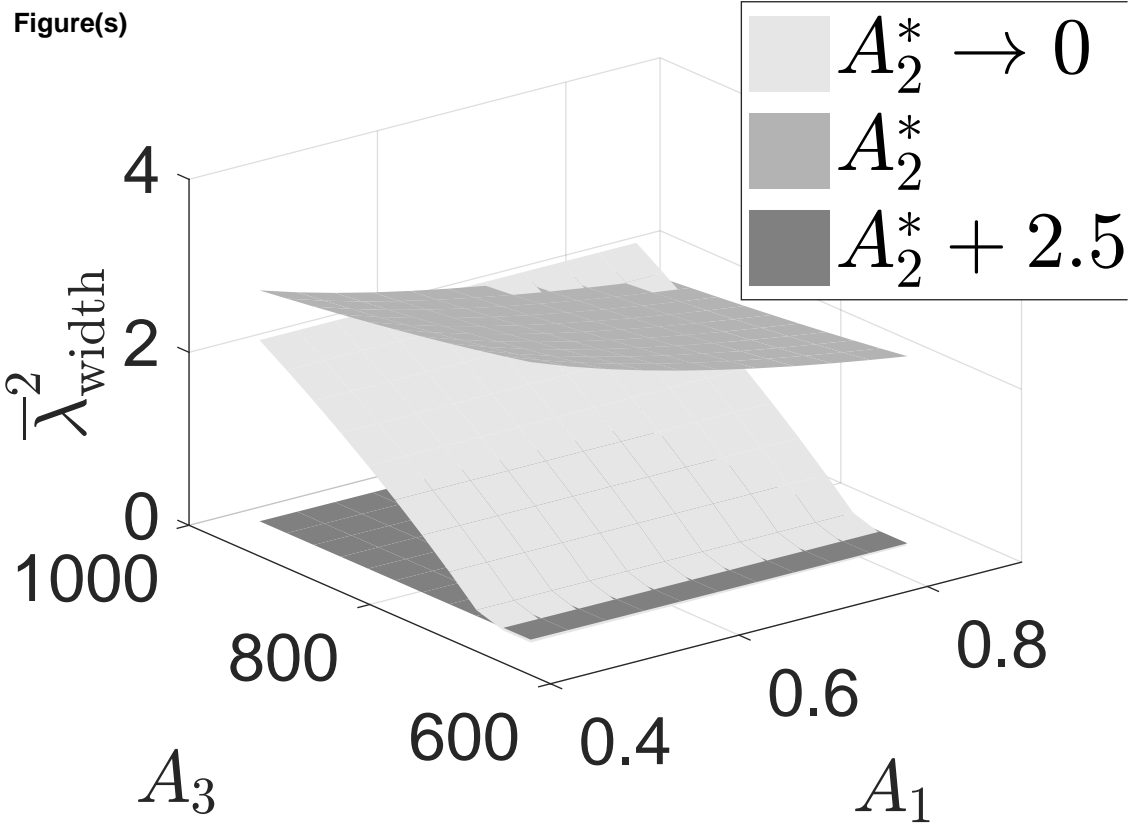
Figure(s)



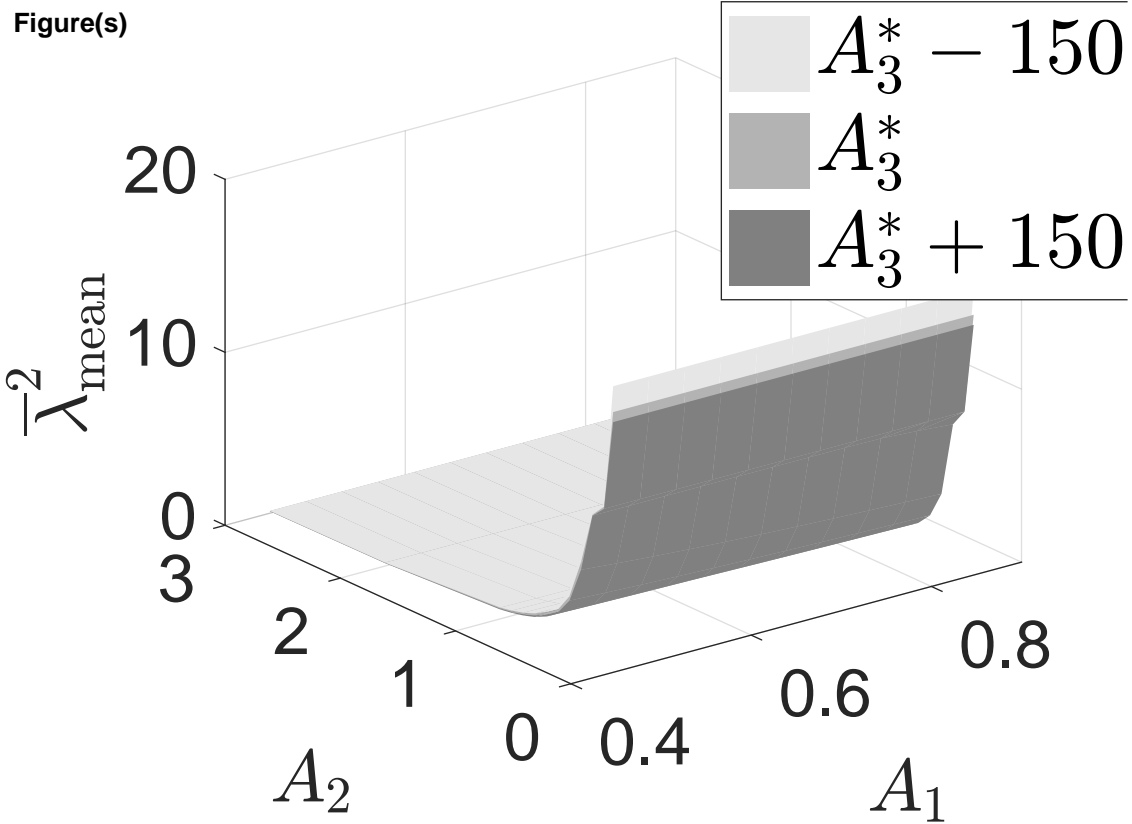
Figure(s)



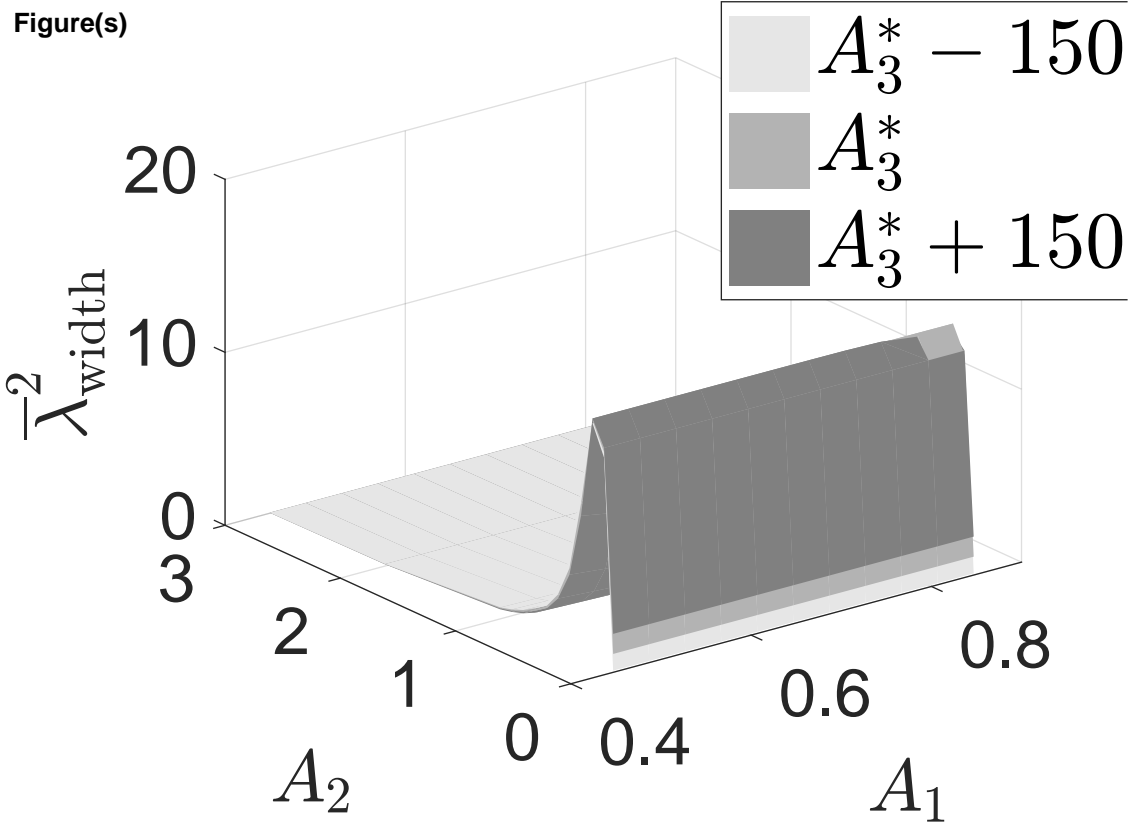
Figure(s)



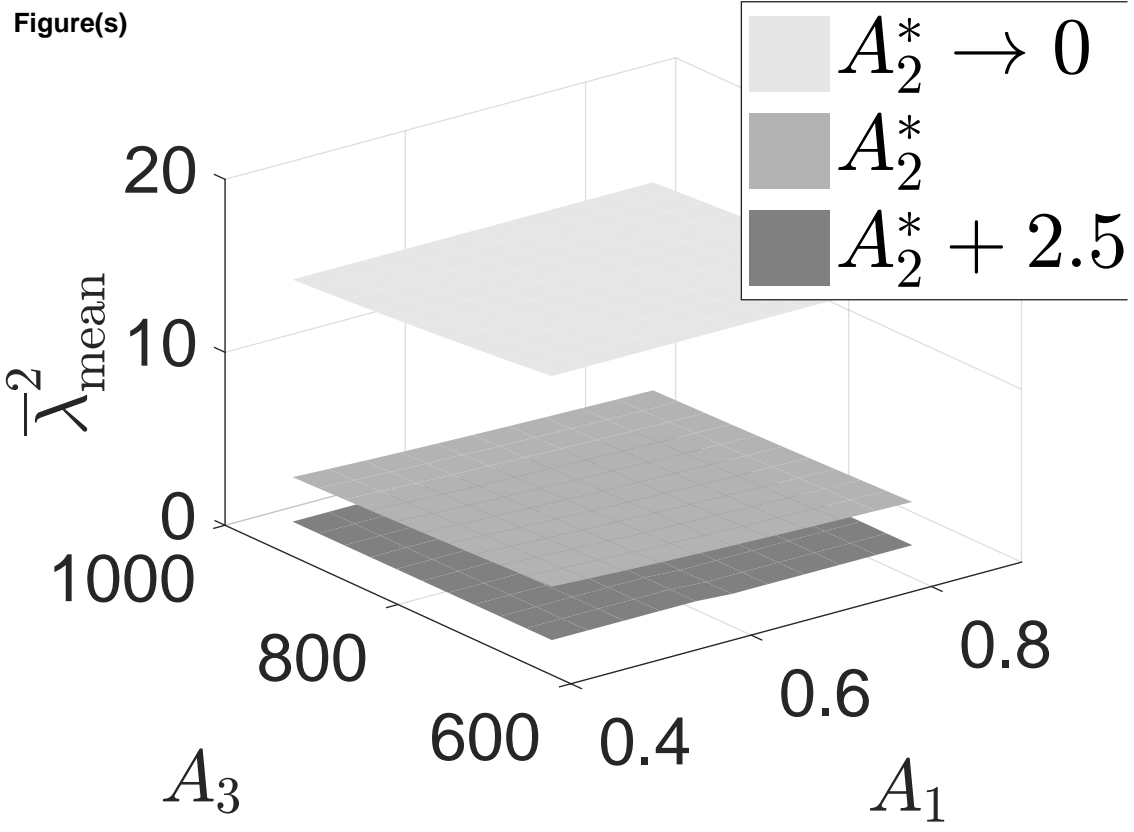
Figure(s)



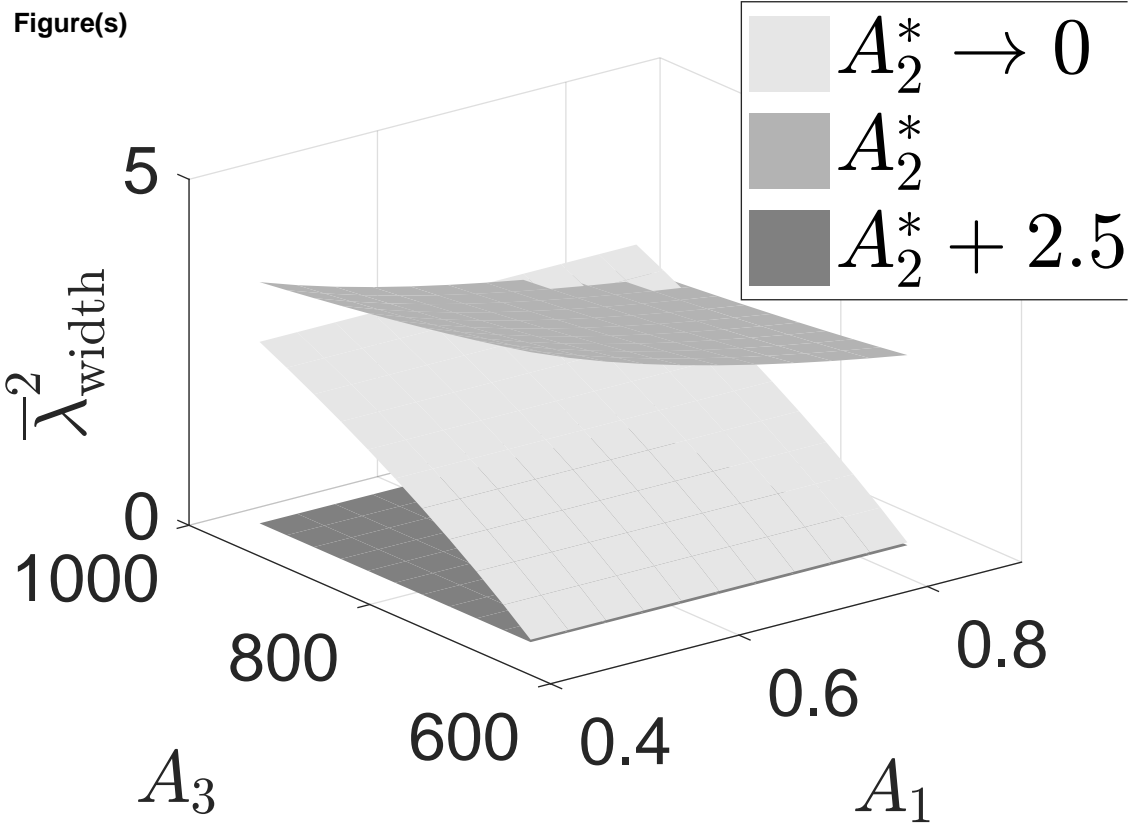
Figure(s)



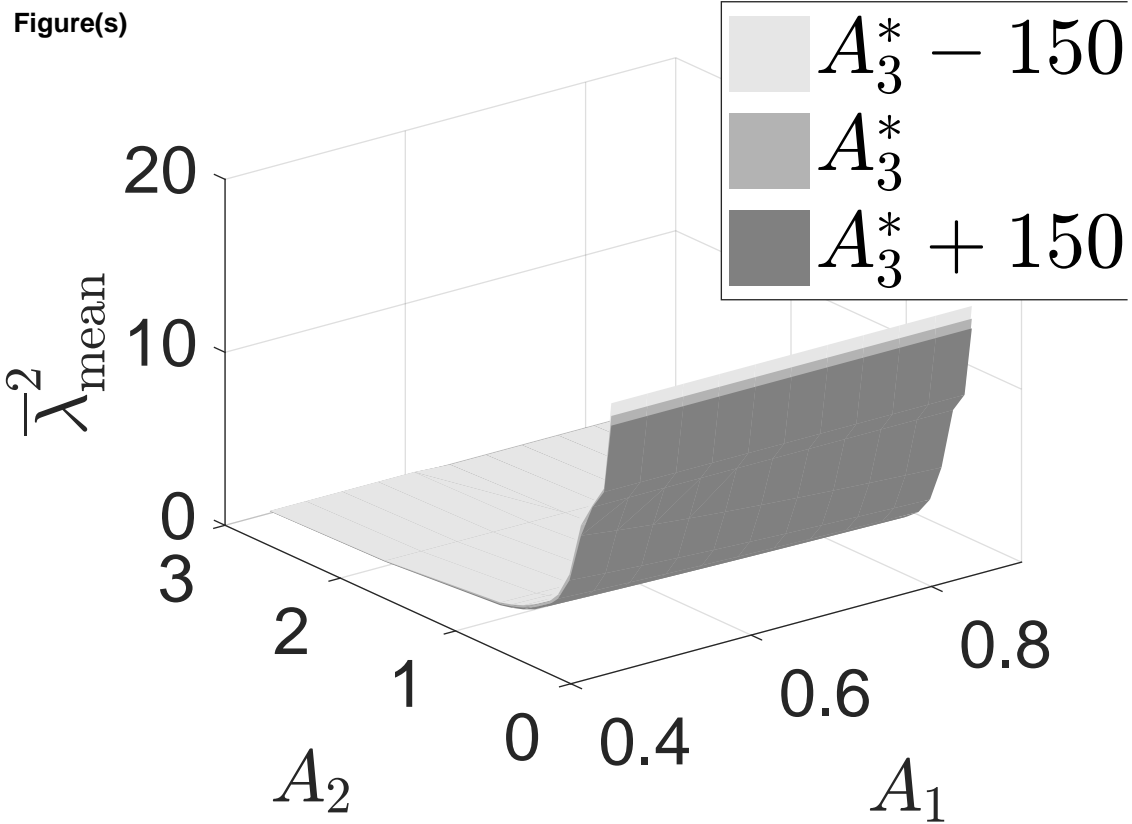
Figure(s)



Figure(s)

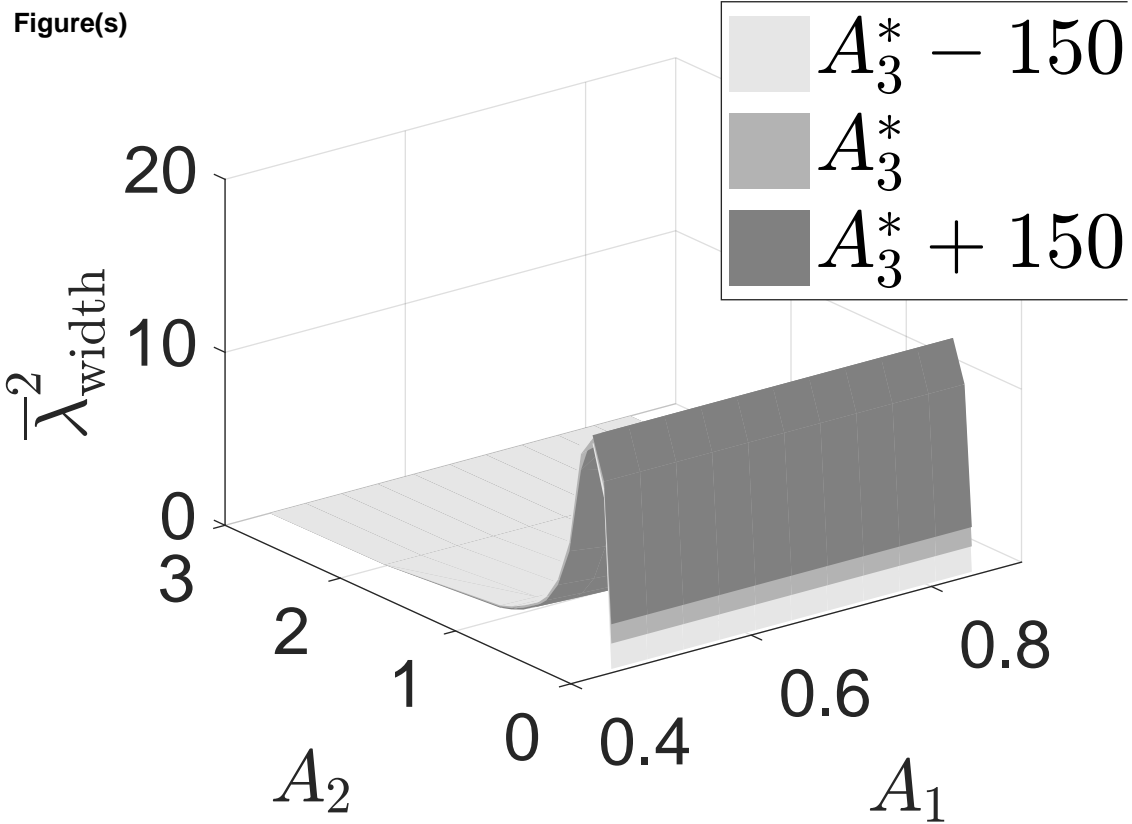


Figure(s)





Figure(s)





## \*Detailed Response to Reviewers

The authors gratefully acknowledge the interest of the referees in reviewing our manuscript, and for their valuable comments and suggestions.

The new version of the manuscript has been sent to a translation agency for grammatical improvement. Some editorial revisions have been made and some figures have been improved in order to get a better quality.

Journal of Sound and Vibration

Author Checklist

Authors should complete the following checklist and submit with their revised manuscript.

Math notation follows requirements on Guide for Authors (GFA) see:

<https://www.elsevier.com/journals/journal-of-sound-and-vibration/0022-460X/guide-for-authors>

Use Roman (normal upright) type for: Total differential operators (e.g.  $d$  in differential);  $i$  or  $j$  (square root of  $-1$ );  $\exp$  or  $e$  (base of natural logarithms);  $\text{Re}$  or  $\text{Im}$  (real or imaginary part);  $\log$ ,  $\ln$ ,  $\sin$ ,  $\cos$ , etc.; abbreviations such as  $c.c.$  (complex conjugate); multiletter symbols (e.g.  $TL$  for transmission loss); subscripts of two or more letters identifiable as words or word-abbreviations (e.g.,  $\text{Apipe}$ ,  $f_{\text{max}}$ )

For more unusual functions, JSV follows Abramowitz and Stegun's book. More detail given in the GFA (see link above).

Unit symbols - These should be upright (e.g.  $\text{kg}$ , not  $kg$ ).

All authors are listed on the manuscript with correct affiliations, correct email address and are in correct order.

Keywords present.

Manuscript is not currently submitted to any other Journal.

If submitting highlights please note that only six may be submitted and each one should be no longer than 85 characters in length.

Novelty of paper has been clearly stated in the Introduction.

References are presented as per GFA.

References not produced in English language to have English translation in brackets.

Figures and Tables and Equations are numbered in sequence correctly. (See GFA).

Nomenclature (if required) appears on second page of submission.

Acknowledgements should appear in a separate section just after the conclusions.

All abbreviations, in both the abstract and main body of document, are defined once only, the first time they appear in the text. (N.B. The Abstract is treated as an independent text, where references are given in full and abbreviations and symbols, if used, are properly defined.)

Figures – if there are multi-parts to a figures each part is labelled (a) (b) (c) etc. and the labels defined in the figure caption.

Figures – Colour can be used for the on-line version. Figures are reproduced in black and white in the printed journal and must therefore be readable in both colour and black & white. (N.B. charges apply for production of colour figures in the printed journal)

Appendices – should appear before the list of references and labelled A, B, C, (please see GFA for further information regarding equations, figures and tables in the appendices.

Copyright – material reproduced from other publications (e.g. Tables, Figures), source is acknowledged.

Statement of Author contribution complete (see GFA)

Revisions made to the manuscript:

- The new version of the manuscript has been revised in order to correct the punctuation after the equations:
  - o Commas: Eq.1, Eq.3, Eq.4, Eq.6, Eq.7, Eq.8, Eq.9, Eq.10, Eq.12, Eq.13, and Eq.14.
  - o Full stops: Eq.2, Eq.5, and Eq.11.